

Organic Structure Directing Agent Free Synthesis of Small
Pore Zeolite Catalysts for the Methanol-to-Olefins Reaction

Thesis by
Yuewei Ji

In Partial Fulfillment of the Requirements for
the degree of
Doctor of Philosophy

CALIFORNIA INSTITUTE OF TECHNOLOGY
Pasadena, California

2017
(Defended August 16, 2016)

© 2017

Yuewei Ji

All Rights Reserved

ACKNOWLEDGEMENTS

I would like to thank my advisor Prof. Mark E. Davis for the opportunity to work in his research group. I am grateful for his support and encouragement, and it was a privilege to work with him.

In the M.E. Davis group, I would like to thank former lab member, Mark Deimund, who helped me get started with experiments and was instrumental in training me. I collaborated with both Mark Deimund and John Birmingham on the MTO project and would like to thank them for their work with reaction testing and TPD experiments. I'd like to thank former graduate student, Yasho, who performed the initial steaming experiments that eventually lead to my thesis work. I would also like to thank Joel, Michiel, Marat, Kramer, Ben and Josh for their assistance throughout the past four years and for helpful suggestions and discussions.

I am grateful to the Dow Chemical Company for generously funding my thesis work. I would like to thank Drs. Andrzej Malek, Yu Liu and Jonathan Lunn at Dow for their time, helpful suggestions and feedback.

I would like to thank Profs. Jay Labinger, Richard Flagan and George Rossman for taking their time to be on my thesis committee.

In the broader Caltech community, I would like to thank Dr. Sonjong Hwang and Magnus at the solid state NMR facility for their help with NMR experiments and Dr. Chi Ma for his help at the GPS SEM facility. I'd like to thank Kathy Bubash and Martha

Hepworth for their help with administrative tasks as well as other Caltech staff including Rick, Steve, Suresh and Memo who provided valuable assistance.

I would like to thank the professors at MIT who taught me and helped me in applying to graduate school. I would especially like to thank Prof. Yuriy Roman, Yuran and William, who first introduced me to catalysis with zeolites.

Finally I would like to thank the friends I made at Caltech, especially Yong and Camille for their friendship and brunch company. Last but not least, I would like to thank my parents who have always supported me and for always being there to listen.

ABSTRACT

Light olefins, ethylene and propylene, are two of the highest produced petrochemicals globally. The methanol-to-olefins (MTO) reaction is a promising route for making these chemicals from non-petroleum feedstocks such as natural gas and coal that has been successfully commercialized. The catalysts employed for this reaction are typically microporous molecular sieves with Brønsted acidity, *e.g.*, zeolites and silicoaluminophosphates, that generally require costly organic structure directing agents (OSDAs) to synthesize.

This thesis explores an alternative, low cost method for synthesizing small pore zeolite catalysts for the MTO reaction without the use of OSDAs. Small pore zeolites are first synthesized in the absence of OSDAs. The resulting high-aluminum materials are then converted into useful catalysts via high temperature (500-800°C) steam treatments that extract a portion of the framework aluminum, thereby modifying the acid site concentration, pore structure and catalytic behavior of the materials. This synthesis method is demonstrated on three small pore zeolite structures that are prepared without using OSDAs: CHA, RHO and KFI. In the as-synthesized forms, these materials deactivate rapidly when evaluated as catalysts for the MTO reaction due to their high aluminum contents. Upon steam treatment, however, improved catalyst lifetimes and olefin selectivities are observed that are attributed to a decrease in the total Brønsted acid site concentration and the creation of mesopores that facilitate transport of reactants and products.

Improvements in the activity were observed for all three of the zeolites chosen for investigation with CHA-type zeolites performing best, though differences in olefin selectivities were observed. Poisoning of acid sites located in the mesopores and on external surface of the steamed zeolites did not change the observed product distribution, suggesting that these differences do not arise from secondary reactions of olefins and instead may be attributed to differences in the pore structures.

Overall, the successful demonstration of this catalyst preparation method on three different zeolite structures suggests that it may be a useful route for converting any small pore zeolite that can be synthesized without using OSDAs into catalysts that may be useful for reactions like MTO.

PUBLISHED CONTENT AND CONTRIBUTIONS

Ji, Y.; Deimund, M.A.; Bhawe, Y.; Davis, M.E. Organic-free synthesis of CHA-type zeolite catalysts for the methanol-to-olefins reaction. *ACS Catal.* **2015**, *5*, 4456-4465. doi: 10.1021/acscatal.5b00404.

Y.J. participated in the conception of the project, synthesized and characterized the materials, prepared the data, and participated in the writing of the manuscript.

Ji, Y.; Birmingham, J.; Deimund, M.A.; Davis, M.E. Steam-dealuminated, OSDA-free RHO and KFI-type zeolites as catalysts for the methanol-to-olefins reaction. *Micropor. Mesopor. Mater.* **2016**, *232*, 126-137. doi:10.1016/j.micromeso.2016.06.012.

Y.J. participated in the conception of the project, synthesized and characterized the materials, prepared the data, and participated in the writing of the manuscript.

TABLE OF CONTENTS

1.	Introduction and Thesis Overview.....	1
1.1.	Thesis Overview	1
1.2.	Introduction to Microporous Molecular Sieves	3
1.3.	Introduction to Methanol-to-Olefins and Motivation	7
1.4.	References	14
2.	OSDA-free synthesis of CHA-type zeolite catalysts for methanol-to-olefins.....	19
2.1.	Abstract	19
2.2.	Introduction.....	20
2.3.	Experimental Section.....	23
2.4.	Results and Discussion	29
2.5.	Conclusions.....	48
2.6.	Acknowledgements.....	49
2.7.	References	50
2.8.	Supporting Information for Chapter 2.....	54
3.	OSDA-free synthesis of RHO and KFI-type zeolite catalysts for methanol-to-olefins	67
3.1.	Abstract	67
3.2.	Introduction.....	68
3.3.	Experimental Section.....	70
3.4.	Results and Discussion	74
3.5.	Conclusions.....	92
3.6.	References	93
3.7.	Supporting Information for Chapter 3.....	95
4.	Role of acid sites internal vs. external to 8MR cages of steamed 8MR zeolites	99
4.1.	Abstract	99
4.2.	Introduction.....	100
4.3.	Experimental Section.....	102

4.4.	Results and Discussion	106
4.5.	Conclusions	116
4.6.	References	117
4.7.	Supporting Information for Chapter 4	121
5.	Conclusion and Future Directions for OSDA-free synthesis of 8MR zeolite catalysts for MTO	126
5.1.	Conclusions	126
5.2.	Recommended Future Work	129
5.3.	References	131
A.	Microporous zincosilicate molecular sieves as catalysts for propane dehydrogenation	132
A.1	Abstract	132
A.2	Introduction	132
A.3	Experimental Section	136
A.4	Results and Discussion	142
A.5	Conclusions and Recommended Future Work	157
A.6	References	158
A.7	Supporting Information for Appendix	161

LIST OF FIGURES

Figure 1-1. Chemical structure of (A) zeolite and (B) SAPO molecular sieve with Brønsted acidity	4
Figure 1-2. Types of shape selectivity ¹	5
Figure 1-3. General schematic for the hydrocarbon pool mechanism	8
Figure 1-4. Proposed mechanism for steam dealumination of zeolite framework	10
Figure 1-5. MTO reaction data for unsteamed SSZ-13 with Si/Al=5	11
Figure 1-6. MTO reaction data for SSZ-13 with Si/Al=5 steamed for 24 h at 750°	11
Figure 2-1. Powder XRD patterns of the as-synthesized CHA, CHA samples steamed at 500°C, 600°C and 700°C with water saturator at 80°C, and the 600°C steamed and acid-washed CHA (bottom to top).....	29
Figure 2-2. ²⁷ Al MAS NMR spectra of the as-synthesized CHA, the CHA samples steamed at 500°C, 600°C and 700°C with water saturator at 80°C, and the 600°C steamed and acid-washed CHA (bottom to top).....	31
Figure 2-3. ²⁹ Si MAS NMR spectra of the as-synthesized CHA, the CHA samples steamed at 500°C, 600°C and 700°C with water saturator at 80°C, and the 600°C steamed and acid-washed CHA (bottom to top).....	32
Figure 2-4. Ar physisorption isotherms of the as-synthesized and 500°C -700°C steamed CHA samples, and 600°C steamed and acid-washed CHA: (A) full isotherms, (B) normalized adsorption isotherms plotted on a semi-logarithmic scale and (C) NLDFT pore size distributions plotted on a semi-logarithmic scale	34
Figure 2-5. Powder XRD patterns of CHA samples steamed at 600°C with varying partial pressures of steam	37
Figure 2-6. ²⁷ Al MAS NMR spectra of CHA samples steamed at 600°C with varying partial pressures of steam	38
Figure 2-7. ²⁹ Si MAS NMR spectra of CHA samples steamed at 600°C in order of increasing steam partial pressures (bottom to top).	38

Figure 2-8. Ar physisorption isotherms of the as-synthesized and 600°C steamed CHA samples under varying steam partial pressures: (A) full isotherms, (B) normalized adsorption isotherms plotted on a semi-logarithmic scale and (C) NLDFT pore size distributions plotted on a semi-logarithmic scale	40
Figure 2-9. Representative MTO reaction data obtained at 400°C for: (A) unsteamed H-CHA, (B) 500°C steamed CHA, (C) 600°C steamed CHA, (D) 700°C steamed CHA, (E) 600°C steamed and acid washed CHA, and (F) SAPO-34	44
Figure 2-10. Representative MTO reaction data for 600°C steamed CHA (CHA-S600B80) obtained at reaction temperatures of (A) 350°C, (B) 400°C, (C) 450°C and (D) 600°C steamed and acid-washed CHA (CHA S600B80A) at a reaction temperature of 450°C	47
Figure 2-11. MTO reaction data for fresh (unsteamed) H-SSZ-13 Si/Al=5	54
Figure 2-12. MTO reaction data for steamed H-SSZ-13 Si/Al=5	55
Figure 2-13. ^{27}Al MAS NMR of as-synthesized K-CHA.....	56
Figure 2-14. Powder XRD patterns of unsteamed NH_4NaY and NH_4NaY samples steamed for 3 h at 550°C in order of increasing steam partial pressure (bottom to top).	59
Figure 2-15. Powder XRD patterns of NH_4NaY samples steamed for 3 h at 650°C in order of increasing steam partial pressure (bottom to top).	60
Figure 2-16. ^{27}Al NMR spectra of unsteamed NH_4NaY and NH_4NaY samples steamed for 3 h at 550°C in order of increasing steam partial pressure (bottom to top).	60
Figure 2-17. ^{27}Al NMR spectra of NH_4NaY samples steamed for 3 h at 650°C in order of increasing steam partial pressure (bottom to top).....	61
Figure 2-18. Powder XRD patterns of $\text{NH}_4\text{Na-Y}$ samples steamed for 8 h at 800°C in order of increasing steam partial pressure (bottom to top)	62
Figure 2-19. ^{27}Al MAS NMR of $\text{NH}_4\text{Na-Y}$ samples steamed for 8 h at 800°C in order of increasing steam partial pressure (bottom to top).....	62
Figure 2-20. Powder XRD patterns of CHA samples steamed for 3 h at 500°C in order of increasing steam partial pressure (bottom to top).....	63
Figure 2-21. ^{27}Al MAS NMR of CHA samples steamed for 3 h at 500°C in order of increasing steam partial pressure (bottom to top).....	64

Figure 2-22. MTO reaction data obtained at 400°C for 600°C steamed CHA during the initial reaction run	65
Figure 2-23. MTO reaction data obtained at 400°C for 600°C steamed CHA after regeneration of spent catalyst.....	65
Figure 2-24. MTO reaction data obtained at 450°C for 600°C steamed and acid washed CHA during the initial reaction test.....	66
Figure 2-25. MTO reaction data obtained at 450°C for 600°C steamed and acid washed CHA after regeneration of spent catalyst	66
Figure 3-1. Powder XRD patterns of as-synthesized and 600, 700 and 800°C steamed RHO (bottom to top).....	74
Figure 3-2. Powder XRD patterns of as-synthesized and 600, 700 and 800°C steamed KFI (bottom to top).....	75
Figure 3-3. ^{27}Al NMR spectra of as-synthesized and 600-800°C steamed RHO (bottom to top). * denotes spinning sideband.....	76
Figure 3-4. ^{27}Al NMR spectra of as-synthesized and 600-700°C steamed KFI (bottom to top). * denotes spinning sideband.....	76
Figure 3-5. ^{29}Si NMR spectra of as-synthesized and 600-800°C steamed RHO (bottom to top).....	77
Figure 3-6. ^{29}Si NMR spectra of as-synthesized and 600-800°C steamed RHO (bottom to top).....	77
Figure 3-7. (A) Ar physisorption isotherms of the as-synthesized and steamed RHO samples, (B) adsorption isotherms in the micropore filling region and (C) NLDFT pore size distributions plotted on a semi-logarithmic scale	79
Figure 3-8. (A) Ar physisorption isotherms of the as-synthesized and steamed KFI samples, (B) adsorption isotherms in the micropore filling region and (C) NLDFT pore size distributions plotted on a semi-logarithmic scale	80
Figure 3-9. Powder XRD patterns of RHO steamed at 800C under increasing steam partial pressures (bottom to top)	83
Figure 3-10. ^{27}Al NMR spectra of RHO steamed at 800°C under increasing steam partial pressures (bottom to top)	83

Figure 3-11. ^{31}Si NMR spectra of RHO steamed at 800°C under increasing steam partial pressures (bottom to top)	84
Figure 3-12. Ar physisorption isotherms of the 800°C steamed RHO samples under varying steam partial pressures (A) full isotherms, (B) adsorption isotherms plotted on a log scale and (C) NLDFT pore size distributions.....	85
Figure 3-13. MTO reaction data obtained at 400°C for (A) as-synthesized, (B) 600°C steamed, (C) 700°C steamed and (D) 800°C steamed RHO samples.....	88
Figure 3-14. MTO reaction data obtained at 400°C for (A) as-synthesized, (B) 600°C steamed and (C) 700°C steamed KFI samples	89
Figure 3-15. MTO reaction data for RHOS800B80 obtained at reaction temperatures of (A) 350°C, (B) 400°C and (C) 450°C	91
Figure 3-16. Powder XRD patterns for (A) 700°C steamed RHO and 700°C steamed RHO after acid washing with (B) 0.1 N HCl or (C) 1 N HCl for 2 h at 100°C	95
Figure 3-17. ^{27}Al MAS NMR for (A) 700°C steamed RHO and 700°C steamed RHO after acid washing with (B) 0.1 N HCl or (C) 1 N HCl for 2 h at 100°C.....	96
Figure 3-18. Powder XRD patterns for (A) 800°C steamed RHO and 800°C steamed RHO after acid washing with (B) 0.1 N HCl or (C) 1 N HCl for 2 h at 100°C	96
Figure 3-19. ^{27}Al MAS NMR for (A) 800°C steamed RHO and 800°C steamed RHO after acid washing with (B) 0.1 N HCl or (C) 1 N HCl for 2 h at 100°C.....	97
Figure 3-20. Powder XRD patterns for (A) 700°C steamed KFI and (B) 700°C steamed and acid washed KFI.....	97
Figure 3-21. ^{27}Al MAS NMR for (A) 700°C steamed KFI and (B) 700°C steamed and acid washed KFI.	98
Figure 4-1. ^{31}P MAS NMR of steamed and phosphite-treated zeolites	108
Figure 4-2. ^{27}Al MAS NMR spectra of the steamed zeolites before and after phosphite treatment.....	109
Figure 4-3. <i>i</i> -Propylamine TPD for steamed and phosphite-treated zeolite samples.....	111
Figure 4-4. MTO reaction data for steamed zeolites before and after phosphite treatment.....	114

Figure 4-5. ^{31}P NMR spectra of trimethylphosphite-exchanged and calcined H-ZSM-5 (A) hydrated and (B) dehydrated	122
Figure 4-6. ^{27}Al NMR spectra of (A) H-ZSM-5 and (B) trimethylphosphite-exchanged and calcined H-ZSM-5	122
Figure 4-7. <i>i</i> -Propylamine TPDs of (A) H-MFI and (B) H-MFI after trimethylphosphite treatment.....	123
Figure 4-8. Powder XRD patterns of NH_4 -exchanged, steamed and phosphite-treated CHA	124
Figure 4-9. Powder XRD patterns of NH_4 -exchanged, steamed and phosphite-treated RHO	124
Figure 4-10. Powder XRD patterns of NH_4 -exchanged, steamed and phosphite-treated KFI	125
Figure 4-11. ^{31}P NMR spectra of trimethylphosphite-treated samples post MTO reaction: (A) CHA-S600-P, (B) RHO-S800-P and (C) KFI-S700-P	125
Figure A-1. Reaction data for (A) Pt/Zn-MFI and (B) Zn-MFI- NH_4	144
Figure A-2. Reaction data for Zn/ SiO_2	145
Figure A-3. Reaction data for (A) Pt/CIT-6A, (B) CIT-6A- NH_4 , (C) CIT-6A-Zn and (D) pure silica BEA.	146
Figure A-4. Reaction data for CIT-6C- NH_4 tested at a propane WHSV of (A) 2.2 h^{-1} and (B) 17.6 h^{-1}	148
Figure A-5. Proposed framework zinc sites in microporous zincosilicates	149
Figure A-6. Reaction data for (A) CIT-6A-C, (B) CIT-6A-Li, (C) CIT-6A- $\text{N}(\text{CH}_3)_4$, (D) CIT-6B- $\text{N}(\text{CH}_3)_4$ -Li,	150
Figure A-7. Reaction data for (A) CIT-6B- NH_4 , (B) Ni/CIT-6B-0.5, (C) CIT-6C- NH_4 and (D) Ni/CIT-6C-2.5	153
Figure A-8. Reaction data for CIT-6C- NH_4 samples (A) after the standard in-situ pre-treatment and (B) after in-situ pre-treatment for platinum-impregnated samples	154
Figure A-9. Reaction data for (A) VPI-8-C and (B) VPI-8- NH_4	156
Figure A-10. Reaction data for CIT-6B-Li	161

Figure A-11. Reaction data for CIT-6B-N(CH ₃) ₄	xv 162
--	-----------

LIST OF TABLES

Table 1-1. Zeolite frameworks studied and their pore dimensions	13
Table 2-1. Summary of steaming conditions, Si/Al ratios and acid site concentrations.....	25
Table 2-2. Micropore volumes of the as-synthesized and steamed CHA	33
Table 2-3. Maximum combined C ₂ -C ₃ olefin selectivities near complete conversion, and deactivation times of catalysts tested.....	43
Table 2-4. Summary of zeolite Y and additional CHA steaming conditions.....	57
Table 3-1. Summary of RHO and KFI steaming conditions and Si/Al ratios.....	71
Table 3-2. Micropore volumes of RHO and KFI samples	78
Table 3-3. Maximum combined C ₂ -C ₃ olefin selectivities near complete conversion, and deactivation times of RHO and KFI catalysts tested.....	86
Table 3-4. Summary of acid washing treatments for steamed RHO and KFI samples and bulk Si/Al Ratios	95
Table 4-1 Si/Al and P/Al ratios of phosphite-treated sample and their estimated tetrahedral / penta-coordinated / octahedral Al (Al _T /Al _P /Al _O) ratios from ²⁷ Al NMR	106
Table 4-2. Summary of MTO reaction data for steamed zeolites before and after trimethylphosphite treatment	113
Table A-1. Summary of catalyst treatments and Si/Zn ratios.....	142
Table A-2. Reaction data at specific time points for Zn-MFI and CIT-6 samples. Reaction conditions: 540°C, 4:1 (mol/mol) propane:inert, 2.2 h ⁻¹ WHSV and 0.4 gcat. unless otherwise specified.....	143

1. Introduction and Thesis Overview

1.1. Thesis Overview

This thesis covers a project that I worked on in Professor Mark E. Davis's group at Caltech investigating the synthesis of small pore zeolite catalysts for the methanol-to-olefins (MTO) reaction without using organic structure directing agents (OSDAs). I also worked on a second project investigating zincosilicate molecular sieves as catalysts for propane dehydrogenation that is included in the Appendix. The end goal of both projects was finding lower cost catalysts that may be useful for obtaining light olefins that are currently in high demand.

Chapter 1 of this thesis will provide a brief introduction to zeolites and molecular sieves, the background and motivation for MTO, the objectives for the project, and the general approach we took in attempting to synthesize catalysts for the reaction without using OSDAs. In brief, this method involved first synthesizing the zeolites in the absence of OSDAs and then converting them into useful catalysts via steam dealumination treatments. We began the project by demonstrating the effectiveness of the preparation method on CHA-type zeolites that were prepared in the absence of OSDAs and post-synthetically dealuminated via steam and acid treatments. The synthesis, characterizations and reaction testing results with CHA are covered in Chapter 2. The success with CHA suggested that the preparation method was effective for other zeolite structures, and thus Chapter 3 covers the results obtained with two other zeolites, RHO and KFI. While the

dealumination method was effective on all three zeolites studied here, the reaction profiles for the three materials revealed differences in their product selectivities. This result led us to hypothesize that secondary reactions may be occurring in the mesopores and/or surface acid sites in the steamed zeolites. We probed the origins of the differences in the product distributions by selectively poisoning the acid sites located external to the 8MR cages and found that secondary reactions do not contribute significantly to the product distributions observed, suggesting that the differences in product selectivities arise from differences in the zeolite cage structures. This study is covered in Chapter 4. Chapter 5 provides a summary of the methanol-to-olefins project and recommendations for future work. This project was performed in collaboration with Mark Deimund and John Birmingham, who performed the reaction testing and TPD experiments that are presented in this work.

Finally, the Appendix details the project investigating microporous zincosilicate molecular sieves as catalysts for propane dehydrogenation. Based on recent reports that single site Lewis acid catalysts are highly selective for propane dehydrogenation (without the addition of platinum that is commonly used in alkane dehydrogenation catalysts), we screened several microporous zincosilicate molecular sieves (silica-based molecular sieves with isomorphic substitution of T-atoms by Zn^{2+} centers) as direct catalysts for propane dehydrogenation. It was found that zincosilicate CIT-6 and Zn-MFI were active for dehydrogenation but less stable compared to standard supported platinum catalysts. Further investigation was conducted to understand the type of zinc sites that are responsible for the catalytic activity and to improve the stability of the material.

1.2. Introduction to Microporous Molecular Sieves

Microporous molecular sieves are porous crystalline materials whose pore diameters are less than 2 nm. The frameworks of these materials are composed of oxide tetrahedra (TO_4) linked together via shared oxygen bridges so that each oxygen atom is shared between two tetrahedra. In a pure silica (SiO_4) material, the framework is neutral in charge as Si is tetravalent. Substitution of AlO_4 units in the framework of a pure silica material generates a negative charge (aluminum is trivalent), that requires an extra-framework cation to maintain a net neutral charge. Such materials composed of only SiO_4 and AlO_4 units are aluminosilicates, or zeolites. The framework charge can be balanced by inorganic cations (e.g., alkali or alkaline earth cations), organic cations, ammonium or protons. When the charge-balancing species are protons (Figure 1-1A), Brønsted acid sites are generated that can be useful in catalysis applications requiring Brønsted acidity. Besides a charge-balancing cation, water is also typically found in the pores. These species are free to diffuse through the pores, and thus ion exchange and reversible hydration-dehydration can occur.

Other chemical compositions are possible besides aluminosilicates. Aluminophosphates (AlPO_4s) are constructed from alternating AlO_4 and PO_4 tetrahedra whose charges balance each other to give rise to a net neutral framework. Substitution of a PO_4 unit with a SiO_4 unit generates a negative framework charge that requires an extra-framework charge-balancing cation. These materials are known as silicoaluminophosphates (SAPOs). Like zeolites, SAPOs also possess Brønsted acidity when the charge balancing

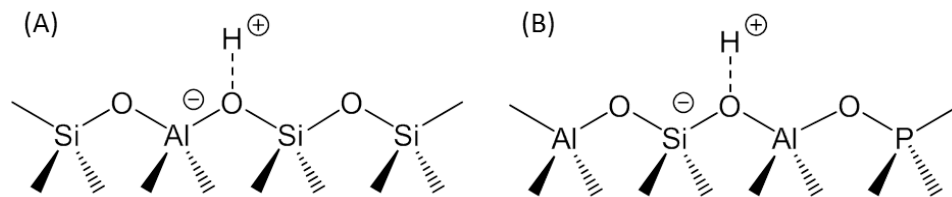


Figure 1-1. Chemical structure of (A) zeolite and (B) SAPO molecular sieve with Brønsted acidity

cations are protons (Figure 1-1B). Lewis acidic microporous materials can also be generated via substitution of isolated tetravalent metal atoms (such as Sn, Ti, Zr and Hf) into tetrahedral positions in pure silica frameworks.

The tetrahedra described above are the basic building units of the zeolite framework that consists of a system of channels and cages. Because the T-O-T angle in the tetrahedra described above is relatively flexible, a large variety of framework structures can be constructed from these units. There are currently more than 200 recognized frameworks for microporous molecular sieves. Each framework is designated by a three letter code assigned by the International Zeolite Association (IZA) structure commission.

Frameworks are typically classified according to the size of the pores that allow diffusion of guest molecules. The smallest pores that allow molecules larger than water to diffuse through are pores circumscribed by 8 tetrahedral atoms (8 membered ring or 8MR) and are typically 0.35 to 0.45 nm in diameter. Frameworks with pores composed of 10, 12 and 14 tetrahedral atoms (10MR, 12MR and 14MR, respectively) also exist. These pores may extend in one, two or all three dimensions.

Their uniform pore sizes that are on the order of the size of small molecules give zeolites and other microporous molecular sieves unique molecular sieving properties. These properties are particularly interesting for catalysis applications. If catalytic sites are located within the pores or cages, only molecules of a certain size may access these sites. Figure 1-2 shows the types of shape selectivity that can arise within the pore structure. Notably, many frameworks contain cages or channel intersections where the internal space is larger than the pores leading to them. Thus, bulky transition states or reactive intermediates may form inside these cavities that are too large to diffuse out and thus remain stabilized inside.

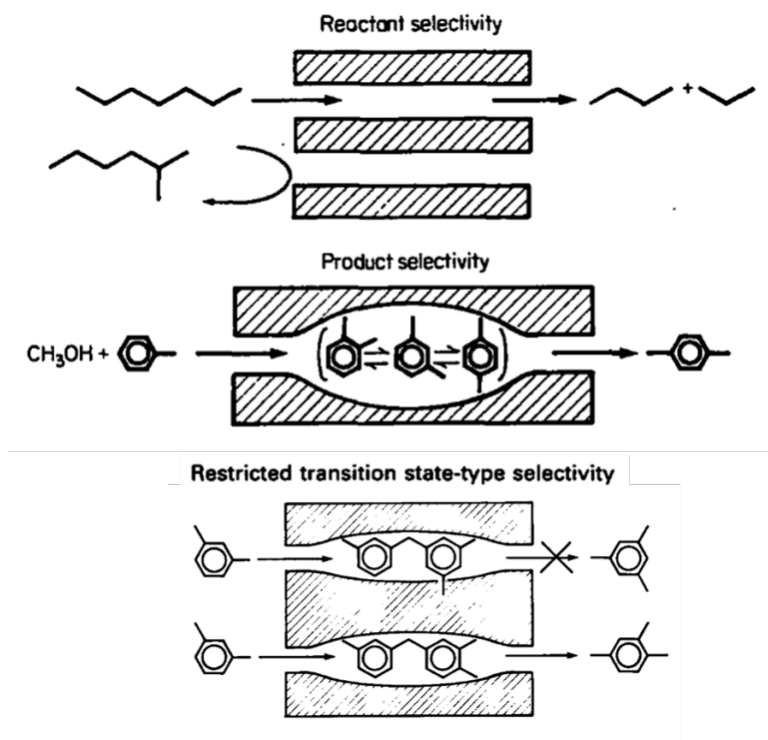


Figure 1-2. Types of shape selectivity ¹

The first synthetic zeolites were prepared hydrothermally starting from an aluminosilicate gel containing alkali hydroxides.² Because of the high concentration of alkali cations, these zeolites contain high aluminum content (typically considered to have Si/Al ratios less than 5) and are typically used as adsorbents and in ion-exchange applications. The addition of organic cations, such as alkylammonium species,^{2,3} facilitated the synthesis of higher Si/Al zeolites as the organic cations are bulkier than alkali cations and thus require less charge density in the framework. With increasing Si/Al ratio, the acidity and hydrothermal stability of the zeolite also improve, making zeolites with higher Si/Al ratios desirable for catalysis applications. SAPO molecular sieves are also interesting materials for catalysis and are typically synthesized from an alumina source, phosphoric acid and organic species, such as a quaternary ammonium.

The use of organic molecules, known as organic structure-directing agents (OSDAs), in the synthesis of zeolites and molecular sieves makes has drawbacks including high cost and require removal by combustion prior to use. The high cost of the organic molecules is often prohibitive to commercialization of new materials.⁴ One approach to lower the cost is to attempt syntheses in the absence of OSDAs by seeding the reaction mixture.⁵ However, the products typically have low yields and lower Si/Al ratios compared to their counterparts that are synthesized in the presence of OSDAs and thus limited catalysis applications in their as-synthesized forms. Another approach has been to combine a less expensive organic species that acts as a void filler with the more expensive OSDA that is required to nucleate crystallization.⁴ It has also been demonstrated that certain OSDAs can be prepared that may be recovered and used again.⁶ Finally, if low Si/Al zeolites are

synthesized in the absence of OSDAs, it may be possible to post-synthetically remove a portion of the framework aluminum to give convert them into useful catalysts.

1.3. Introduction to Methanol-to-Olefins and Motivation

Light olefins, ethylene and propylene, are two of the highest produced chemicals worldwide. Conventionally, they have been produced via cracking of naphtha. In light of growing demand for these chemicals, there has been great interest in utilizing non-petroleum feed stocks, e.g., natural gas, coal and biomass. A promising and industrially viable route that has been extensively studied is to convert these feed stocks to methanol as an intermediate followed by conversion of methanol to olefins (MTO). The MTO reaction can be carried over microporous molecular sieves with Brønsted acidity, e.g., zeolites and SAPOs. The current commercial catalyst is SAPO-34, a SAPO molecular sieve with the chabazite (CHA) framework that is currently utilized in commercial MTO plants in China.⁷ Depending upon reaction conditions, combined ethylene and propylene selectivities near 85-90% can be achieved.⁸

CHA is one of several small-pore frameworks that contain cage structures accessible via 8-ring pores, a feature that is critical to achieving high olefin selectivities in the MTO reaction.^{9,10} It is generally accepted that the reaction occurs via the hydrocarbon pool mechanism that has been supported by both experimental evidence and theoretical calculations.¹¹⁻¹⁴

Figure 1-3 shows a general schematic of the hydrocarbon pool mechanism (there is still debate on the mechanism by which the first C-C bond forms)¹³. In this reaction

scheme, polymethylbenzenes form within the cages of the zeolite and remain trapped inside the cages. These species serve as intermediates in the reaction where the side chains are continuously methylated by methanol and olefins are eliminated. In some instances, polymethylated benzene species have been observed to be confined within the zeolite cages.¹⁵⁻¹⁷ Frameworks containing 8MR cages possess the appropriate shape selectivity in that the cages have 8-ring faces that are large enough to allow small linear molecules to diffuse in and out while branched and aromatic species, including polymethylbenzene intermediates, remain trapped within the cages.

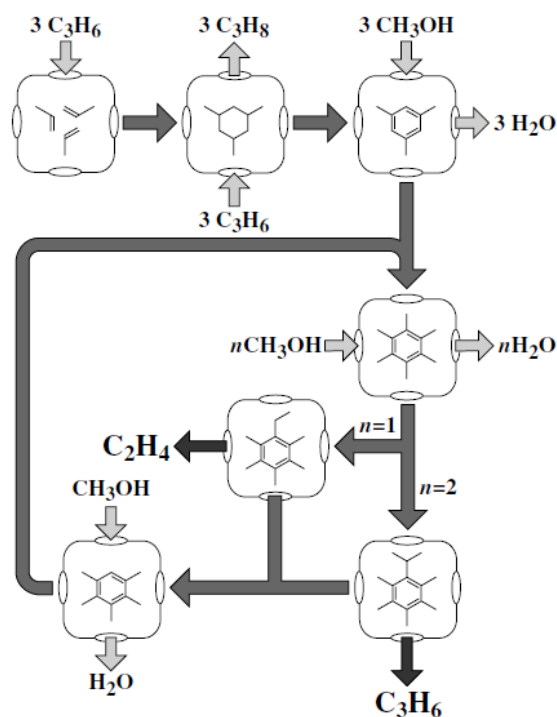


Figure 1-3. General schematic for the hydrocarbon pool mechanism¹⁸

With increasing time-on-stream, the polymethylbenzene species age into other aromatic species (such as methylnaphthalene and phenanthrene) that are the precursors for coke. Coke deposition at the active sites within the pore system leads to eventual catalyst deactivation. Depending upon the material, the activity can be regenerated by burning off the coke.

In addition to shape selectivity, the density of acid sites is also of importance for the reaction. It has been reported that faster catalyst deactivation occurs for zeolites with higher acid site densities¹⁹⁻²¹ as higher acid site densities allow molecules to undergo a greater number of successive reaction steps within the zeolite crystallites as well as facilitate bimolecular hydride transfer reactions. Thus, researchers have explored methods of synthesizing various small-pore zeolites with high Si/Al ratios using OSDAs. Among these materials, AEI²², LEV²³, AFX²³, and RTH²⁴ have shown promising results for MTO. Besides MTO, 8MR zeolites with high Si/Al ratios are also currently of interest as deNO_x catalysts.

An alternative approach to obtain high Si/Al materials is to post-synthetically remove a portion of the framework aluminum. One common dealumination strategy is treatment with high temperature steam (typically above 500°C), which preferentially hydrolyzes Si-O-Al bonds and extracts aluminum from the framework and leaves behind hydroxyl nest vacancies as well as amorphous material (Figure 1-4). It is generally believed that the amorphous material serves as a source of mobile silicon species that may heal the vacancies, and mesopores are generated in this process.^{25, 26} Amorphous debris remains

within the zeolite pores but may be removed by acid leaching. This method of steaming and acid leaching is commonly employed in the preparation of ultrastable Y zeolites that serve as fluid catalytic cracking (FCC) catalysts.²⁷ It is also possible to remove framework aluminum via acid leaching alone if the zeolite pores are large enough to accommodate removal of the dissolved species. For 8MR zeolites, the pores do not allow removal of aluminum from intact cages. However, it may be possible to remove aluminum from these materials if mesopores are created via steaming.

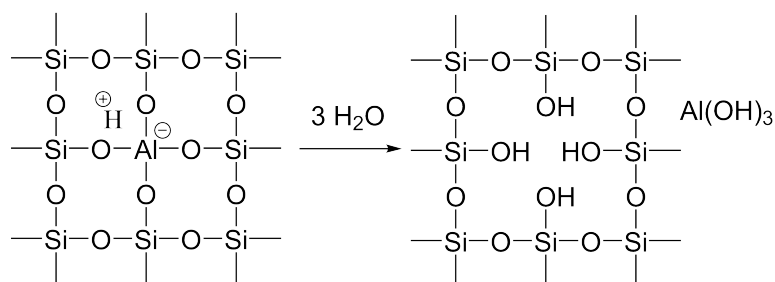


Figure 1-4. Proposed mechanism for steam dealumination of zeolite framework

Dealumination treatments increase the framework Si/Al ratio and thereby modify the catalytic behavior. This effect was demonstrated in our group using SSZ-13 for the MTO reaction. SSZ-13 is a synthetic aluminosilicate with the CHA framework (isostructural to SAPO-34) that can be prepared with a wide range of Si/Al ratios using the N,N,N-trimethyladamantylammonium OSDA.²⁸ In a previous study²⁹, it was shown that SSZ-13 synthesized at a low Si/Al ratio of 5 could be steamed to yield a catalyst with

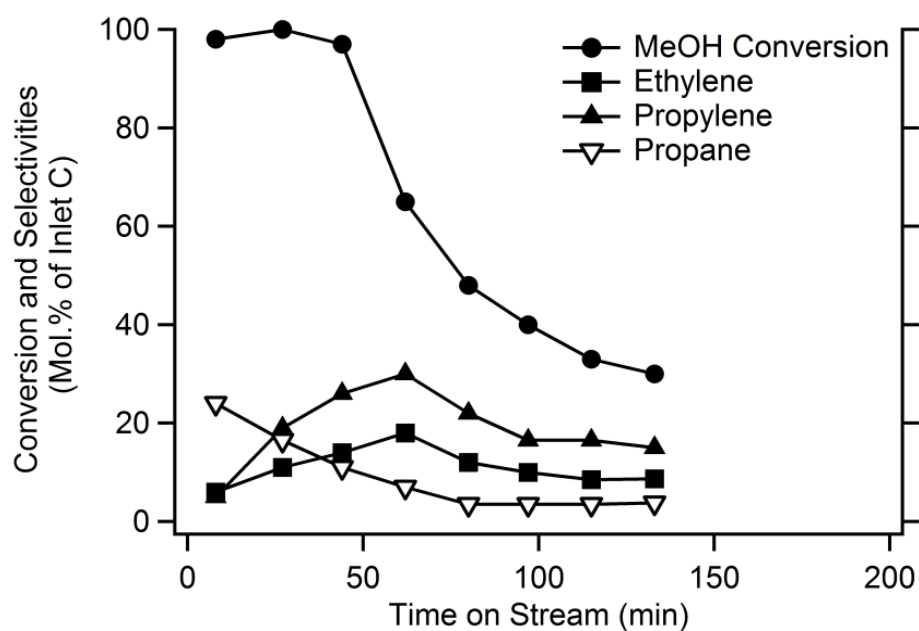


Figure 1-5. MTO reaction data for unsteamed SSZ-13 with Si/Al=5²⁹

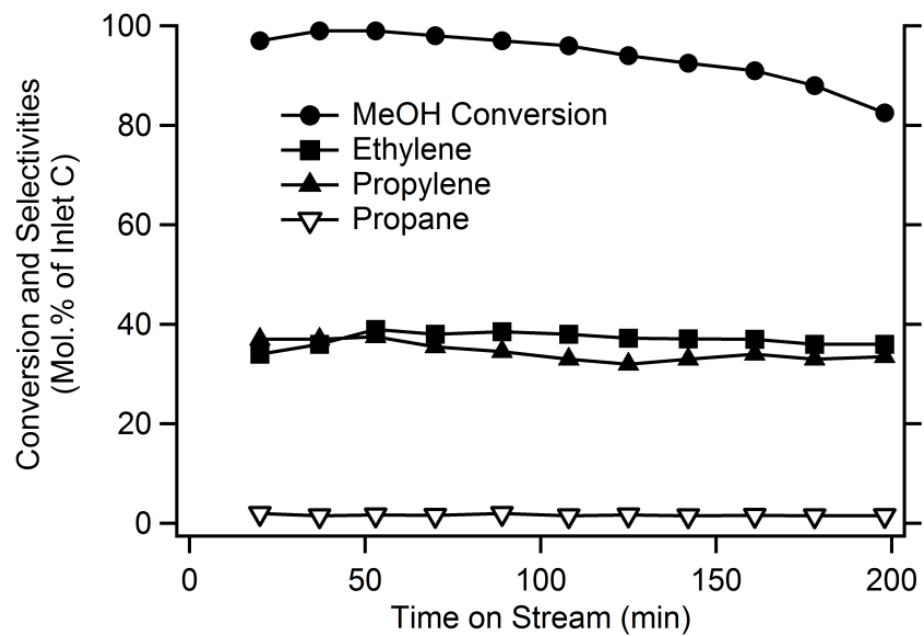


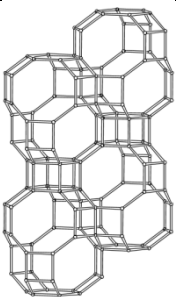
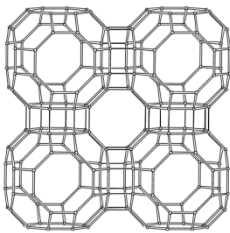
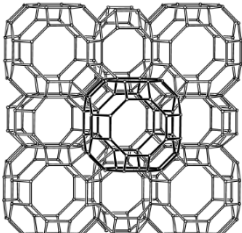
Figure 1-6. MTO reaction data for SSZ-13 with Si/Al=5 steamed for 24 h at 750°C²⁹

improved activity for MTO. While the as-synthesized catalyst deactivates rapidly (Figure 1-5), the steamed sample (Figure 1-6) shows an increased lifetime and olefin selectivities. The behavior of the steamed SSZ-13 now resembles that of an SSZ-13 with a higher Si/Al ratio. Similar improvements have been reported by Cartlidge et al.³⁰, who prepared CHA-type zeolites at a Si/Al ratios greater than 2.5 using the hexamethylenetetramine OSDA and dealuminated the samples by steam and acid treatments. These reaction data suggested that it may be possible to modify the catalytic behavior of zeolites synthesized with low Si/Al ratios via dealumination treatments to convert them into useful catalysts for MTO. Several small pore zeolites can be synthesized without using OSDAs and consequently have low Si/Al ratios ($\text{Si/Al} < 5$). These materials have not been explored extensively for MTO because of their high aluminum contents.

The objective for this project was to synthesize 8MR zeolite catalysts for MTO without using OSDAs. We approached this problem by first synthesizing the zeolites in the absence of OSDAs and then post-synthetically extracting the aluminum via steam and, in some instances, acid leaching treatments. This method was first demonstrated to be effective on CHA-type zeolites that were prepared without an OSDA. We then applied this method on two other 8MR zeolites, RHO and KFI, to show that this method is effective on any 8MR zeolite that can be prepared without an OSDA to create an useful MTO catalyst. Table 1-1 provides the cage structures and pore dimensions of the zeolites studied. These structures contain cage structures with three-dimensional channel systems and can be readily synthesized on a large scale without using OSDAs. CHA-type zeolites can be synthesized via an interzeolite conversion from Y zeolites (faujasite) in the presence of

potassium hydroxide.³¹ CHA obtained via this method is commonly used for gas separations. RHO and KFI-type zeolites can be synthesized using alkali hydroxides.^{32, 33} These materials have been previously explored as catalysts for the synthesis of methylamines^{34, 35} but have not yet been evaluated in the as-synthesized form for MTO. The catalyst preparation method presented here provides a low-cost method for synthesizing small pore zeolite catalysts that may be useful for reactions like MTO and enables the exploration of new zeolite structures that may not have been previously considered for MTO because of their high aluminum content in the as-synthesized form.

Table 1-1. Zeolite frameworks studied and their pore dimensions

	CHA	RHO	KFI
Framework structure^a			
Pore diameter^a	3.8 Å	3.6 Å	3.9 Å
Maximum diameter of a sphere that can be included within cage^a	7.37 Å	10.43 Å	10.67 Å
Maximum diameter of a sphere that can diffuse along a-,b- and c-axis^a	a: 3.72 Å b: 3.72 Å c: 3.72 Å	a: 4.06 Å b: 4.06 Å c: 4.06 Å	a: 4.04 Å b: 4.04 Å c: 4.04 Å

^a All data from IZA online database (Ref 36)

1.4. References

- (1) Csicsery, S.M. Shape-selective catalysis in zeolites. *Zeolites* **1984**, 4, 3, 202-213.
- (2) Cundy, C.S.; Cox, P.A. The hydrothermal synthesis of zeolites: history and development from the earliest days to the present time. *Chem. Rev.* **2003**, 103, 663-702.
- (3) Barrer, R.M.; Denny, P.J. Hydrothermal chemistry of the silicates. Part IX. Nitrogenous aluminosilicates. *J. Chem. Soc.* **1961**, 201, 971-982.
- (4) Zones, S.I., Translating new materials discoveries in zeolite research to commercial manufacture. *Micropor. Mesopor. Mater.* **2011**, 144, 1-8.
- (5) Iyoki, K.; Itabashi, K.; Okubo, T. Progress in seed-assisted synthesis of zeolites without using organic structure-directing agents. *Micropor. Mesopor. Mater.* **2014**, 189, 22-30.
- (6) Lee, H.; Zones, S.I.; Davis, M.E. A combustion-free methodology for synthesizing zeolites and zeolite-like materials. *Nature* **2003**, 425, 385-388.
- (7) Liu, Z.; Sun, C.; Wang, G.; Wang, Q.; Cai, G. New progress in R&D of lower olefin synthesis. *Fuel Process. Tech.* **2000**, 62, 161-172.
- (8) Chen, J.Q.; Bozzano, A.; Glover, B.; Fuglerud, T.; Kvisle, S. Recent advancements in ethylene and propylene production using the UOP/Hydro MTO process. *Catal. Today* **2005**, 106, 103-107.
- (9) Wilson, S.; Barger, P. The characteristics of SAPO-34 which influence the conversion of methanol to light olefins. *Micropor. Mesopor. Mater.* **1999**, 29, 117-126.

- (10) Deimund, M.A.; Schmidt, J.E.; Davis, M.E. Effect of pore and cage size on the formation of aromatic intermediates during the Methanol-to-Olefins Reaction. *Top. Catal.* **2015**, *58*, 416-423.
- (11) Dahl, I.M.; Kolboe, S. On the reaction-mechanism for hydrocarbon formation from methanol over SAPO-34 .1. Isotopic labeling studies of the co-reaction of ethene and methanol. *J. Catal.* **1994**, *149*, 458-464.
- (12) Haw, J.F.; Song, W.; Marcus, D.M.; Nicholas, J.B. The mechanism of methanol to hydrocarbon catalysis. *Acc. Chem. Res.* **2003**, *36*, 317-326.
- (13) Stocker, M. Methanol-to-hydrocarbons: catalytic materials and their behavior. *Micropor. Mesopor. Mater.* **1999**, *29*, 3-48.
- (14) Arstad, B.; Nicholas, J.B.; Haw, J.F. Theoretical study of the methylbenzene side-chain hydrocarbon pool mechanism in methanol to olefin catalysis. *J. Am. Chem. Soc.* **2004**, *126*, 2991-3001.
- (15) Li, J.; Wei, Y.; Chen, J.; Tian, P.; Su, X.; Xu, S.; Qi, Y.; Wang, Q.; Zhou, Y.; He, Y.; Liu Z. Observation of heptamethylbenzenium cation over SAPO-type molecular sieve DNL-6 under real MTO conversion conditions. *J. Am. Chem. Soc.* **2012**, *134*, 836-839.
- (16) Xu, S.; Zheng, A.; Wei, Y.; Chen, J.; Li, J.; Chu, Y.; Zhang, M.; Wang, Q.; Zhou, Y.; Wang, J.; Deng, F.; Liu, Z. Direct observation of cyclic carbenium ions and their role in the catalytic cycle of the methanol-to-olefin reaction over chabazite zeolites. *Angew. Chem. Int. Ed.* **2013**, *52*, 11564-11568.

- (17) Bjørgen, M.; Bonino, F.; Kolboe, S.; Lillerud, K.P.; Zecchina, A.; Bordiga S. Spectroscopic evidence for a persistent benzenium cation in zeolite H-Beta. *J. Am. Chem. Soc.* **2003**, *125*, 15863-15868.
- (18) Haw, J.F.; Marcus, D.M. Well-defined (supra)molecular structures in zeolite methanol-to-olefin catalysis. *Top. Catal.* **2005**, *34*, 41-48.
- (19) Zhu, Q.J.; Kondo, J.N.; Ohnuma, R.; Kubota, Y.; Yamaguchi, M.; Tatsumi, T. The study of methanol-to-olefin over proton type aluminosilicate CHA zeolites. *Micropor. Mesopor. Mater.* **2008**, *112*, 153-161.
- (20) Dahl, I.M.; Mostad, H.; Akporiaye, D.; Wendelbo, R. Structural and chemical influences on the MTO reaction: a comparison of chabazite and SAPO-34 as MTO catalysts. *Micropor. Mesopor. Mater.* **1999**, *29*, 185-190.
- (21) Park, J.W.; Kim, S.J.; Seo, M.; Kim, S.Y.; Sugi, Y.; Seo, G. Product selectivity and catalytic deactivation of MOR zeolites with different acid site densities in methanol-to-olefin (MTO) reactions. *App. Catal. A: Gen.* **2008**, *349*, 76-85.
- (22) Dusselier, M.; Deimund, M.A.; Schmidt, J.E.; Davis, M.E. Methanol-to-olefins catalysis with hydrothermally treated zeolite SSZ-39. *ACS Catal.* **2015**, *5*, 6078-6085.
- (23) Bhawe, Y.; Moliner-Marin, M.; Lunn, J.D.; Liu, Y.; Malek, A.; Davis M.E. Effect of cage size on the selective conversion of methanol to light olefins. *ACS Catal.* **2012**, *2*, 2490-2495.
- (24) Schmidt, J.E.; Deimund, M.A.; Xie, D.; Davis, M.E. Synthesis of RTH-type zeolites using a diverse library of imidazolium cations. *Chem. Mater.* **2015**, *27*, 3756-3762.

- (25) van Donk, S.; Janssen, A.H.; Bitter, J.H.; de Jong, K.P. Generation, characterization, and impact of mesopores in zeolite catalysts. *Catal. Rev.* **2003**, *45*, 297-319.
- (26) Scherzer, J., The Preparation and Characterization of Aluminum-Deficient Zeolites, in *Catalytic Materials: Relationship Between Structure and Reactivity*. 1984, American Chemical Society, 157-200.
- (27) Lutz, W. Zeolite Y: Synthesis, Modification, and Properties - A Case Revisited. *Advances in Materials Science and Engineering* **2014**, *20*.
- (28) Zones, S.I. Zeolite SSZ-13 and its method of preparation, U.S. Patent 4,544,538, October 1, 1985.
- (29) Bhawe, Y., "Structure-Property Relationships for Zeolite Catalyzed Conversion of Methanol to Light Olefins." California Institute of Technology. Pasadena, CA, 2012. PhD Thesis Seminar.
- (30) Carlidge, S.; Patel, R. Hydrothermally stable chabazites for the selective preparation of olefins from methanol, in *Zeolites: Facts, Figures, Future*, P.A. Jacobs and R.A. vanSanten, Editors. 1989, Elsevier: Amsterdam. p. 1151-1161.
- (31) Bourgogne, M.; Guth, J.L.; Wey, R. U.S. Patent 4,503,024, March 5, 1985.
- (32) Robson, H.E. Zeolite RHO, U.S. Patent 3,904,738, September 9, 1975.
- (33) Robson, H.E. Method for preparing a small pore synthetic zeolite, U.S. Patent 3,720,753, February 22, 1971.
- (34) Shannon, R.D.; Keane, M.; Abrams, L.; Staley, R.H.; Gier, T.E.; Sonnichsen, G.C. Selective synthesis of dimethylamine over small-pore zeolites. *J. Catal.* **1989**, *115*, 79-85.

- (35) Corbin, D.R.; Keane, M.; Abrams, L.; Farlee, R.D.; Bierstedt, P.E.; Bein, T.

Designing zeolite catalysts for shape-selective reactions: Chemical modification of surfaces for improved selectivity to dimethylamine in synthesis from methanol and ammonia. *J. Catal.* **1990**, *124*, 268-280.

- (36) Baerlocher, C.; McCusker, L.B.; Olson, D.H. *Atlas of Zeolite Framework Types*.

6th revised ed. 2007, Amsterdam: Elsevier.

2. OSDA-free synthesis of CHA-type zeolite catalysts for methanol-to-olefins

This chapter has been published as: Y. Ji, M.A. Deimund, Y. Bhawe, M.E. Davis, Organic-free Synthesis of CHA-Type Zeolite Catalysts for the Methanol-to-Olefins Reaction, *ACS Catal.* 5, (2015) 4456-4465. doi: 10.1021/acscatal.5b00404.

2.1. Abstract

Chabazite (CHA)-type zeolites are prepared from the hydrothermal conversion of faujasite (FAU)-type zeolites, dealuminated by high-temperature steam treatments (500°C-700°C), and evaluated as catalysts for the methanol-to-olefins (MTO) reaction. The effects of temperature and partial pressure of water vapor during steaming are investigated. Powder X-ray diffraction (XRD) and Ar physisorption data show that the steam treatments cause partial structural collapse of the zeolite with the extent of degradation increasing with steaming temperature. ^{27}Al MAS NMR spectra of the steamed materials reveal the presence of tetrahedral, pentacoordinate and octahedral aluminum. NH_3 and *i*-propylamine temperature-programmed desorption (TPD) demonstrate that steaming removes Brønsted acid sites, while simultaneously introducing larger pores into the CHA materials that make the remaining acid sites more accessible. Acid washing the steamed CHA-type zeolites removes a significant portion of the extra-framework aluminum, producing an increase in the bulk Si/Al ratio as well as the adsorption volume. The proton form of the as-

synthesized CHA (Si/Al = 2.4) rapidly deactivates when tested for MTO at a reaction temperature of 400°C and atmospheric pressure. CHA samples steamed at 600°C performed the best among the samples tested, showing increased olefin selectivities as well as catalyst lifetime compared to the unsteamed CHA. Both lifetime and C₂-C₃ olefin selectivities are found to increase with increasing reaction temperature. At 450°C, CHA steamed at 600°C reached a combined C₂-C₃ olefin selectivity of 74.2% at 100% methanol conversion, with conversion remaining above 80% for more than 130 minutes of time-on-stream (TOS) before deactivating. More stable time-on-stream behavior is observed for 600°C steamed CHA that underwent acid washing; conversion above 90% for more than 200 minutes of TOS at 450°C with a maximum total C₂-C₃ olefin selectivity of 71.4% at 100% conversion.

2.2. Introduction

The methanol-to-olefins (MTO) reaction is an industrially viable route for making the light olefins, ethylene and propylene, using feedstocks other than petroleum, e.g., natural gas, coal and biomass.¹ The reaction can be carried out over solid acid catalysts such as microporous aluminosilicate² and silicoaluminophosphate (SAPO)^{3,4} molecular sieves. The industrial catalyst for the MTO reaction is SAPO-34,^{5,6} a small-pore SAPO molecular sieve with the chabazite (CHA) framework topology that is currently utilized in commercial MTO plants in China. Depending upon reaction conditions, SAPO-34 can convert methanol to ethylene and propylene at 85-90% selectivity.⁷ The high selectivity towards light olefins is attributed to the material's optimal acidity (acid site strength and density)⁸ as well as the topology of the CHA framework,^{9,10} consisting of relatively large

cavities ($8.35 \text{ \AA} \times 8.35 \text{ \AA} \times 8.23 \text{ \AA}^{11}$) that are accessible through 8-membered ring (8MR) pore openings ($3.8 \times 3.8 \text{ \AA}^{11}$). Only small linear molecules (alcohols and linear alkenes) can diffuse through the 8MR pores, while larger branched and aromatic compounds, including methylated aromatic intermediates,^{9,12} remain trapped inside the cages.

Despite its success, SAPO-34 suffers the shortcoming of requiring the use of an organic structure-directing agent (OSDA) to crystallize. Aluminosilicates (zeolites) also catalyze the reaction, but synthesizing them at high Si/Al ratios that are desirable for catalytic applications, typically requires the use of OSDAs. The high cost and environmental concerns associated with removal of the OSDA from the materials prior to use has generated considerable interest in developing OSDA-free synthesis methods. While the earliest synthetic zeolites were prepared in the absence of OSDAs, using only inorganic cations as the structure-directing species, they typically have high aluminum content ($\text{Si/Al} < 5$) and thus limited uses, particularly in applications requiring solid acidity.

CHA-type zeolites can be prepared in the absence of OSDAs, but their Si/Al ratios are too low to be of use in catalyzing reactions like MTO. However, it may be possible to remove aluminum from the framework through post-synthetic treatments, thereby modifying the acidity and catalytic behavior of the materials. Since CHA is an 8MR zeolite, the extracted aluminum cannot be removed from intact cages. However, if mesoporosity is formed during the dealumination, then it may be possible to extract the extra-framework aluminum via the larger pores. Here, we show that CHA-type zeolites

synthesized without OSDSAs can be subjected to dealumination to provide active MTO catalysts. This strategy may enable the preparation of low cost MTO catalysts. Additionally, there are a number of other framework topologies that may be interesting catalysts for the MTO reaction that have yet to be evaluated because of their low Si/Al. The dealumination strategy provided here will allow for investigation of other framework types (we are currently exploring several other zeolites, and the results will be reported at a later time).

SSZ-13¹³ is the synthetic aluminosilicate analog of SAPO 34, and can be synthesized over a wide range of Si/Al ratios using the N,N,N-trimethyladamantylammonium OSDA. While also active for converting methanol to olefins, SSZ 13 deactivates more rapidly than SAPO 34, and initially produces a significant amount of C1-C4 alkanes.^{14,15} Recently, our research group showed that an SSZ-13 synthesized with high aluminum content (Si/Al=5) could be steamed to obtain a catalyst with improved olefin selectivities and lifetime, comparable to that of an SSZ-13 with Si/Al=15. Reaction data from this study are provided in the Supporting Information (Figures 2-11 and 2-12). In a similar study, Cartledge et al.¹⁶ prepared CHA-type zeolites at Si/Al ratios of greater than 2.5 using the hexamethylenetetramine OSDA, dealuminated the samples by steam and acid treatments, and observed improved olefin selectivities.

Based on these results, we hypothesized that a dealumination strategy could be applied to aluminum-rich CHA-type zeolites prepared without the use of an OSDA to create selective catalysts for converting methanol to light olefins. CHA-type zeolite is

prepared from the hydrothermal conversion of zeolite Y (FAU), and then steamed at temperatures of 500°C, 600°C or 700°C to partially extract the framework aluminum. CHA steamed at 600°C is additionally acid washed to remove the extra-framework aluminum. The effects of the dealumination treatments on the solids are analyzed by powder X-ray diffraction (XRD), energy-dispersive X-ray spectroscopy (EDS), and Ar physisorption. Removal of aluminum from the zeolite framework is observed by ^{27}Al and ^{29}Si MAS NMR. The acid site concentrations of the samples were measured by temperature programmed desorption (TPD) using NH_3 and *i*-propylamine. The catalytic performance of the materials is evaluated by the use of the MTO reaction.

2.3. Experimental Section

2.3.1. CHA Synthesis

CHA-type zeolites were prepared from the hydrothermal conversion of zeolite Y (FAU) following the method of Bourgogne et al.¹⁷ In a typical synthesis, 238 mL of deionized water was mixed with 32.2 mL of 45 wt.% aqueous potassium hydroxide solution (Aldrich), to which 30 g of USY (Zeolyst, CBV712, $\text{SiO}_2/\text{Al}_2\text{O}_3=12$) was added. The mixture was shaken for about 30 s and heated in a sealed polypropylene vessel at 100°C for 4 days under static conditions. The solid product was recovered by centrifugation, washed with water and acetone, and dried overnight at 100°C. The as-synthesized product, that had potassium as the counter-cation (designated K-CHA), was ion-exchanged three times with 1 M aqueous ammonium nitrate solution at 90°C for 2 h at a ratio of 100 mL of liquid per gram of solid to obtain the NH_4^+ form (designated NH_4 -CHA).

2.3.2. Steaming and Acid Washing Treatments

Table 2-1 provides a summary of the steaming and acid washing treatments. Steaming was conducted under atmospheric pressure in an MTI OTF-1200X horizontal tube furnace fitted with a 3 in. ID mullite tube. $\text{NH}_4\text{-CHA}$ samples (approximately 1.2 g in a typical experiment) were loaded in ceramic calcination boats and placed in the center of the tube furnace. The furnace was ramped at $1^\circ\text{C}/\text{min}$ to the desired steaming temperature, held at temperature for 8 h, and then allowed to cool. The entire process was carried out under a flow of moist air that was created by bubbling zero-grade air at 50 cc/min through a heated water saturator (bubbler) upstream of the furnace. Samples were steamed at temperatures of 500°C , 600°C and 700°C with the bubbler held at 80°C (water saturation pressure of 47.3 kPa) and the resulting materials designated CHA-S500B80 , CHA-S600B80 and CHA-S700B80 , respectively. The effect of the partial pressure of steam was investigated by two additional steaming experiments at 600°C where the bubbler temperature was changed to 60°C and 90°C (water saturation pressures of 19.9 and 70.1 kPa, respectively). For each of the bubbler temperatures tested (60°C , 80°C and 90°C), the air was approximately 50% saturated with water vapor. A dry calcination of $\text{NH}_4\text{-CHA}$ was conducted in the same tube furnace for 8 h at 600°C ($1^\circ\text{C}/\text{min}$ ramp) under 50 cc/min of zero-grade air, and the product was designated CHA-C600 . A portion of the CHA steamed at 600°C with the bubbler held at 80°C was additionally acid washed with 0.1 N aqueous hydrochloric acid at a liquid-to-solid ratio of 100:1 (w/w) for 2 h at 100°C in a sealed vessel. The product, designated CHA-S600B80A , was recovered by filtering, washed extensively with water and dried overnight at 100°C .

Table 2-1. Summary of steaming conditions, Si/Al ratios and acid site concentrations

Entry	Sample	Steaming Conditions		Si/Al Bulk	Si/Al _T ^b	Acid Site Conc. by NH ₃ TPD [mmol/g]	Acid Site Conc. by <i>i</i> -propylamine TPD [mmol/g]
		Steaming Temp. ^a	Water Saturator Temp.				
1	CHA-S500B80	500°C	80°C	2.4	11	1.07	0.24
2	CHA-S600B80	600°C	80°C	2.4	16	0.94	0.30
3 ^c	CHA-S600B80A	600°C	80°C	7.8	12	0.80	0.39
4	CHA-S700B80	700°C	80°C	2.3	17	0.72	0.20
5	CHA-S600B90	600°C	90°C	2.5	16	0.84	0.29
6	CHA-S600B60	600°C	60°C	2.4	15	0.92	0.16
7	CHA-C600	600°C	Dry Calcination	2.7	38	0.09	0.08

^a Furnace was held at temperature for 8 h for all samples^b Calculated from ²⁷Al NMR, Al_T denotes tetrahedral Al only^c Steamed sample was acid washed with 0.1 N HCl for 2 h at 100°C

2.3.3. Characterizations

Powder X-ray diffraction (XRD) patterns were obtained on a Rigaku MiniFlex II instrument with Cu K α radiation ($\lambda=1.54184$ Å) at a sampling window of 0.01° and scan speed of 0.05°/min. Scanning electron microscopy/energy dispersive spectroscopy (SEM/EDS) was used to determine the morphology and bulk elemental composition of the materials and was conducted on a ZEISS 1550VP instrument equipped with an Oxford X-Max SDD energy dispersive X-ray spectrometer. Powder patterns were normalized to the highest intensity peak.

Solid-state ^{27}Al MAS NMR spectra were acquired on a Bruker AM 300 MHz spectrometer operated at 78.2 MHz using a 90° pulse length of 2 μs and a cycle delay time of 1 s. Samples were loaded in a 4 mm ZrO_2 rotor and spun at 12 kHz. Chemical shifts were referenced to 1 M aqueous aluminum nitrate solution. Solid-state ^{29}Si MAS NMR spectra were acquired on a Bruker Avance 200 MHz spectrometer operated at 39.78 MHz with ^1H decoupling. A 90° pulse length of 4 μs and a cycle delay time of 60 s were used for recording. Samples were loaded in a 7 mm ZrO_2 rotor and spun at 4 kHz, and chemical shifts were referenced to tetramethylsilane. Reported spectra are scaled to the same maximum intensity.

Argon physisorption was conducted on a Quantachrome Autosorb iQ instrument. Prior to adsorption measurements, samples were outgassed by heating (at a rate of $10^\circ\text{C}/\text{min}$) the sample under vacuum for 1 h at 80°C , 3 h at 120°C and 10 h at 350°C . Adsorption isotherms were collected using argon at 87.45 K using the constant dose (quasi-equilibrium) method. Micropore volumes were obtained from the adsorption branch of the isotherms using the t-plot method ($0.1 < P/P_0 < 0.3$). Pore size analyses were obtained from the adsorption branches using the non-local density functional theory (NLDFT) model provided by Micromeritics (based on model of Ar at 87 K on a zeolite with cylindrical pores).

NH_3 and *i*-propylamine TPD were performed on each ammonium-exchanged, steamed CHA sample to quantify the number and accessibility of the Brønsted acid sites present, NH_3 TPD is able to titrate essentially all acid sites both external to and within the

8MR pore system, while *i*-propylamine only accesses acid sites external to the 8MR pore system (and in areas of mesoporosity created by the steam treatment), as *i*-propylamine is too large to fit within the 8MR pores. When *i*-propylamine desorbs from a Brønsted acid site, it reacts with the site to form propylene and ammonia. The propylene desorption peak was integrated to determine the number of Brønsted acid sites accessible to *i*-propylamine.

The materials were pelletized, crushed, and sieved, with particles between 0.6 mm and 0.18 mm being retained and loaded between quartz wool beds in a continuous-flow quartz-tube reactor (part of an Altamira AMI-200 reactor). A thermocouple inserted directly into the bed monitored temperature, and a Dymaxion mass spectrometer monitored desorbing products. Once loaded, samples were heated to 150°C for 1 h at 10°C/min and then to 600°C for 1 h at 10°C/min in flowing helium (50 sccm) to remove any adsorbed species. For NH₃ TPD, samples were then cooled to 160°C, and NH₃ was dosed onto each sample. After a 6 h purge in flowing argon (50 sccm) at 50°C to remove any physisorbed NH₃, the sample was heated to 600°C at a rate of 10°C/min in 30 sccm argon while the mass spectrometer monitored desorbing products, namely $m/z = 17$ fragments corresponding to NH₃. The sample was held at 600°C for 2 h to ensure all species had fully desorbed. For *i*-propylamine TPD, after the initial heating to 600°C, samples were cooled to 50°C, and *i*-propylamine was dosed onto each sample by means of a vapor saturator. The sample was then purged in a flow of helium (50 sccm) for 6 h before heating to 600°C at 10°C/min, with the mass spectrometer monitoring the main propylene and NH₃ signals ($m/z = 41$ and 17, respectively) formed by the decomposition reaction of the *i*-propylamine at Brønsted acid sites in the sample.

2.3.4. MTO Reaction Testing

Samples used for reaction testing were approximately 200 mg of pure zeolite that had been pelletized, crushed and sieved to obtain particles between 0.6 mm and 0.18 mm. A sample was supported between glass wool beds in a tubular, continuous flow reactor. Prior to reaction, all samples were calcined in-situ under a flow of breathing-grade air, during which the temperature was ramped at 1°C/min to 150°C, held for 3 hours, then ramped at 1°C/min to 580°C and held for 12 hours. The reaction was conducted at 350°C, 400°C or 450°C with a feed of 10% methanol/inert at a WHSV of 1.3 h⁻¹. Reaction testing of unsteamed CHA was conducted on a sample in the H⁺ form (H-CHA), which was obtained by calcining the NH₄-CHA in-situ. Regeneration of spent catalysts was conducted in-situ by heating at 1°C/min from the reaction temperature to 580°C, holding for 6 h, and then cooling at 1°C/min back to the reaction temperature, all under a flow of breathing-grade air. Conversions and selectivities are computed on a carbon mole basis according to Equations 2-1 and 2-2, respectively, where n_i and $n_{c,i}$ represent the molar flow rate for species i and carbon number for species i , respectively. Carbon balances are reported based on the moles of methanol converted (Equation 2-3).

$$X_{MeOH} = \frac{n_{MeOH,in} - n_{MeOH,out}}{n_{MeOH,in}} \cdot 100\% \quad (2-1)$$

$$S_i = \frac{n_{i,out} \cdot n_{c,i}}{\sum_{i=All\ Products} n_{i,out} \cdot n_{c,i}} \cdot 100\% \quad (2-2)$$

$$Carbon\ balance = \frac{\sum_{i=All\ Products} n_{i,out} \cdot n_{c,i}}{n_{MeOH,in} - n_{MeOH,out}} \cdot 100\% \quad (2-3)$$

2.4. Results and Discussion

2.4.1. Sample Characterizations

2.4.1.1. Effect of Steaming Temperature and Acid Washing

The powder XRD patterns of the as-synthesized $\text{NH}_4\text{-CHA}$ and the CHA samples steamed at 500°C-700°C under the same steam partial pressure are shown in Figure 2-1. The baseline signal increases relative to the peaks for the steamed samples, indicating the presence of amorphous material and a loss of crystallinity upon steaming. Increasing the steaming temperature, and thus the severity of steaming, results in increasingly greater

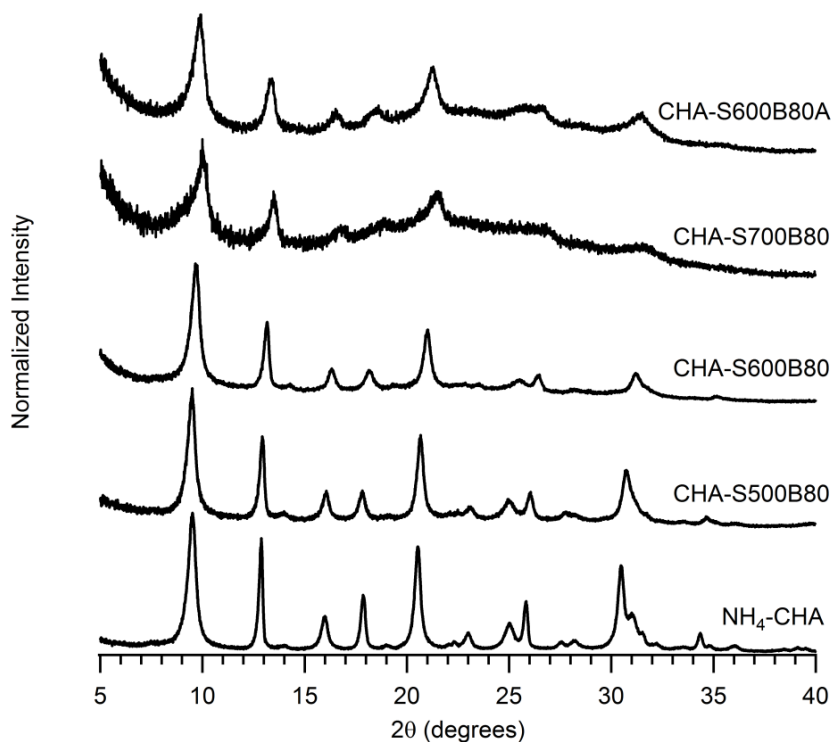


Figure 2-1. Powder XRD patterns of the as-synthesized CHA, CHA samples steamed at 500°C, 600°C and 700°C with water saturator at 80°C, and the 600°C steamed and acid-washed CHA (bottom to top)

structural degradation, with the 700°C steamed sample showing the greatest loss in crystallinity. Further, the XRD peaks are shifted to lower d-spacings for the steamed samples, which can be attributed to contractions of the unit cell due to extraction of framework aluminum. The bulk Si/Al ratios of the steamed samples (Table 2-1) are essentially the same as that of the starting CHA (Si/Al=2.4), accommodating for minor deviations that are within measurement error. Acid washing the 600°C steamed CHA sample results in additional degradation and produces an increase in the bulk Si/Al ratio from 2.4 to 7.8.

Indications that aluminum is removed from the zeolite framework after the steam and acid treatments are provided by the ^{27}Al MAS NMR spectra that are shown in Figure 2-2. The spectra of both the as-synthesized K-CHA (Supporting Information Figure 2-13) and NH_4^+ -exchanged CHA show a single sharp resonance centered at approximately 55 ppm, corresponding to tetrahedral, framework aluminum. In addition to this resonance, the spectra of the steamed samples show two additional resonances centered at approximately 30 ppm and 0 ppm that are attributed to pentacoordinated and octahedral aluminum species, respectively.

As the steaming temperature is raised from 500°C to 700°C, an increasing fraction of aluminum is converted from tetrahedral to penta- and hexacoordination (indicated by increases in the intensities of the resonances centered at 30 ppm and 0 ppm relative to the resonance centered at 55 ppm). Accordingly, the silicon to tetrahedral aluminum ($\text{Si}/\text{Al}_\text{T}$) ratios (Table 2-1), calculated from the bulk Si/Al and deconvolution of the ^{27}Al NMR,

increase with increasing steaming temperature. The intensities of the resonances associated with penta- and hexacoordinated aluminum are reduced after acid washing the 600°C steamed CHA, with nearly complete removal of the pentacoordinated aluminum species. These NMR data for the acid treated sample are consistent with the elemental analyses in that the bulk Si/Al increases after acid treatment. These results also suggest that the bulk of the higher-coordinated (above 4) aluminum is extra-framework.

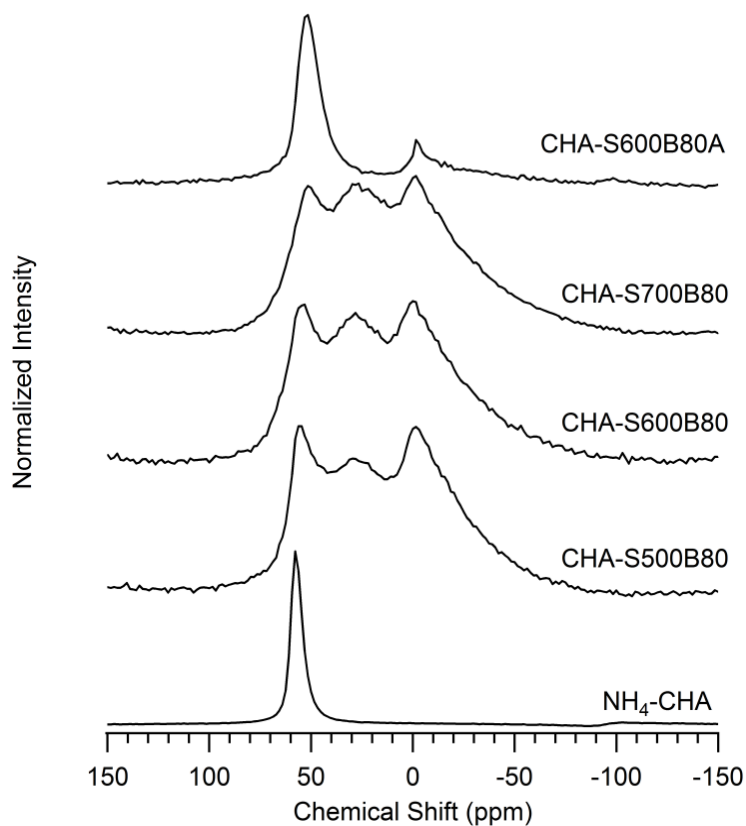


Figure 2-2. ^{27}Al MAS NMR spectra of the as-synthesized CHA, the CHA samples steamed at 500°C, 600°C and 700°C with water saturator at 80°C, and the 600°C steamed and acid-washed CHA (bottom to top).

Further indication that the aluminum content of the zeolite framework changes after steaming is provided by the ^{29}Si MAS NMR spectra (Figure 2-3) of the steamed CHA. The spectrum of the as-synthesized $\text{NH}_4\text{-CHA}$ shows four resonances centered at approximately -109 ppm, -104 ppm, -98 ppm and -93 ppm that can be attributed to Si(0Al) , Si(1Al) , Si(2Al) and Si(3Al) environments, respectively. The silicon environment changes to predominantly Si(0Al) and Si(1Al) after steaming, with the Si(0Al) resonance becoming the largest peak

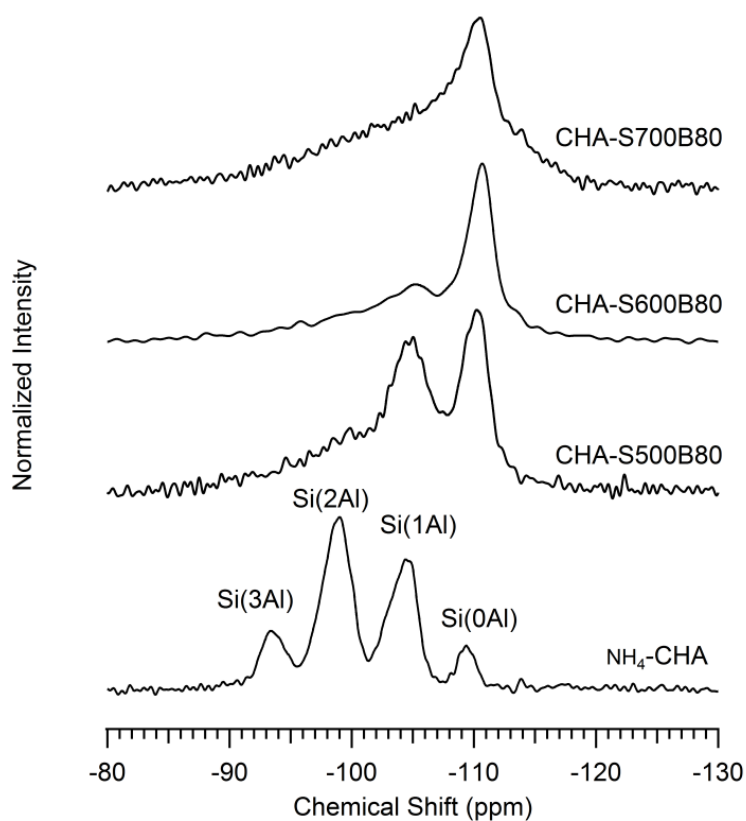


Figure 2-3. ^{29}Si MAS NMR spectra of the as-synthesized CHA, the CHA samples steamed at 500°C, 600°C and 700°C with water saturator at 80°C, and the 600°C steamed and acid-washed CHA (bottom to top).

Figure 2-4A shows the full Ar physisorption isotherms of the as-synthesized NH_4 -CHA and steamed CHA samples along with the isotherm of a pure silicon dioxide sample (Si CHA) that is used as a control for illustrating the adsorption isotherm for a pure (cation-free) CHA material. The steamed CHA samples show decreased micropore adsorption volumes (Table 2-2) compared to the NH_4 -CHA due to partial collapse of the framework.

The micropore filling region is illustrated in Figure 2-4B that shows the adsorption branches of the isotherms (on a semi-logarithmic scale) normalized by the adsorption volume of Si CHA at $P/P_0 = 0.1$. Acid washing the 600°C steamed CHA produces a significant increase in the adsorption volume that can be attributed to the removal of extra-framework aluminum localized within the channels and pores of the sample prior to acid leaching. This treatment, however, does not produce an increase in the micropore volume (Figure 2-4B).

Table 2-2. Micropore volumes of the as-synthesized and steamed CHA

Sample	Micropore Volume (cc/g)
Pure Si CHA	0.221
NH_4 -CHA	0.190
CHA-S500B80	0.149
CHA-S600B80	0.0765
CHA-S700B80	0.0379
CHA-S600B60	0.0466
CHA-S600B90	0.0753

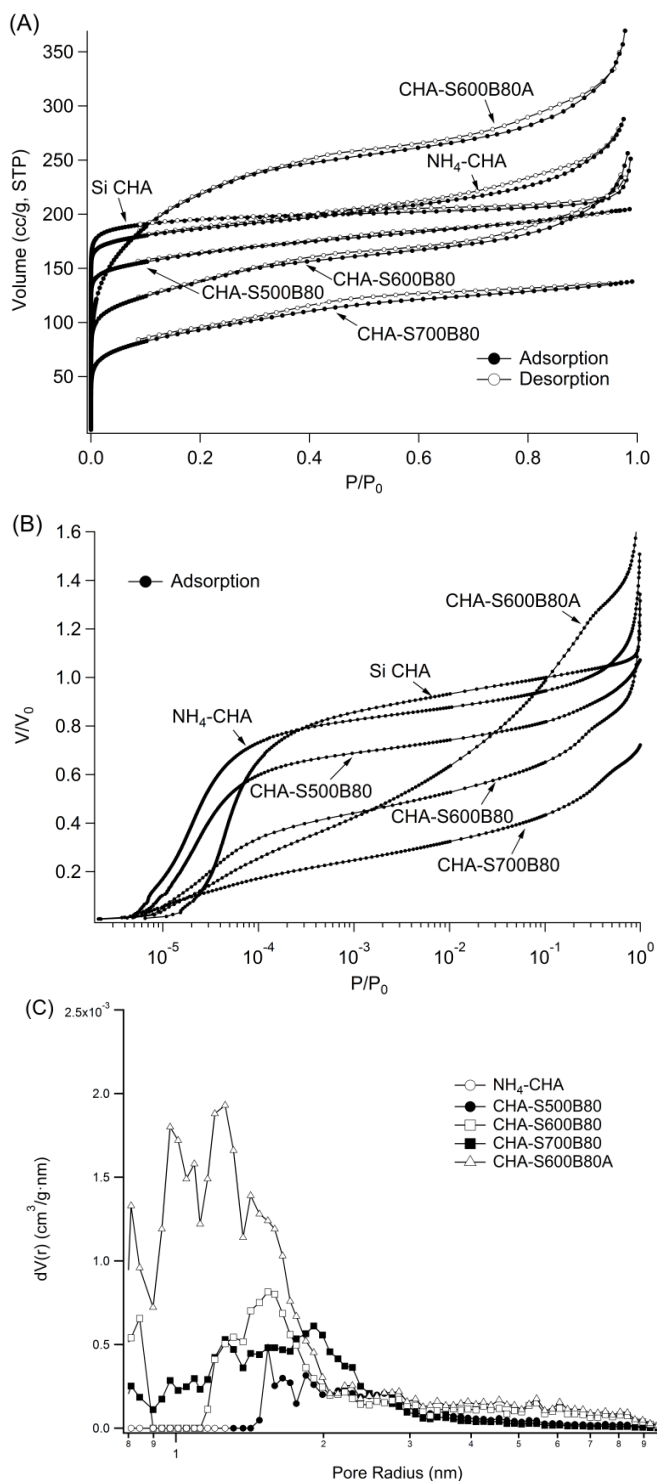


Figure 2-4. Ar physisorption isotherms of the as-synthesized and 500°C -700°C steamed CHA samples, and 600°C steamed and acid-washed CHA: (A) full isotherms, (B) normalized adsorption isotherms plotted on a semi-logarithmic scale and (C) NLDFT pore size distributions plotted on a semi-logarithmic scale

At pressures above the micropore filling P/P_0 range, the adsorption isotherms of the steamed samples differ in shape from that of the $\text{NH}_4\text{-CHA}$ and Si CHA in that the adsorption volumes of the steamed samples increase continuously and at a higher rate per P/P_0 compared to the unsteamed samples. The pore size distributions (obtained from the NLDFT method on the adsorption branches of the isotherms) are illustrated in Figure 2-4C that show the distributions in the mesopore range (greater than 2 nm diameter). While the $\text{NH}_4\text{-CHA}$ does not show any pores with diameters larger than 2 nm, the steamed samples show a contribution in their distributions from pores between 2-6 nm in diameter. These data suggest that mesopores are created by the steam treatments. The pore size distribution of the acid-washed sample shows an even greater contribution from these larger pores, consistent with the removal of amorphous debris from the mesopores.

Entries 1, 2 and 4 of Table 2-1 also demonstrate how steaming decreases the total number of Brønsted acid sites from 3.75 mmol/g for the unsteamed material ($\text{NH}_4\text{-CHA}$ by NH_3 TPD) to 1.07 mmol/g, 0.94 mmol/g and 0.72 mmol/g for the CHA samples steamed at 500°C, 600°C and 700°C, respectively. The number of Brønsted acid sites decreases as steaming temperature increases, consistent with increasing framework aluminum removal and degradation. These total acid site densities also correlate well with the predicted numbers based on the amount of tetrahedral aluminum remaining in each sample by ^{27}Al NMR.

The sites accessible by *i*-propylamine (presumably accessible via the mesopores introduced by steaming) exhibit a maximum with increasing steaming temperature at CHA-

S600B80. This result suggests that the steaming process has an optimal temperature (600°C for CHA) before framework degradation becomes too severe and access to acid sites decreases. For comparison, the unsteamed NH₄-CHA has 0.08 mmol/g of acid sites by *i*-propylamine TPD. Acid washing of the steamed CHA-S600B80 sample (Entry 3 in Table 2-1) reveals the presence of fewer total Brønsted acid sites, but a higher fractional accessibility, as indicated by the reduced NH₃ and increased *i*-propylamine acid site counts, respectively, from the TPDs.

These TPD results are consistent with the other characterization data for the samples that suggest steaming converts tetrahedral framework aluminum to pentacoordinate or octahedral aluminum species, consequently eliminating Brønsted acid sites (as seen via ²⁷Al NMR and NH₃ TPD), and introduces mesoporosity (as seen via Ar adsorption and *i*-propylamine TPD). The samples steamed at 600°C demonstrate the best balance of access to Brønsted acid sites without excessive framework degradation.

2.4.1.2. *Effect of Steam Partial Pressure*

Figure 2-5 shows the XRD patterns of the samples steamed at 600°C with varying partial pressures of steam. The XRD patterns show that lowering the steam partial pressure results in increased amorphization, as indicated by an increasing baseline intensity relative to the peak intensities. Almost complete collapse of the structure was observed when NH₄-CHA is calcined under dry air for 8 h at 600°C. The ²⁷Al NMR spectra of the steamed samples (Figure 2-6), however, do not show significant differences in the relative intensities of the tetrahedral, pentacoordinated and hexacoordinated aluminum signals,

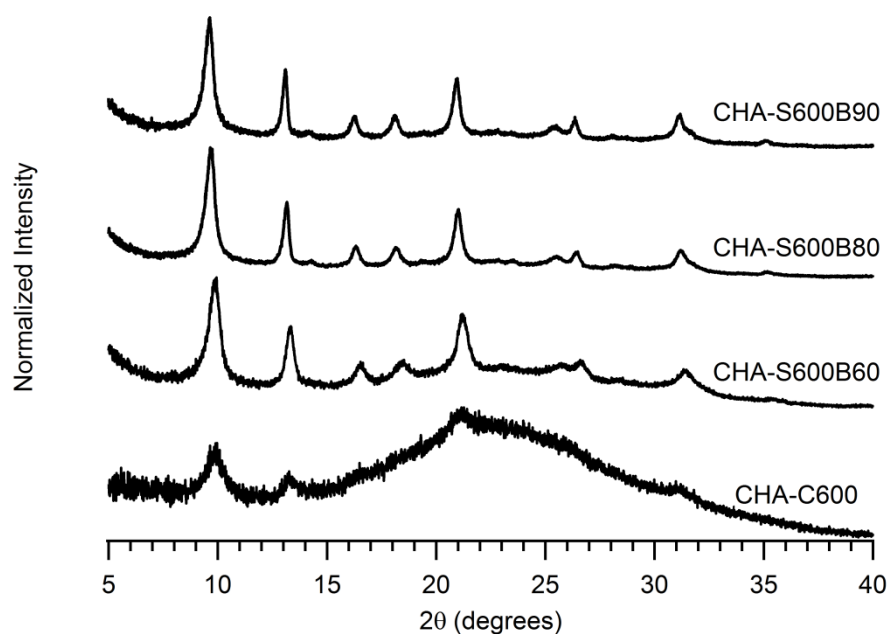


Figure 2-5. Powder XRD patterns of CHA samples steamed at 600°C with varying partial pressures of steam

although the intensity of the tetrahedral aluminum signal relative to the higher coordinated aluminum was the lowest for the CHA calcined under dry conditions. ^{29}Si NMR spectra of the samples steamed under varying steam partial pressures is shown in Figure 2-7, that shows differences in the silicon environments for the samples steamed under varying water vapor pressures.

Ar physisorption measurements on the steamed samples (Figure 2-8A) show that with decreasing steam partial pressure, the samples show decreasing adsorption volume. This trend is also observed in the micropore filling region of the isotherms (Figure 2-8B) and corroborated by the intact micropore volumes (Table 2-2). The pore size distributions of the samples (Figure 2-8C) show that they have mesopore sizes that are approximately in

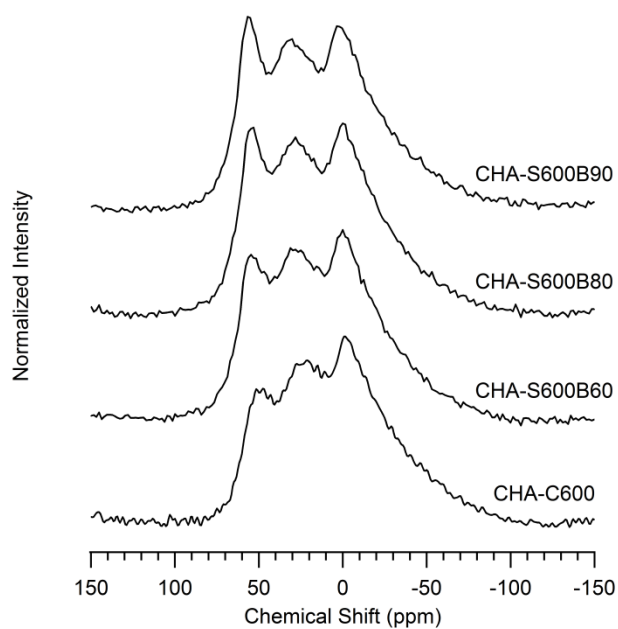


Figure 2-6. ^{27}Al MAS NMR spectra of CHA samples steamed at 600°C with varying partial pressures of steam

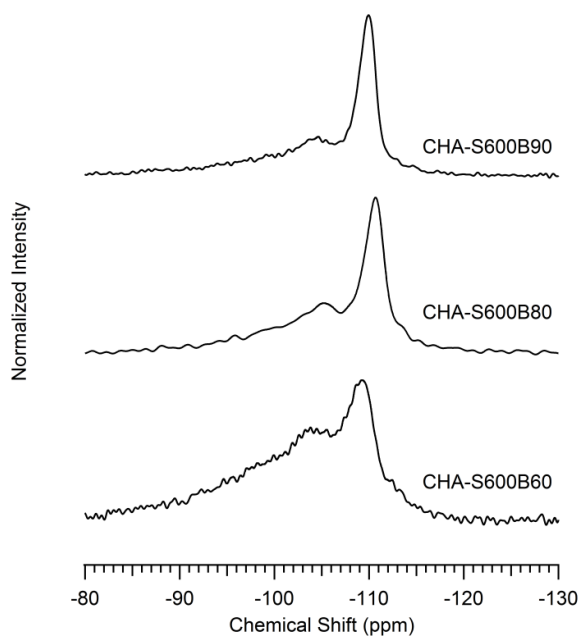


Figure 2-7. ^{29}Si MAS NMR spectra of CHA samples steamed at 600°C in order of increasing steam partial pressures (bottom to top).

the same range, with the size of these pores increasing slightly with the steam partial pressure.

Interestingly, as steam partial pressure decreases, the total Brønsted acid sites titrated by NH_3 TPD remain relatively similar (Entries 2, 5 and 6 in Table 2-1, consistent with the ^{27}Al NMR results), with a maximum value at CHA-S600B80. The *i*-propylamine TPD results are quite different, however, with the greatest accessibility observed for the two samples that were steamed with the water saturator at 80°C and 90°C (CHA-S600B80 and CHA-S600B90, respectively). The sample with the lowest steam partial pressure, CHA-S600B60, has approximately half the *i*-propylamine accessibility of these other samples

The trend of increased degradation with decreasing steam partial pressure is the opposite of what has been reported for larger pore zeolites such as zeolites Y, ^{18,19} (FAU) and ZSM-5 ²⁰ (MFI). Our steaming experiments with zeolite Y at 550°C and 650°C using a similar steam procedure to those reported by Wang et al.¹⁹, are consistent with the literature results in that zeolite Y samples calcined in the presence of steam undergo greater dealumination compared to samples calcined in dry air. Characterizations (powder XRD patterns and ^{27}Al NMR) for the 550°C and 650°C steamed zeolite Y samples are provided in the Supporting Information (Table 2-4 and Figures 2-14 through 2-17). However, when zeolite Y is steamed under more severe conditions (8 h at 800°C) using the same steaming procedure. that was used with the CHA zeolites, the results (Supporting Information Table 2-4 and Figures 2-18 and 2-19) show the reversed trend of greater degradation with

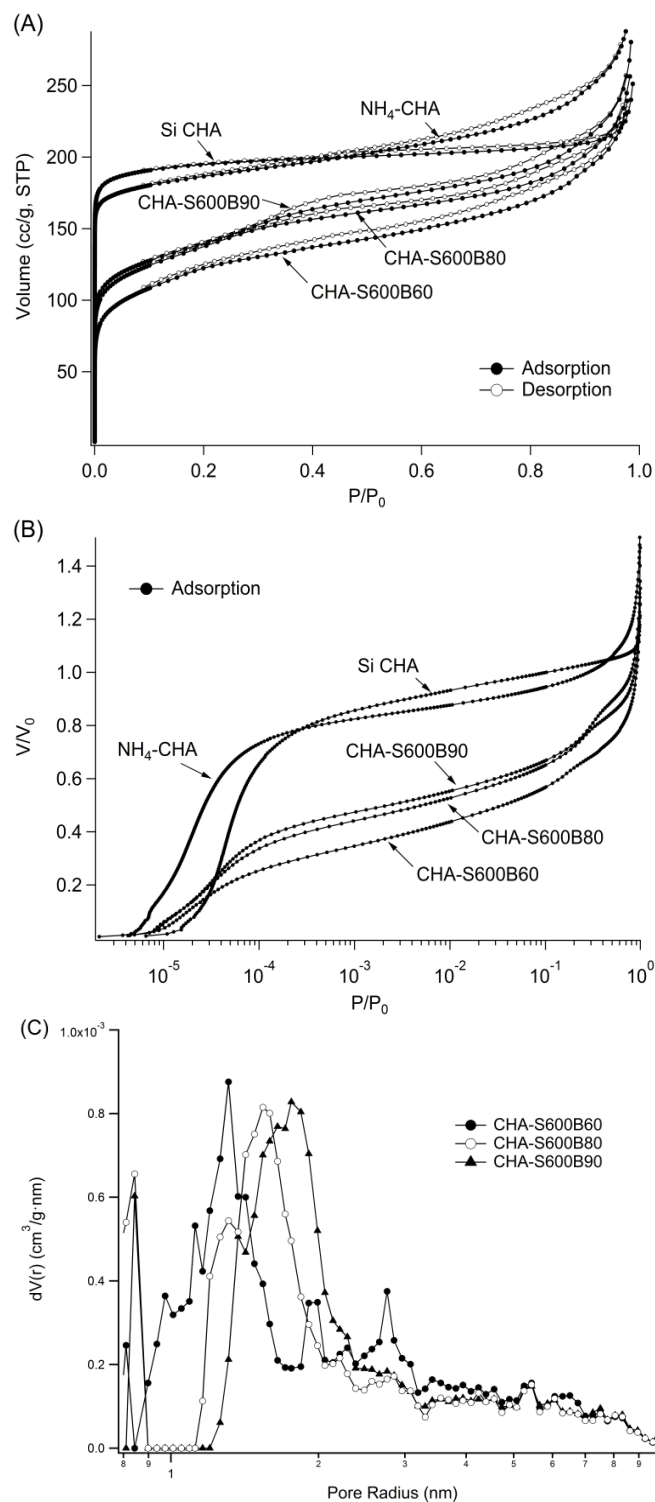


Figure 2-8. Ar physisorption isotherms of the as-synthesized and 600°C steamed CHA samples under varying steam partial pressures: (A) full isotherms, (B) normalized adsorption isotherms plotted on a semi-logarithmic scale and (C) NLDFT pore size distributions plotted on a semi-logarithmic scale

decreasing steam partial pressure, consistent with the behavior of the CHA zeolites.

Furthermore, steam treatment of CHA at milder conditions (3 h at 500°C) using the 550°C and 650°C Y steaming procedure produces increasing dealumination with increasing steam partial pressure (Supporting Information Table 2-4 and Figures 2-20 and 2-21), consistent with the behavior of zeolite Y at the lower steaming temperatures. The similar behaviors between CHA and zeolite Y at these steaming conditions suggest that the trend reported here is not unique to CHA.

It has been proposed that the steaming involves hydrolyses of Al-O-Si bonds by water vapor at high temperatures, resulting in extra-framework aluminum species and the formation of vacant silanol nests.^{19,21,22} As an increasing number of the framework aluminum is extracted, portions of the zeolite collapse, forming amorphous regions. Investigations on the steam dealumination of Y zeolites further suggest that in the presence of steam, silicon may migrate in the form of ortho-silicic acid (H_4SiO_4) to fill in the aluminum vacancies and thus “heal” the structure so that the resulting structure shows increased thermal stability.^{22,23}

It is likely that a similar stabilization process may be occurring during the heating period for the zeolites studied here. When heated to temperatures at which the zeolite normally becomes amorphous under dry conditions (600°C for CHA and 800°C for Y in this study), the presence of steam provides stabilization of the structure. Due to the slow ramp rate (1°C/min) used during the steaming experiments for CHA and Y where the reversed trend of increased degradation with decreasing steam partial pressure was

observed, the samples spend approximately the first half of the duration of the steaming experiment in heating under a steam atmosphere. A significant portion of the steaming process would thus occur in the heating period, during which the dealumination and healing steps described above are occurring at the same time. Under the higher steam partial pressures tested, healing of the framework may be facilitated and occurs at a rate that is fast enough to compensate for the dealumination process, and thus the structure is stabilized during the heating period. At a low steam partial pressure, the rate of healing could be too slow to compensate for dealumination and dehydroxylation and thus significant loss of crystallinity occurs. The ^{29}Si NMR of the samples steamed under varying steam partial pressures suggest that as the steam partial pressure is increased, the Si(0Al) peak grows in intensity relative to the downfield peaks, which would be consistent with increasing formation of Si-O-Si bonds with increasing availability of water during steaming.

2.4.2. MTO Reaction Testing

2.4.2.1. *Effect of Steaming Temperature and Acid Washing*

Figure 2-9 illustrates representative TOS reaction data obtained at 400°C for the as-synthesized CHA, the CHA samples steamed at 500°C-700°C with the water saturator at 80°C, and a SAPO-34. Table 2-3 provides a summary of the reaction data that includes the maximum methanol conversion, maximum combined C₂-C₃ olefin selectivity at maximum conversion. Each of the catalysts is initially active in producing C₂-C₄ olefins when methanol conversion is close to 100%. With increasing TOS, methanol conversion decreases, and is accompanied by a decrease in olefin selectivities and a simultaneous

increase in dimethyl ether (DME) production. C₃-C₅ alkanes, mainly propane and butane, are also observed among the products at the start of the reaction, with selectivities decreasing with increasing TOS. Lower alkanes (methane and ethane) are not observed among the products. and the approximate time to deactivation (arbitrarily defined as the first time point where the conversion drops below 80%).

The as-synthesized CHA, while initially active in producing ethylene and propylene, has the shortest catalyst lifetime. Methanol conversion starts at 100%, but decreases rapidly after approximately 45 min (0.93 g MeOH/g-cat) TOS, and DME becomes the main reaction product. The fast deactivation may be attributed to the high

Table 2-3. Maximum combined C₂-C₃ olefin selectivities near complete conversion, and deactivation times of catalysts tested

Sample	Reaction Temperature	Maximum MeOH Conversion	Combined C ₂ -C ₃ Olefin Selectivity at Max. MeOH Conversion	Time to Deactivation ^a
H-CHA	400°C	100.0%	59.0%	61 min (1.3 g MeOH/g cat)
CHA-S500B80	400°C	100.0%	55.3%	80 min (1.6 g MeOH/g cat)
CHA-S600B80	350°C	98.6%	58.6%	59 min (1.2 g MeOH/g cat)
	400°C	100.0%	65.6%	108 min (2.3 g MeOH/g cat)
	450°C	100.0%	74.2%	152 min (3.2 g MeOH/g cat)
CHA-S700B80	400°C	97.4%	58.8%	69 min (1.4 g MeOH/g cat)
CHA-S600B80A	400°C	94.4%	58.9%	240 min (5.0 g MeOH/g cat)
	450°C	100.0%	71.4%	>439 min (> 9.0 g MeOH/g cat)
SAPO-34	400°C	100.0%	86.3%	>448 min (> 9.8 g MeOH/g cat)

^a First time point where methanol conversion drops below 80%

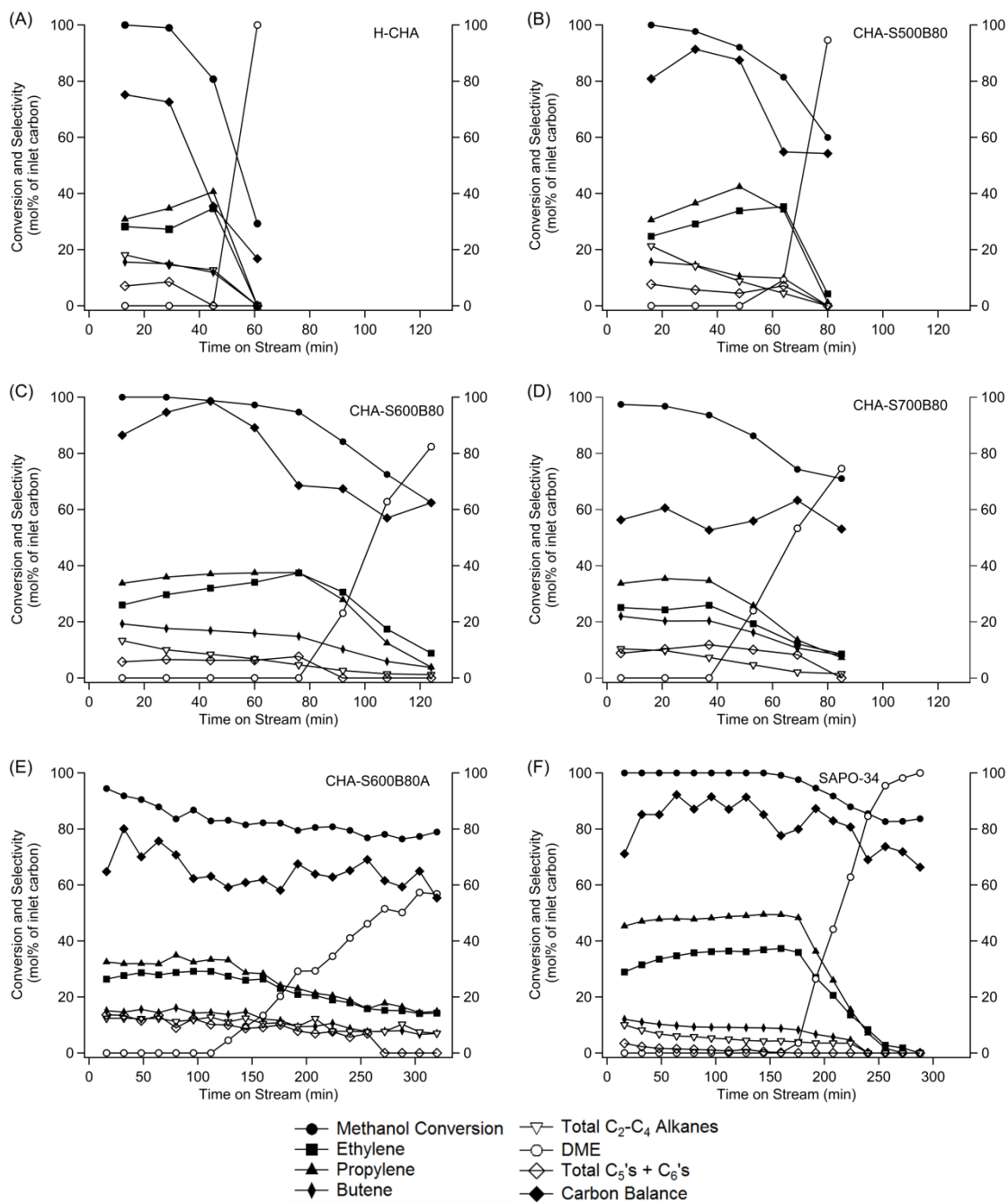


Figure 2-9. Representative MTO reaction data obtained at 400°C for: (A) unsteamed H-CHA, (B) 500°C steamed CHA, (C) 600°C steamed CHA, (D) 700°C steamed CHA, (E) 600°C steamed and acid washed CHA, and (F) SAPO-34

framework aluminum content of the as-synthesized CHA (Si/Al = 2.4) that leads to rapid coke deposition.

Whereas deactivation occurs abruptly for the as-synthesized CHA, the steamed materials show more gradual deactivation profiles that vary depending on the severity of steaming. CHA steamed at 500°C has a slightly improved lifetime compared to the as-synthesized CHA. Methanol is initially completely converted and remains above 80% conversion for 64 min (1.3 g MeOH/g cat) TOS. However, olefin selectivities for CHA-S500B80 are comparable to the unsteamed CHA.

CHA steamed at 600°C shows the most stable reaction profile and longest lifetime among the steamed samples. Methanol conversion starts at 100% and remains above 80% for more than 92 min (2.0 g MeOH/g cat) TOS before deactivation occurs, with DME becoming the main product. Importantly, improved olefin selectivities are also observed for this sample. C₂-C₃ olefin selectivities increase gradually with increasing TOS when conversion is near 100% and reach maximum selectivities of 29.7% and 35.9%, respectively, at complete conversion, and approaches olefin selectivities for SAPO-34 (Figure 2-9F). Upon regeneration of the spent catalyst, similar olefin selectivities are observed with only a slight decrease in catalyst lifetime (Supporting Information Figures 2-22 and 2-23).

The lifetime of the 600°C steamed CHA is improved further after acid washing (Figure 2-9E). Methanol conversion decreases slowly and remains steady around 80% until approximately 240 min (5.0 g-MeOH/g-cat) TOS. The combined ethylene and propylene

selectivity remains steady at approximately 61% for 100 min TOS before gradually declining.

Increasing the steaming temperature further to 700°C gives poorer MTO activity compared to CHA S600B80, likely due to the increased severity of steaming at 700°C. Ethylene and propylene reach selectivities of 24.3% and 35.4%, respectively, at 96.8% methanol conversion (21 min TOS). Conversion drops below 80% by approximately 60 min TOS, giving a reaction profile similar to the 500°C steamed CHA.

The improvements in selectivities and catalyst lifetime of the 600°C-steamed CHA may be attributed to modifications in the acidity of the catalysts resulting from the extraction of framework aluminum. It is also likely that the mesoporosity created by steaming plays a role in the extended lifetimes. It has been observed that the introduction of mesopores in microporous zeolite catalysts facilitates mass transport to the micropores and leads to longer catalyst lifetimes.²⁴ This trend has been reported by Wu et al.,²⁵ who evaluated hierarchical SSZ-13 that was synthesized using the N,N,N-trimethyladamantylammonium OSDA in combination with a mesoporegen. These introduced mesopores result in improved lifetimes for the MTO reaction by allowing greater utilization of the micropore volume. As demonstrated by the NH₃ and *i*-propylamine TPD data, the 600°C-steamed CHA sample appears to have the best balance of intact Brønsted acid sites and access to those sites via the mesoporosity introduced by the steaming process that could account for the excellent reaction behavior observed.

2.4.2.2. Effect of Reaction Temperature

The effects of reaction temperature on the activity of CHA-S600B80 and CHA-S600B80A are illustrated in Figure 2-10. The most apparent trend in the reaction profiles for CHA S600B80 when the reaction temperature is increased from 350°C to 450°C is the increase in catalyst lifetime. At 350°C, methanol conversion is initially near 100%, but declines below 80% after approximately 59 min (1.3 g MeOH/g cat) of TOS, while at

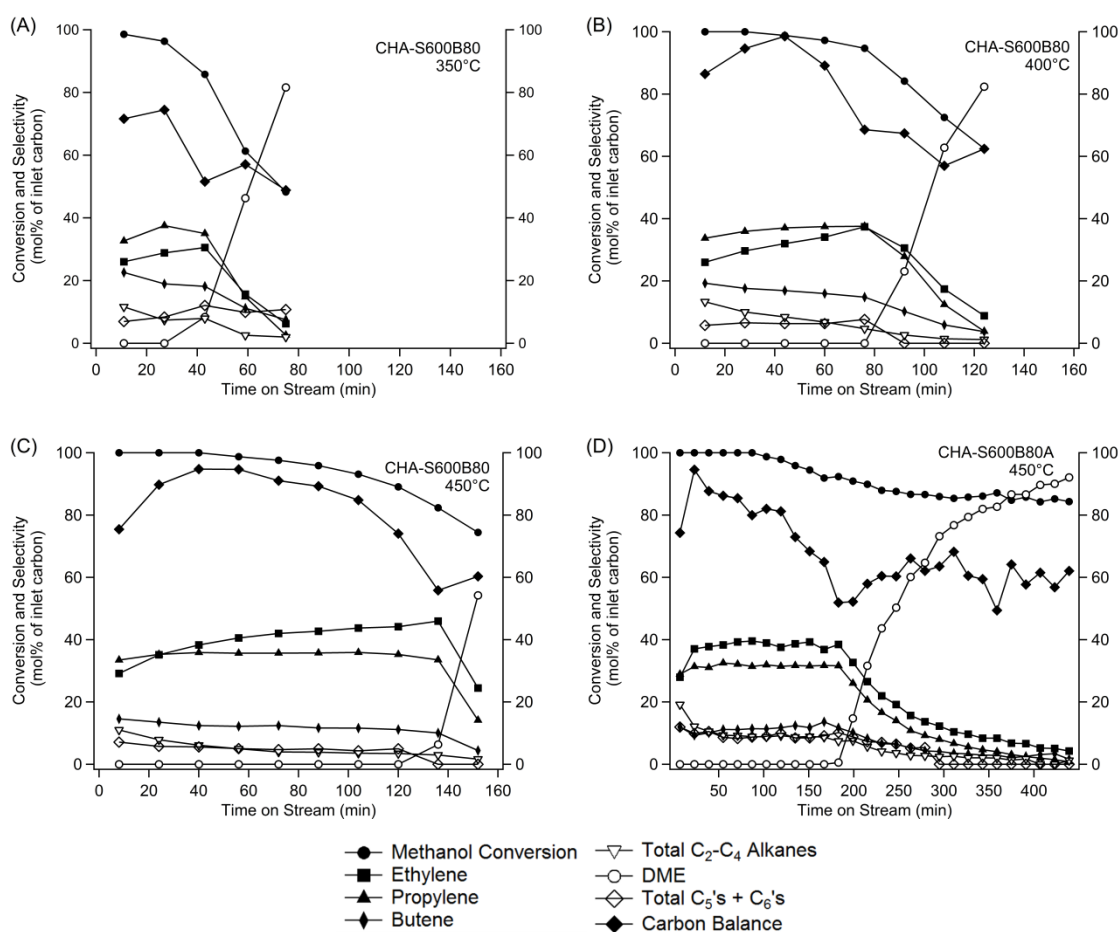


Figure 2-10. Representative MTO reaction data for 600°C steamed CHA (CHA-S600B80) obtained at reaction temperatures of (A) 350°C, (B) 400°C, (C) 450°C and (D) 600°C steamed and acid-washed CHA (CHA S600B80A) at a reaction temperature of 450°C

400°C, the lifetime was 108 min (2.3 g MeOH/g cat). Increasing the reaction temperature further to 450°C results in the longest lifetime at 152 min (3.2 g MeOH/g cat). Further, the maximum combined ethylene and propylene selectivity increases at 450°C to 74.2% at 100% conversion, approaching olefin selectivities observed for SAPO-34 (Figure 2-9F).

Similarly, the acid washed sample shows increases in lifetime and olefin selectivities at 450°C. CHA-S600B80A converts methanol to ethylene and propylene steadily at an average of 69% combined selectivity for almost 200 min (4.1 g MeOH/g cat) TOS before DME becomes the main product. Further, ethylene selectivities increase for both CHA S600B80 and CHA S600B80A when the reaction temperature is increased from 400°C to 450°C so that more ethylene than propylene is produced at 450°C. Regeneration of CHA S600B80A at 450°C results in some loss in olefin selectivities and lifetime (Supporting Information Figures 2-24 and 2-25).

2.5. Conclusions

CHA type zeolites were prepared from the hydrothermal conversion of zeolite Y, NH_4^+ -exchanged, and dealuminated post-synthetically by steam and acid treatments to create selective catalysts for converting methanol to olefins. Characterizations by XRD and Ar physisorption of the steamed samples showed that partial collapse of the framework occurs during the steaming process with the degree of degradation increasing with steaming temperature. ^{27}Al MAS NMR spectra of the steamed samples revealed the presence of tetrahedral, pentacoordinate and octahedral aluminum species. NH_3 and *i*-propylamine TPD results further corroborated that steaming converted tetrahedral

aluminum to pentacoordinate and octahedral species while also introducing pores larger than 8MR pores to the samples (simultaneously reduced the number of total Brønsted acid sites, but made them more accessible). As steaming temperature increases, the total Brønsted acid sites decreased, but accessibility via mesopores exhibited a maximum when samples were steamed at 600°C.

When evaluated for the MTO reaction, the unsteamed H-CHA (Si/Al = 2.4) deactivated quickly whereas the steamed samples showed longer lifetimes and increased olefin selectivities. CHA steamed at 600°C achieved the highest olefin selectivities (comparable to that of the commercial catalyst) and lifetime among the steamed samples, and the activity was retained upon regeneration of the spent catalyst. The results presented here show that the acidity and catalytic behavior of an aluminum-rich CHA zeolite prepared without using an OSDA can be modified by post-synthetic dealumination treatments to create a selective catalyst for converting methanol to olefins. It is likely that this dealumination strategy may be effective for preparing useful catalysts starting from small-pore zeolites of other topologies that are currently of interest for applications such as MTO and deNO_x.

2.6. Acknowledgements

The authors thank the Dow Chemical Company for financial support of this work. The authors also thank Drs. Andrzej Malek, Jonathan Lunn and Yu Liu from the Dow Chemical Company for helpful discussions.

2.7. References

- (1) Vora, B.; Chen, J. Q.; Bozzano, A.; Glover, B.; Barger, P. Various routes to methane utilization—SAPO-34 catalysis offers the best option. *Catal. Today* **2009**, *141*, 77-83.
- (2) Froment, G. F.; Dehertog, W. J. H.; Marchi, A. J. Zeolite catalysis in the conversion of methanol into olefins. In *Catalysis*; Spivey, J. J., Ed; Specialist Periodical Reports: Catalysis, Vol.9; The Royal Society of Chemistry: Cambridge, 1992; p 1-64.
- (3) Dai, W.; Wang, X.; Wu, G.; Guan, N.; Hunger, M.; Li, L. Methanol-to-olefin conversion on silicoaluminophosphate catalysts: effect of Brønsted acid sites and framework structures. *ACS Catal.* **2011**, *1*, 292-299.
- (4) Kaiser, S. W. Using silicoaluminophosphate molecular sieve catalyst. U.S. Patent 4,499,327, February 12, 1985.
- (5) Liang, J.; Li, H.; Zhao, S.; Guo, W.; Wang, R.; Ying, M. Characteristics and performance of SAPO-34 catalyst for methanol-to-olefin conversion. *Appl. Catal.* **1990**, *64*, 31-40.
- (6) Vora, B. V.; Marker, T. L.; Barger, P. T.; Nilsen, H. R.; Kvisle, S.; Fuglerud, T. Economic route for natural gas conversion to ethylene and propylene. In *Natural Gas Conversion IV*; de Pontes, M., Espinoza, R. L., Nicolaides, C. P., Scholtz, J. H., Scurrell, M.S., Eds.; *Stud. Surf. Sci. Catal.*, Vol. 107; Elsevier: Amsterdam, 1997; pp 87-98.

- (7) Chen, J. Q.; Bozzano, A.; Glover, B.; Fuglerud, T.; Kvisle, S. Recent advancements in ethylene and propylene production using the UOP/Hydro MTO process. *Catal. Today* **2005**, *106*, 103-107.
- (8) Bleken, F.; Bjørgen, M.; Palumbo, L.; Bordiga, S.; Svelle, S.; Lillerud, K.-P.; Olsbye, U. The effect of acid strength on the conversion of methanol to olefins over acidic microporous catalysts with the CHA topology. *Top. Catal.* **2009**, *52*, 218-228.
- (9) Haw, J. F.; Marcus, D. M. Well-defined (supra)molecular structures in zeolite methanol-to-olefin catalysis. *Top. Catal.* **2005**, *34*, 41-48.
- (10) Wilson, S.; Barger, P. The characteristics of SAPO-34 which influence the conversion of methanol to light olefins. *Micropor. Mesopor. Mater.* **1999**, *29*, 117-126.
- (11) Baerlocher, C.; McCusker, L. B.; Olson, D. H. *Atlas of Zeolite Framework Types*, 6th revised ed.; Elsevier: Amsterdam, 2007.
- (12) Arstad, B.; Nicholas, J. B.; Haw, J. F. Theoretical study of the methylbenzene side-chain hydrocarbon pool mechanism in methanol to olefin catalysis. *J. Am. Chem. Soc.* **2004**, *126*, 2991-3001.
- (13) Zones, S. I. Zeolite SSZ-13 and its method of preparation. U.S. Patent 4,544,538, October 1, 1985.
- (14) Yuen, L.-T.; Zones, S. I.; Harris, T. V.; Gallegos, E. J.; Auroux, A. Product selectivity in methanol to hydrocarbon conversion for isostructural compositions of AFI and CHA molecular sieves. *Microporous Mater.* **1994**, *2*, 105-117.

- (15) Zhu, Q. J.; Kondo, J. N.; Ohnuma, R.; Kubota, Y.; Yamaguchi, M.; Tatsumi, T.
The study of methanol-to-olefin over proton type aluminosilicate CHA zeolites.
Microporous Mesoporous Mater. **2008**, *112*, 153-161.
- (16) Carlidge, S.; Patel, R. Hydrothermally stable chabazites for the selective preparation of olefins from methanol. In *Zeolites: Facts, Figures, Future Part A - Proceedings of the 8th International Zeolite Conference*; Jacobs, P. A., van Santen, R. A., Eds.; *Stud. Surf. Sci. Catal.*, Vol. 49; Elsevier: Amsterdam, 1989; pp 1151-1161.
- (17) Bourgogne, M.; Guth, J. L.; Wey, R. Process for the preparation of synthetic zeolites, and zeolites obtained by said process. U.S. Patent 4,503,024, March 5, 1985.
- (18) Engelhardt, G.; Lohse, U.; Patzeolová, V.; Mägi, M.; Lippmaa, E. High resolution ²⁹Si N.M.R. of dealuminated Y-zeolites 1. The dependence of the extent of dealumination on the degree of ammonium exchange and the temperature and water vapour pressure of the thermochemical treatment. *Zeolites* **1983**, *3*, 233-238.
- (19) Wang, Q.L.; Giannetto, G.; Torrealba, M.; Perot, G.; Kappenstein, C.; Guisnet, M. Dealumination of zeolites II. Kinetic study of the dealumination by hydrothermal treatment of a NH₄NaY zeolite. *J. Catal.* **1991**, *130*, 459-470.
- (20) Lago, R.M.; Haag, W.O.; Mikovsky, R.J.; Olson, D.H.; Hellring, S.D.; Schmitt, K.D.; Kerr, G.T. The nature of the catalytic sites in HZSM-5- activity enhancement. In *Proceedings of the 7th International Zeolite Conference*; Murakami, Y., Iijima, A., Ward, J.W., Eds.; *Stud. Surf. Sci. Catal.*, Vol. 28; Elsevier: Amsterdam, 1986; pp 677-684.

- (21) Malola, S.; Svelle, S.; Bleken, F.L.; Swang, O. Detailed reaction paths for zeolite dealumination and desilication from density functional calculations. *Angew. Chem. Int. Ed.* **2012**, *51*, 652-655.
- (22) Lutz, W. Zeolite Y: Synthesis, modification, and properties—A case revisited. *Adv. Mater. Sci. Eng.* [Online] **2014**, *2014*, DOI:10.1155/2014/724248.
- (23) Scherzer, J. The preparation and characterization of aluminum-deficient zeolites. In *Catalytic Materials: Relationship Between Structure and Reactivity*. Whyte, T. E.; Dalla Betta, R. A.; Derouane, E. G.; Baker, R. T. K., Eds.; ACS Symposium Series 248; American Chemical Society: Washington, DC, 1984; pp 157-200.
- (24) Hartmann, M. Hierarchical zeolites: a proven strategy to combine shape selectivity with efficient mass transport. *Angew. Chem. Int. Ed.* **2004**, *43*, 5880-5882.
- (25) Wu, L.; Degirmenci, V.; Magusin, P. C. M. M.; Lousberg, N. J. H. G. M.; Hensen, E. J. M. Mesoporous SSZ-13 zeolite prepared by a dual-template method with improved performance in the methanol-to-olefins reaction. *J. Catal.* **2013**, *298*, 27-40.

2.8. Supporting Information for Chapter 2

2.8.1. Study on the effect of steam treatment on SSZ-13 for MTO

SSZ-13 was synthesized following the method reported in literature¹³ at a Si/Al ratio of 5 using the N,N,N-trimethyladamantylammonium hydroxide SDA. The product was calcined, NH_4^+ -exchanged and then steamed for 24 h at 750°C under a flow of water vapor/inert mixture, which was accomplished by bubbling inert through a water saturator held at 75°C. Reaction testing of the samples was conducted at 400°C using a 10% methanol/inert feed at a WHSV of 1.3 h⁻¹. The MTO reaction profiles for the fresh (unsteamed) SSZ-13 with Si/Al = 5 and steamed SSZ-13 are shown in Figure 2-11 and 2-12, respectively. The unsteamed SSZ-13 initially converts methanol at 100% but

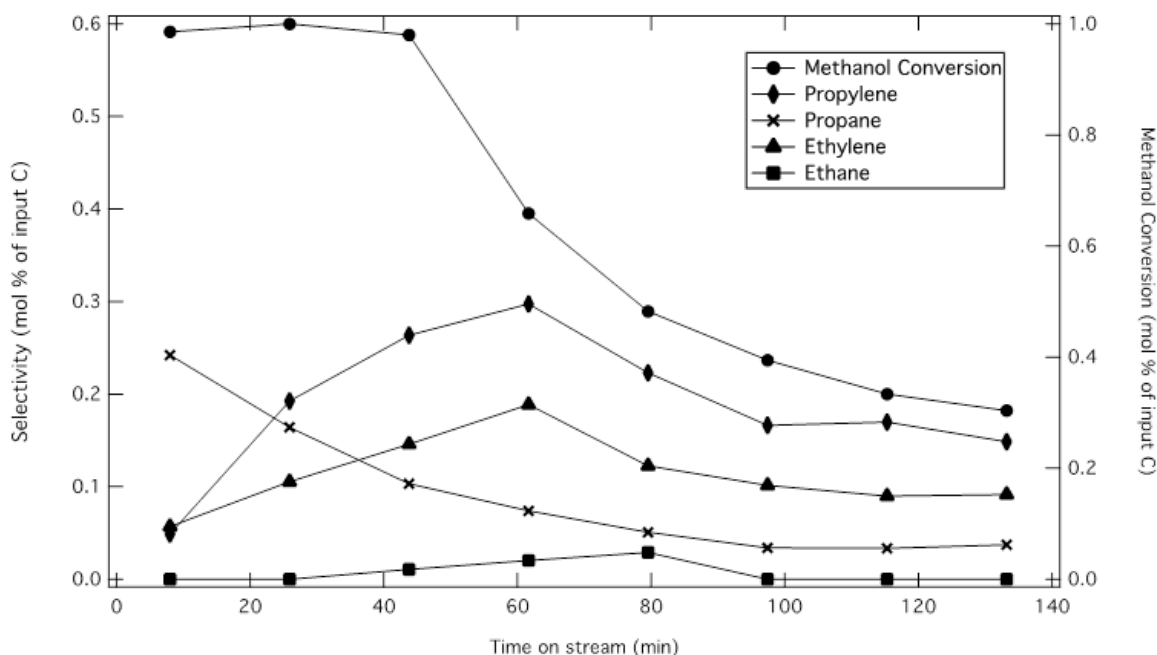


Figure 2-11. MTO reaction data for fresh (unsteamed) H-SSZ-13 Si/Al=5

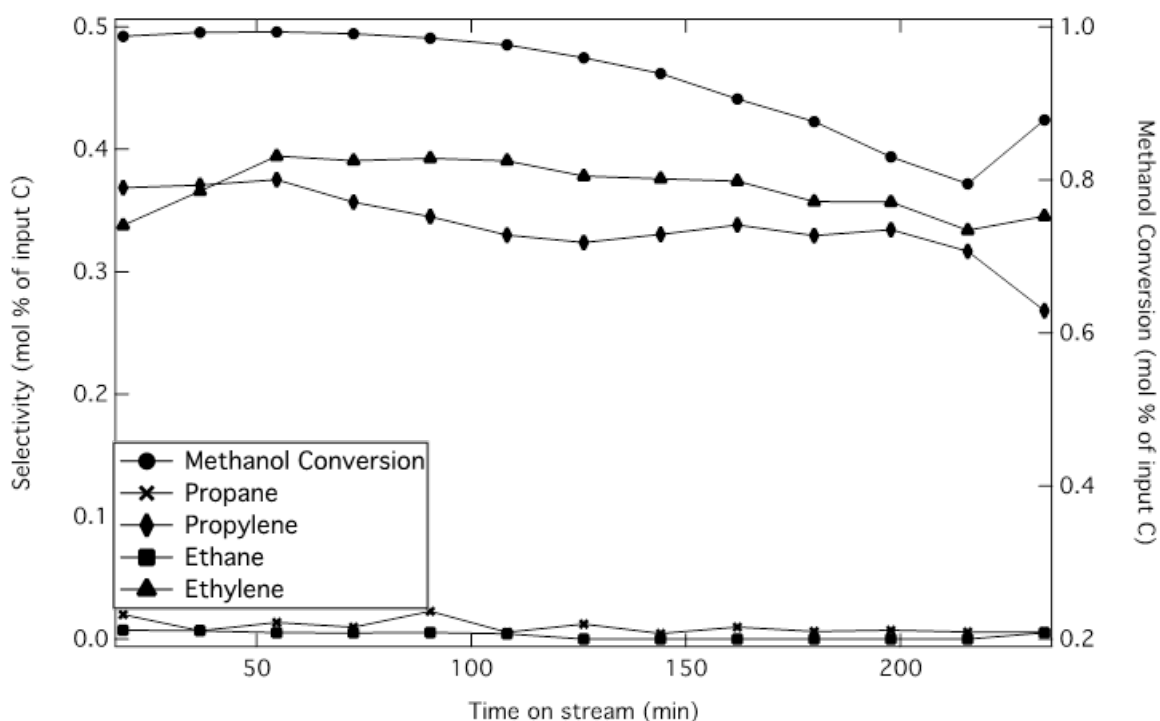


Figure 2-12. MTO reaction data for steamed H-SSZ-13 Si/Al=5

deactivates rapidly after approximately 45 min TOS. Both the catalyst lifetime and olefin selectivities are improved after steam treatment. Methanol conversion remains above 80% for more than 200 min TOS for the steamed SSZ-13. Further, whereas the unsteamed SSZ-13 shows a transient period at the start of the reaction in which a significant amount of propane is observed in addition to rising olefin selectivities, the steamed material has a more stable reaction profile, similar to SAPO-34 (Figure 2-9F).

2.8.2. Further Characterization of Catalysts

A ^{27}Al MAS NMR spectrum of the as-synthesized K-CHA was obtained and is shown in Figure 2-13. The spectrum contains only a single sharp peak centered at

approximately 55 ppm, corresponding to tetrahedral aluminum, and indicates that all aluminum is initially incorporated in the framework.

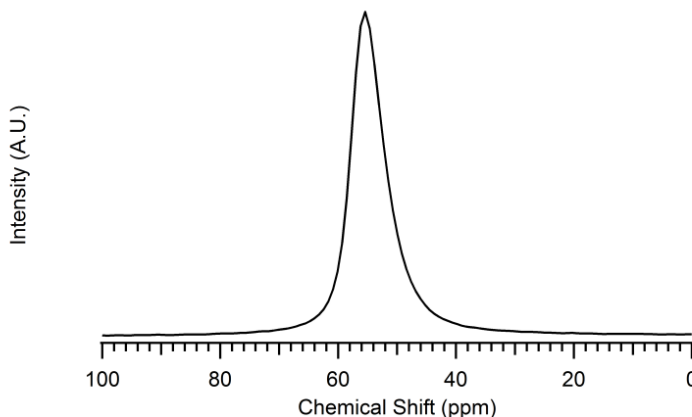


Figure 2-13. ^{27}Al MAS NMR of as-synthesized K-CHA

2.8.3. Steaming Experiments with Zeolite Y and CHA

Three series of steaming experiments were conducted using zeolite Y (FAU) for the purposes of verifying that the steaming and dry calcination results previously reported in the literature on Y can be reproduced as well as determining whether the trend observed with CHA under varying partial pressures is also observed in Y when steamed using the same procedure. For all of the Y steaming experiments, the starting zeolite was a commercial NaY with Si/Al=2.97 that had been NH_4^+ exchanged three times for 2 h at 90°C with 1 M NH_4NO_3 . The NH_4^+ exchanged Y, designated NH_4NaY , had a Na/Al ratio of 0.28 (measured by EDS) and was steamed using the same tube furnace set up as that used for the CHA samples.

A summary of the steaming conditions is provided in Table 2-4. Two sets of steaming experiments were conducted at 550°C and 650°C under similar conditions reported by Wang et al.¹⁹, who investigated the effect of the water partial pressure on steaming of zeolite Y. Samples were heated at 5°C/min to the steaming temperature (550°C or 650°C) under 50 cc/min of dry air and then subjected to flowing steam (created by

Table 2-4. Summary of zeolite Y and additional CHA steaming conditions

Sample	Heating Ramp Rate	Steaming Time	Steaming Temp.	Bubbler Temp.	Duration of Flowing Steam	Al _T /Al _{Total}
NH ₄ NaY-S550B90	5°C/min	3 h	550°C	90°C	At steaming temperature only	0.144
NH ₄ NaY-S550B80	5°C/min	3 h	550°C	80°C	At steaming temperature only	0.288
NH ₄ NaY-S550B60	5°C/min	3 h	550°C	60°C	At steaming temperature only	0.387
NH ₄ NaY-C550	5°C/min	3 h	550°C	-	Dry calcination	0.822
NH ₄ NaY-S650B90	5°C/min	3 h	650°C	90°C	At steaming temperature only	0.394
NH ₄ NaY-S650B80	5°C/min	3 h	650°C	80°C	At steaming temperature only	0.325
NH ₄ NaY-S650B60	5°C/min	3 h	650°C	60°C	At steaming temperature only	0.308
NH ₄ NaY-C650	5°C/min	3 h	650°C	-	Dry calcination	0.444
NH ₄ NaY-S800B90	1°C/min	8 h	800°C	90°C	Entire period	0.230
NH ₄ NaY-S800B80	1°C/min	8 h	800°C	80°C	Entire period	0.670
NH ₄ NaY-S800B60	1°C/min	8 h	800°C	60°C	Entire period	0.713
NH ₄ NaY-C800	1°C/min	8 h	800°C	-	Dry calcination	0.234
CHA-S500B90	5°C/min	3 h	500°C	90°C	At steaming temperature only	0.139
CHA-S500B60	5°C/min	3 h	500°C	60°C	At steaming temperature only	0.156
CHA-C500	5°C/min	3 h	500°C	-	Dry calcination	0.201

bubbling 50 cc/min of dry air through a heated water saturator) for 3 h at the steaming temperature. Samples were cooled under 50 cc/min of dry air flow at the end of the 3 h steaming period. Steaming experiments were conducted with the bubbler (providing approximately a 50% saturated air and water vapor mixture) held at 60°C, 80°C and 90°C, for which the water saturation pressures are 19.9 kPa, 47.3 kPa and 70.1 kPa, respectively. An additional dry calcination was carried out on the NH_4NaY using the same temperature profile under flowing dry air (50 cc/min).

In the third set of steaming experiments, NH_4NaY samples were steamed under more severe conditions using the same procedure that was used for the CHA samples steamed at 600°C under varying steam partial pressures. Samples were heated at 1°C/min to 800°C and held for 8 h at the steaming temperature. The entire process, including heating and cooling, was carried out under flowing air. An additional dry calcination was conducted under 50 cc/min of dry air using the same temperature profile.

To determine whether CHA would also show the same trend that was observed with Y steamed at 550°C and 650°C, an additional series of steaming experiments was conducted with CHA using the same steaming procedures that were used for the 550°C and 650°C zeolite Y steaming experiments, where $\text{NH}_4\text{-CHA}$ samples were steamed for 3 h at 500°C under varying steam partial pressures. The furnace was ramped at 5°C/min to 500°C under 50 cc/min of dry air, steam was introduced for 3 h at 500°C only, and the sample was then allowed to cool under flowing dry air (50 cc/min).

Figures 2-14 and 2-15 show the powder XRD patterns of the NH_4NaY samples steamed at 550°C and 650°C, respectively. ^{27}Al MAS NMR spectra of the 550°C and 650°C steamed samples are shown in Figures 2-16 and 2-17. At both steaming temperatures, the ^{27}Al NMR indicates that a greater fraction of tetrahedral aluminum is converted to pentacoordinated and octahedral aluminum for the steamed NH_4NaY samples compared to the dry calcined samples, consistent with what has been reported by Wang et al.¹⁹

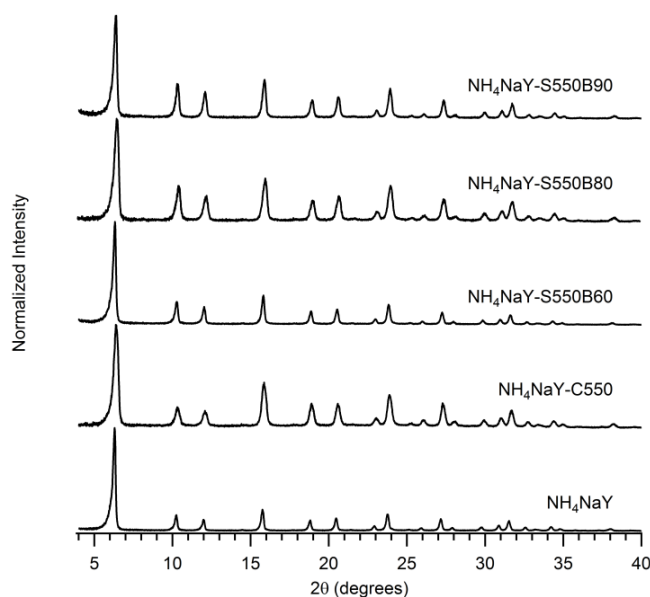


Figure 2-14. Powder XRD patterns of unsteamed NH_4NaY and NH_4NaY samples steamed for 3 h at 550°C in order of increasing steam partial pressure (bottom to top).

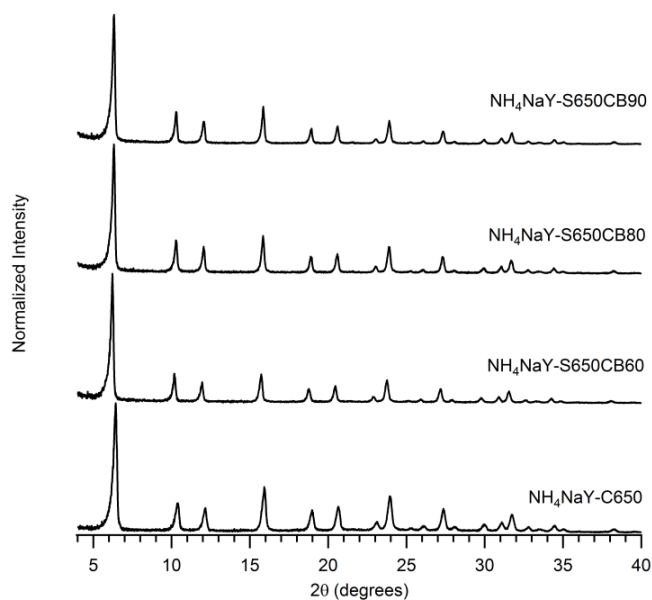


Figure 2-15. Powder XRD patterns of NH_4NaY samples steamed for 3 h at 650°C in order of increasing steam partial pressure (bottom to top).

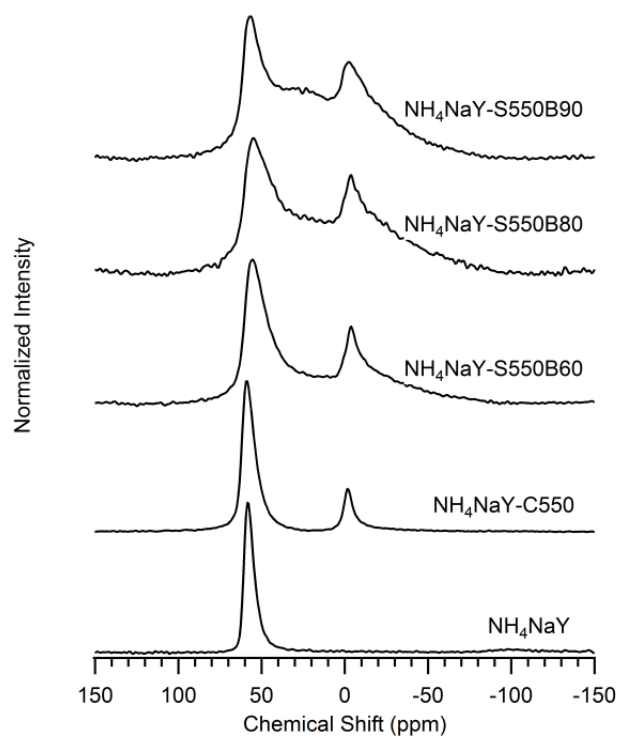


Figure 2-16. ^{27}Al NMR spectra of unsteamed NH_4NaY and NH_4NaY samples steamed for 3 h at 550°C in order of increasing steam partial pressure (bottom to top).

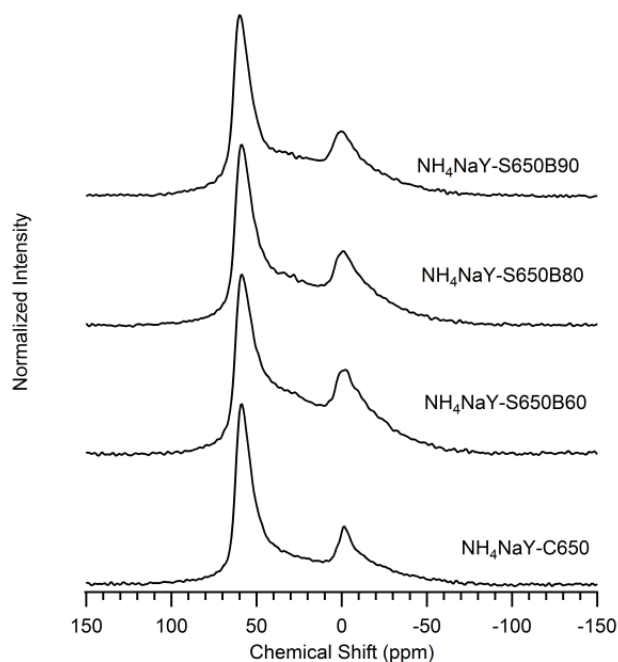


Figure 2-17. ^{27}Al NMR spectra of NH_4NaY samples steamed for 3 h at 650°C in order of increasing steam partial pressure (bottom to top)

The powder XRD patterns and ^{27}Al NMR spectra of the NH_4NaY samples steamed at 800°C are shown in Figures 2-18 and 2-19, respectively. At these conditions, the NH_4NaY samples show increased degradation when the water partial pressure is lowered, with the sample calcined under dry air showing the greatest degradation. The ^{27}Al NMR is consistent with the XRD data in that the amount of pentacoordinated and octahedral aluminum increase relative to the tetrahedral aluminum as the water partial pressure is lowered. This trend is the opposite of what was observed for the 550°C and 650°C steamed NH_4NaY but consistent with the behavior of CHA steamed at 600°C under varying steam partial pressures. The similarity in the behavior of steamed Y compared to CHA at these conditions suggests that the trend of increased degradation with decreasing steam partial pressure is not unique to CHA.

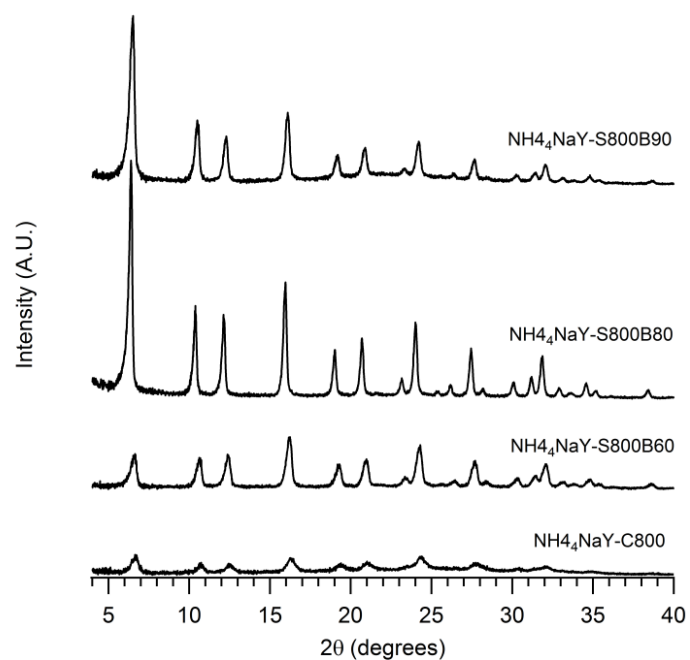


Figure 2-18. Powder XRD patterns of $\text{NH}_4\text{Na-Y}$ samples steamed for 8 h at 800°C in order of increasing steam partial pressure (bottom to top)

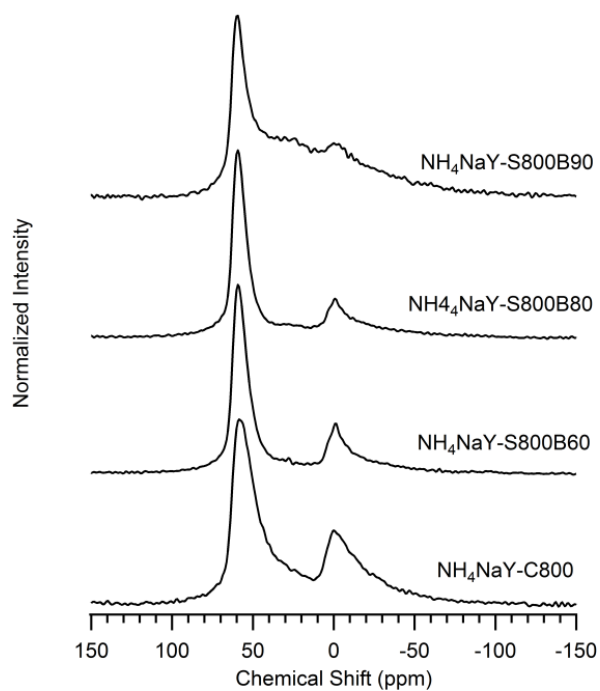


Figure 2-19. ^{27}Al MAS NMR of $\text{NH}_4\text{Na-Y}$ samples steamed for 8 h at 800°C in order of increasing steam partial pressure (bottom to top)

Figures 2-20 and 2-21 show the powder XRD patterns and ^{27}Al MAS NMR, respectively, of the CHA samples steamed at 500°C where steam is introduced at 500°C only. While the powder XRD patterns of the steamed samples are very similar to each other, the ^{27}Al NMR spectra indicate that as the steam partial pressure is increased, an increasing portion of the tetrahedral aluminum is converted to pentacoordinated and octahedral aluminum and is consistent with what was observed for the 550°C and 650°C steamed Y.

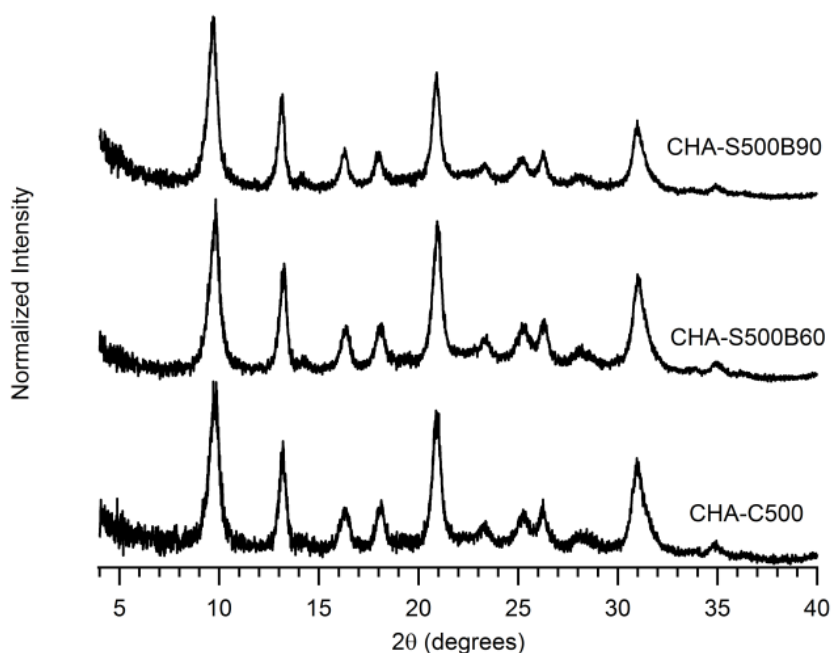


Figure 2-20. Powder XRD patterns of CHA samples steamed for 3 h at 500°C in order of increasing steam partial pressure (bottom to top)

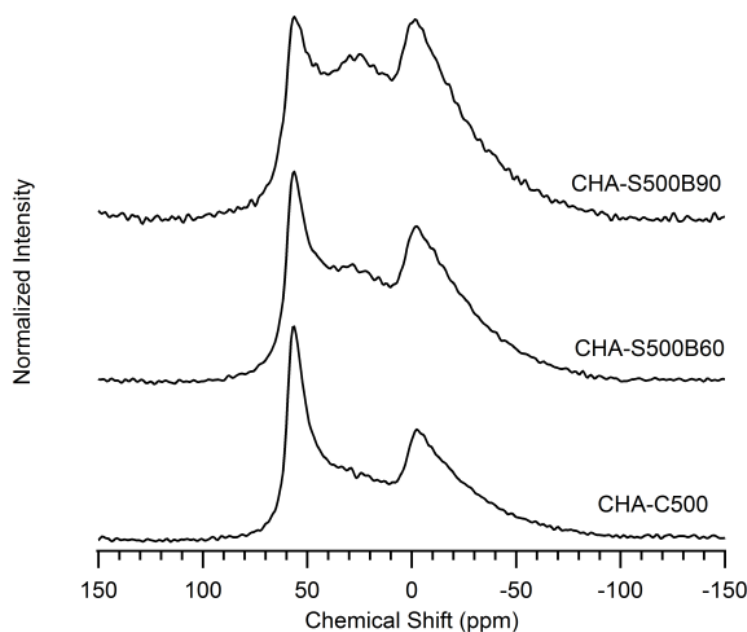


Figure 2-21. ^{27}Al MAS NMR of CHA samples steamed for 3 h at 500°C in order of increasing steam partial pressure (bottom to top)

2.8.4. MTO Reaction Data for Fresh and Regenerated Steamed CHA

An additional batch of steamed CHA was prepared to determine whether the activity could be recovered by regeneration. CHA was steamed for 8 h at 600°C under a steam partial pressure of 47.3 kPa, and a portion of the steamed material was acid washed in the same manner as described in the Experimental section. Reaction testing was conducted using a 10% methanol/inert feed at a WHSV of 1.3 h^{-1} . The reaction profiles at 400°C of the fresh and regenerated 600°C steamed CHA are shown in Figures 2-22 and 2-23, respectively. The activity of the 600°C steamed and acid washed CHA was evaluated over two reaction cycles at 450°C and the reaction profiles are shown in Figures 2-24 and 2-25.

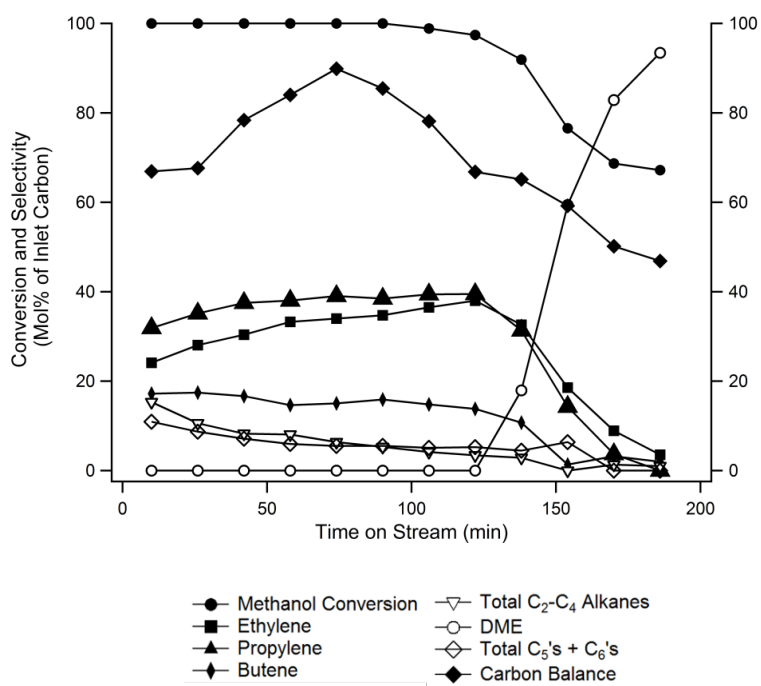


Figure 2-22. MTO reaction data obtained at 400°C for 600°C steamed CHA during the initial reaction run

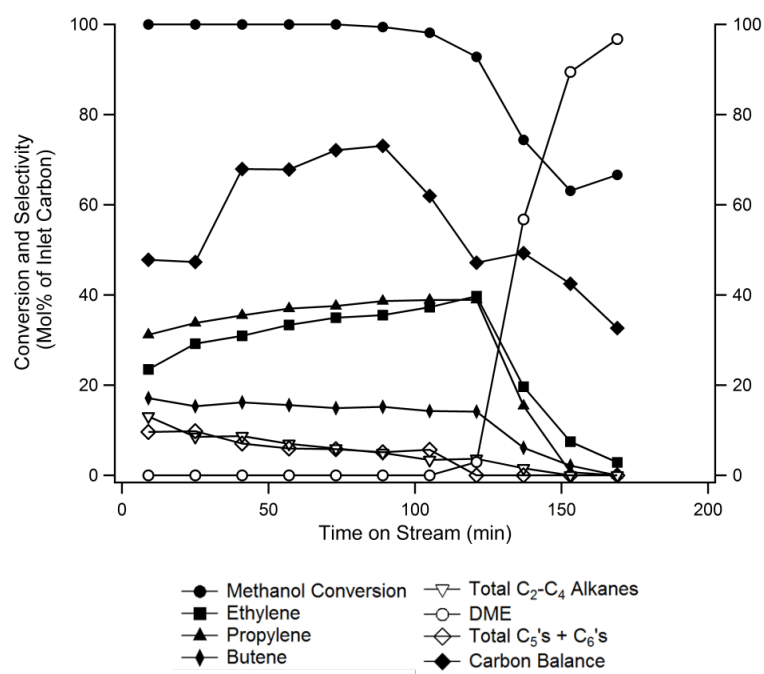


Figure 2-23. MTO reaction data obtained at 400°C for 600°C steamed CHA after regeneration of spent catalyst

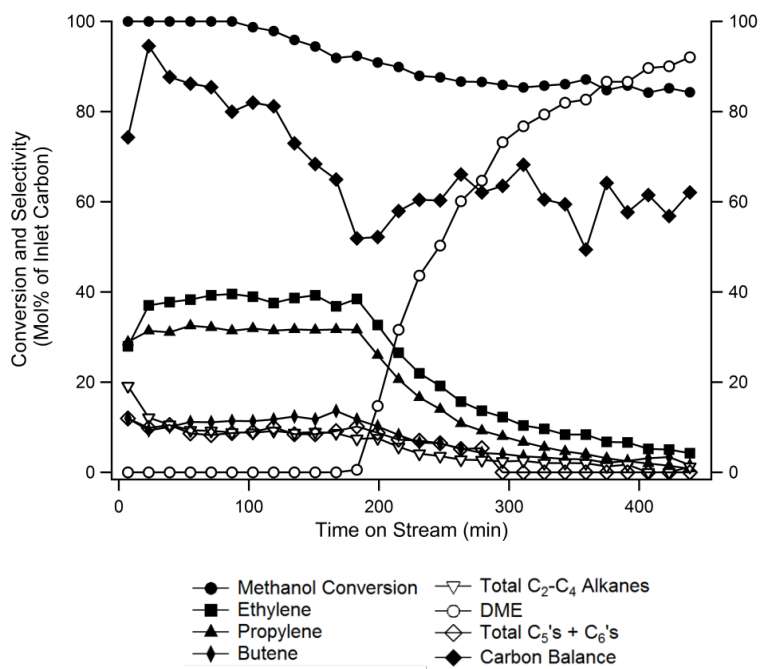


Figure 2-24. MTO reaction data obtained at 450°C for 600°C steamed and acid washed CHA during the initial reaction test

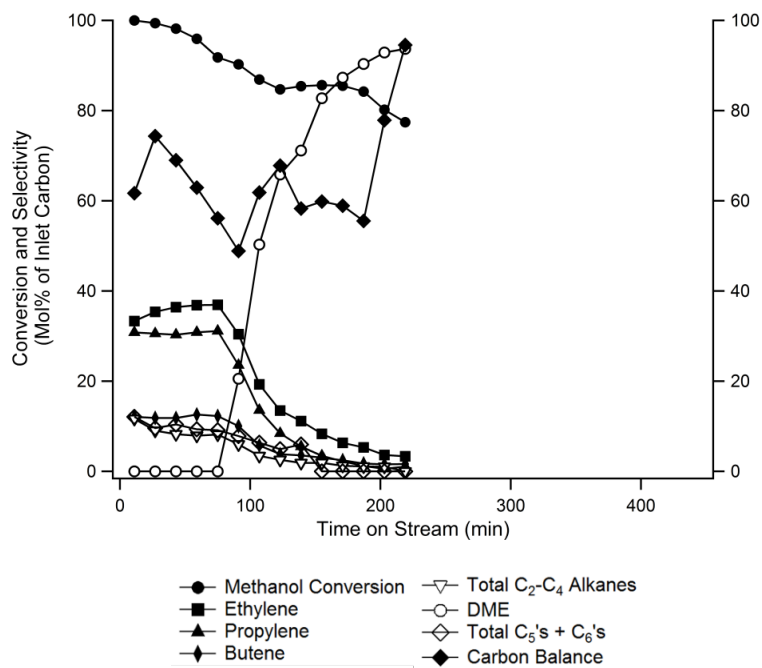


Figure 2-25. MTO reaction data obtained at 450°C for 600°C steamed and acid washed CHA after regeneration of spent catalyst

3. OSDA-free synthesis of RHO and KFI-type zeolite catalysts for methanol-to-olefins

Information in this chapter has been published in: Ji, Y.; Birmingham, J.; Deimund, M.A.; Davis, M.E. Steam-Dealuminated, OSDA-free RHO and KFI-Type Zeolites as Catalysts for the Methanol-to-Olefins Reaction. *Micropor. Mesopor. Mater.* **2016**, 232, 126-137. doi:10.1016/j.micromeso.2016.06.012.

3.1. Abstract

The steam dealumination strategy is extended to two other 8MR zeolites: RHO and KFI. RHO and KFI-type zeolites are synthesized in the absence of organic structure-directing agents (OSDAs), post-synthetically dealuminated via high temperature (600-800°C) steam treatments, and evaluated as catalysts for converting methanol-to-light olefins (MTO). The proton forms of the as-made zeolites deactivate rapidly when tested for the MTO reaction (conducted at 400°C and atmospheric pressure) due to their high aluminum content. Steam treatments lead to improvements in olefin selectivities and catalyst lifetimes with samples steamed at 600°C giving the best combination of lifetime and olefin selectivity. The effects of steaming temperature and partial pressure of water are investigated, and similar trends are observed compared to those for CHA. Zeolite characterizations by ^{27}Al NMR, ^{29}Si NMR and argon physisorption indicate that the steam

treatments extract framework aluminum, leading to reductions in the total number of Brønsted acid sites and the creation of mesopores that can facilitate transport of reactants.

3.2. Introduction

Ethylene and propylene are key components of the petrochemical industry that are currently obtained primarily from cracking of naphtha. The methanol-to-olefins (MTO) reaction provides a route for producing these light olefins from non-petroleum feedstocks such as natural gas, coal or biomass. Microporous molecular sieves with Brønsted acidity, *i.e.*, aluminosilicates (zeolites) and silicoaluminophosphates (SAPOs), can be used to catalyze the conversion of methanol into light olefins. Among these materials, SAPO-34, a microporous SAPO molecular sieve with the chabazite (CHA) topology, is currently utilized in commercial MTO plants in China¹.

Molecular sieves with frameworks containing cages that have limiting pore sizes consisting of 8 tetrahedral atoms (8MR pores) possess the appropriate shape selectivity for MTO.² The pores of 8MR frameworks (typically 0.35-0.45 nm in diameter) allow small molecules such as methanol and linear alkenes to diffuse through the cages while restricting larger branched and aromatic species that may form. These cages also stabilize polymethylated benzene intermediates that act as a hydrocarbon pool for continuous methanol addition and olefin elimination.³⁻⁵

Zeolites with high Si/Al ratios are desirable for catalysis requiring Brønsted acidity as high aluminum zeolites possess poor acidity and hydrothermal stability. Researchers have explored direct syntheses of small-pore zeolites at high Si/Al ratios,⁶⁻¹¹ but the

materials typically utilize organic structure-directing agents (OSDAs) in order to facilitate low framework charges. The use of these organic molecules has drawbacks such as high cost¹² that typically cannot be recovered as they are removed via combustion prior to use. An incentive therefore exists to develop low-cost catalyst preparation methods without the use of OSDAs. While various zeolites can be synthesized in the absence of OSDAs, the resulting materials typically have Si/Al ratios that are too low to be of use for catalytic applications requiring Brønsted acidity. However, it may be possible to post-synthetically remove framework aluminum and thus modify the acidity of the materials.

We have recently explored a post-synthetic dealumination strategy to convert high aluminum 8MR zeolites that are prepared without the use of OSDAs into useful catalysts for MTO and demonstrated the preparation method with CHA-type zeolites.¹³ CHA was synthesized in the absence of OSDAs at a Si/Al ratio of 2.4, steam-treated to extract a portion of the framework aluminum and evaluated for MTO. While the as-made CHA deactivated quickly due to the high aluminum content, the dealuminated samples showed increased olefin selectivities and lifetimes. The results were attributed to a reduction in the number of Brønsted acid sites and the introduction of mesopores that increase the reactant accessibility to the remaining acid sites.

The results obtained with CHA suggest that the preparation method used is broadly applicable to any 8MR zeolite that can be synthesized without using OSDAs. Here, we show that two additional high-aluminum 8MR zeolites prepared in the absence of OSDAs, zeolite rho (RHO) and ZK-5 (KFI), can also be dealuminated by steam treatments to make them active for MTO. The RHO framework has a three-dimensional channel system

consisting of cubic *lta* cages whose faces are connected with each other via double 8-rings (pore size 0.36 x 0.36 nm).¹⁴ Zeolite ZK-5 (pore size 0.39 x 0.39 nm)¹⁴ also possesses a three-dimensional channel system consisting of alternating 8MR *lta* and *paulingite* cages that are connected via shared 8-ring faces. These two zeolites can be synthesized in the absence of OSDAs using alkali hydroxides and have been previously explored for the synthesis of methylamines.¹⁵ However, neither material has been evaluated for MTO because of their high aluminum content in the as-synthesized form.

3.3. Experimental Section

3.3.1. RHO and KFI Syntheses

RHO- and KFI-type zeolites were synthesized following methods described in the patent literature.^{16,17} For RHO, a synthesis gel was prepared with molar composition $0.3 \text{ Na}_2\text{O} / 0.1 \text{ Al}_2\text{O}_3 / 1 \text{ SiO}_2 / 0.04 \text{ Cs}_2\text{O} / 8\text{H}_2\text{O}$. In a typical synthesis, 1.78 g of alumina (Catapal B) source was dissolved in a solution containing 3.17 g NaOH (Mallinckrodt pellets) and 4.67 g water and heated at 110°C until a clear solution formed. 3.2 g of CsOH (Aldrich 50 wt% aqueous solution) was then added followed by 20 g colloidal silica (Ludox HS-40). The reaction mixture was covered and stirred for 72 h at room temperature, transferred to a Teflon-lined autoclave, and heated for 1-3 days at 100°C. The crystallized product was recovered by centrifugation, washed with water followed by acetone and dried overnight at 100°C.

KFI was prepared from a synthesis gel with molar composition $0.24 \text{ K}_2\text{O} / 0.167 \text{ Al}_2\text{O}_3 / 1 \text{ SiO}_2 / 0.030 \text{ Cs}_2\text{O} / 7.5 \text{ H}_2\text{O}$. In a typical synthesis, 3.295 g of $\text{Al}(\text{OH})_3$ (JT Baker)

was added to a solution of 3.825 g KOH (Macron pellets) and 1.396 g CsOH·H₂O (Aldrich powder) in 2 g water. The mixture was heated at 110°C until a clear solution formed and 25 g of colloidal silica (Ludox LS-30) was added. The gel was stirred until homogenous, transferred to a Teflon-lined autoclave and heated at 100°C for 4.5 days. The product was recovered by centrifugation, washed extensively with water followed by acetone, and dried overnight at 100°C.

3.3.2. Steam Treatments

Prior to steaming, the as-synthesized zeolites were ion-exchanged into the NH₄⁺ form by exchanging three times with 1 M ammonium nitrate aqueous solution (100 mL liquid per gram of solid) for 2 h at 90°C. The solids were recovered by centrifugation, washed with water followed by acetone, and dried overnight at 100°C. Steaming was

Table 3-1. Summary of RHO and KFI steaming conditions and Si/Al ratios

Entry	Sample	Steaming Conditions		Si/Al Bulk	Si/Al _T ^a
		Steaming Temperature ^a	Water Saturator Temperature		
1	NH ₄ -RHO	-	-	2.8	2.8
2	RHO-S600B80	600°C	80°C	3.2	25
3	RHO-S700B80	700°C	80°C	3.2	27
4	RHO-S800B80	800°C	80°C	3.2	27
5	RHO-S800B60	800°C	60°C	3.1	39
6	RHO-S800B90	800°C	90°C	3.1	32
7	RHO-C800	800°C	Dry Calcined	-	-
8	NH ₄ -KFI	-	-	3.1	3.1
9	KFI-S600B80	600°C	80°C	3.1	17
10	KFI-S700B80	700°C	80°C	3.2	23
11	KFI-S800B80	800°C	80°C	3.0	35

^a Calculated from ²⁷Al NMR and bulk Si/Al, Al_T denotes tetrahedral Al only

conducted in a horizontal tube furnace (MTI OTF-1200X) under a flowing mixture of steam and air that was generated by bubbling zero-grade air (50 cc/min) through a water saturator held at 80°C upstream of the sample. Samples were exposed to flowing steam and heated at 1°C/min to the desired steaming temperature (600, 700 or 800°C) and held there for 8 h. An additional series of steaming experiments were conducted with RHO where samples were steamed for 8 h at 800°C under different steam partial pressures that were varied by changing the bubbler temperature (60, 80 or 90°C). Table 3-1 provides a summary of the steaming conditions for RHO and KFI.

3.3.3. Characterizations

Powder X-ray diffraction (XRD) patterns were obtained on a Rigaku MiniFlex II instrument with Cu K α radiation ($\lambda = 1.54184$ Å) at a sampling window of 0.01° and scan speed of 0.3°/min. Powder patterns were normalized to the highest intensity peak. Bulk elemental analysis was conducted by energy dispersive spectroscopy (EDS) on a ZEISS 1550VP instrument equipped with an Oxford X-Max SDD.

Solid-state ^{27}Al were acquired on a Bruker DSX 500 MHz spectrometer. ^{27}Al NMR spectra were recorded with the spectrometer operating at 130.3 MHz using a 90° pulse length of 6 μs , a recycle time of 2 s, and a spinning rate of 12 kHz. Samples were hydrated overnight over a saturated KCl solution and loaded in a 4 mm ZrO₂ rotor. Chemical shifts were referenced to 1 M aqueous aluminum nitrate solution. Solid-state ^{29}Si MAS NMR spectra were acquired on a Bruker Avance 200 MHz spectrometer operated at 39.78 MHz with ^1H decoupling. Spectra were recorded using a 90° pulse length of 4 μs and a cycle delay time of 60 s, and a spinning rate of 4 kHz. Samples were loaded in a 7 mm ZrO₂

rotor, and chemical shifts were referenced to tetramethylsilane. Reported spectra are scaled to the same maximum intensity.

Argon physisorption was conducted on a Quantachrome Autosorb iQ instrument. Prior to adsorption measurements, samples were outgassed by heating (at a rate of 1°C/min) the sample under vacuum for 0.5 h at 60°C, 0.5 h at 120°C and 5 h at 350°C. Adsorption isotherms were collected using argon at 87.45 K using the constant dose (quasi-equilibrium) method. Micropore volumes were obtained from the adsorption branch of the isotherms using the t-plot method ($0.1 < P/P_0 < 0.3$). Pore size analyses were obtained from the adsorption branches using the nonlocal density functional theory (NLDFT) model provided by Quantachrome's data reduction software (modeling Ar at 87 K on a zeolite with cylindrical pores).

3.3.4. MTO Reaction Testing

Catalysts for reaction testing were crushed and sieved to obtain particles between 0.15 mm and 0.6 mm. Approximately 200 mg of the sieved catalyst was supported between quartz wool beds in a tubular, continuous flow reactor (Autoclave Engineers BTRS, Jr. SS-316). Samples were calcined in-situ by heating (at a rate of 1°C/min) for 3 h at 150°C and then 12 h at 580°C under a flow of breathing-grade air. Reactions were conducted at 400°C and atmospheric pressure with a feed of 10% methanol in inert (5% Ar, bal. He) pumped at a WHSV of 1.3 h⁻¹. Effluent gases were monitored by an on-stream GC/MS (Agilent 6890/MSD5793N). Methanol conversion, product selectivities and carbon balances are reported on a carbon mole basis and calculated as previously described (Equations 2-1 through 2-3).

3.4. Results and Discussion

3.4.1. Effects of Steaming Temperature

The as-made RHO and KFI have Si/Al ratios of 2.8 and 3.1, respectively. In order to extract aluminum from their frameworks, the zeolites were NH_4^+ exchanged and steamed at temperatures of 600, 700 or 800°C. Figures 3-1 and 3-2 show the PXRD patterns of the as-synthesized (NH_4 form) and the RHO and KFI samples steamed at 600-800°C with the bubbler held at 80°C (water vapor pressure of 47.3 kPa). At steaming temperatures up to 800°C, the crystallinity of the RHO sample is still preserved. An x-ray amorphous material was obtained when RHO was steamed at 850°C (not shown). The steamed KFI samples show good crystallinity up to a steaming temperature of 700°C. Steaming of KFI at 800°C

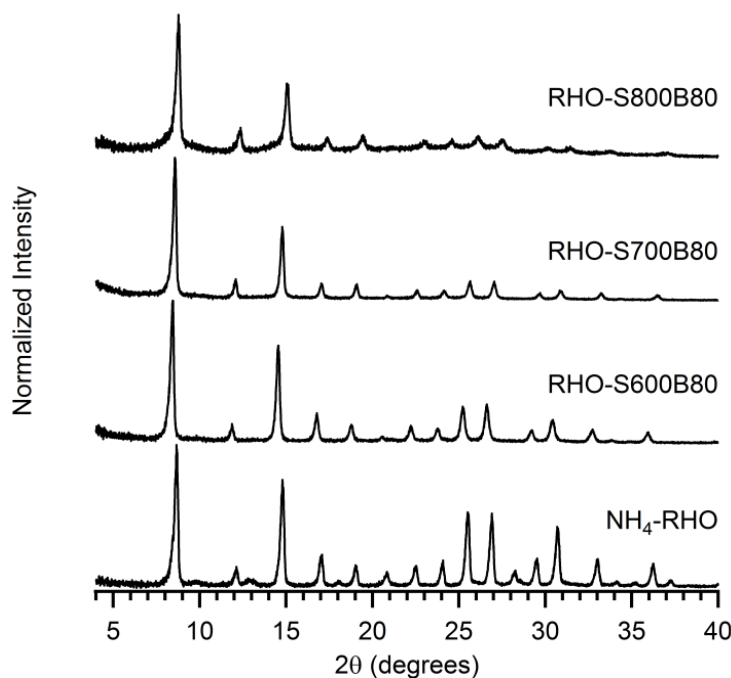


Figure 3-1. Powder XRD patterns of as-synthesized and 600, 700 and 800°C steamed RHO (bottom to top)

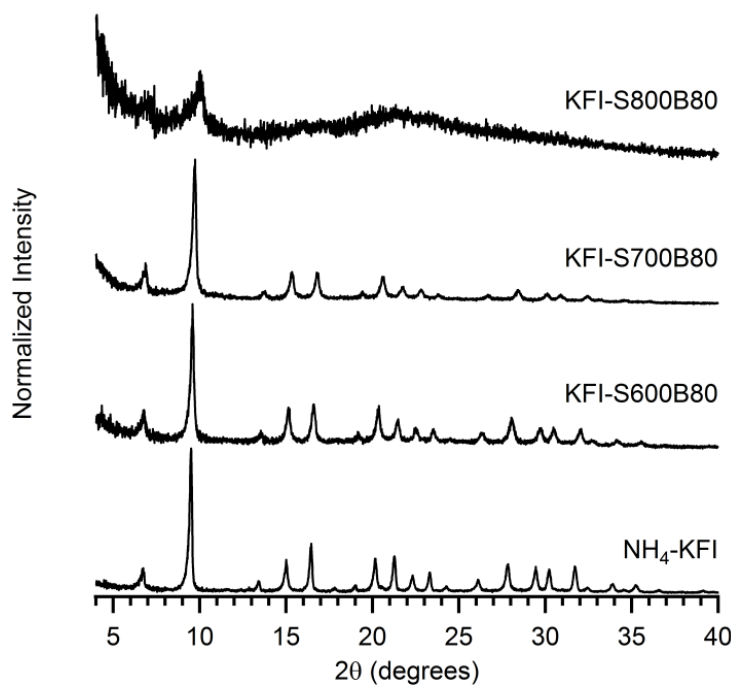


Figure 3-2. Powder XRD patterns of as-synthesized and 600, 700 and 800°C steamed KFI (bottom to top)

produced an X-ray amorphous material (this sample was not further characterized). With increasing steaming temperature, peaks are shifted further to lower d-spacings, consistent with a decreasing unit cell size due to decreasing framework aluminum in the zeolites.

Evidence for extraction of framework aluminum is provided by the ^{27}Al and ^{29}Si MAS NMR spectra of the materials (Figures 3-3 through 3-6). The ^{27}Al MAS NMR spectra of the as-made materials show that all of the aluminum is in tetrahedral (framework) coordination (Figures 3-3 and 3-4). After steaming, the samples show additional peaks at approximately 30 and 0 ppm, which are assigned to penta-coordinated and octahedrally-coordinated aluminum. The results of the ^{27}Al NMR and bulk Si/Al ratios (measured by

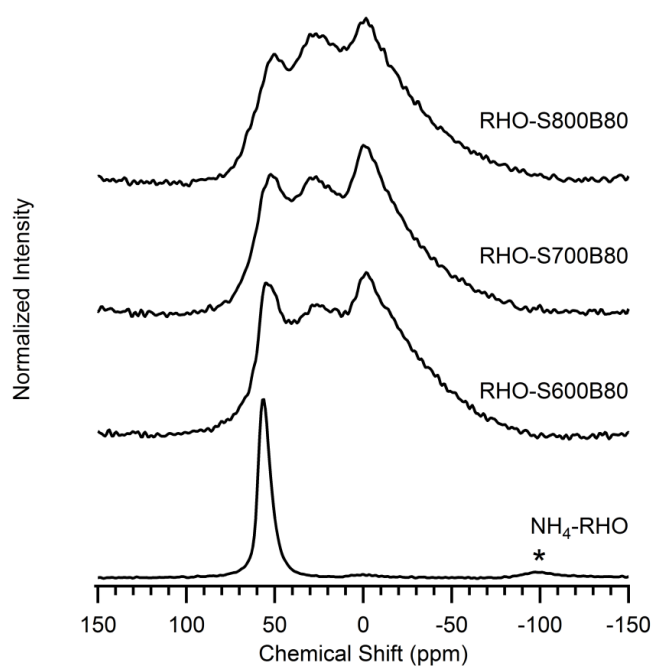


Figure 3-3. ^{27}Al NMR spectra of as-synthesized and 600-800°C steamed RHO (bottom to top) * denotes spinning sideband.

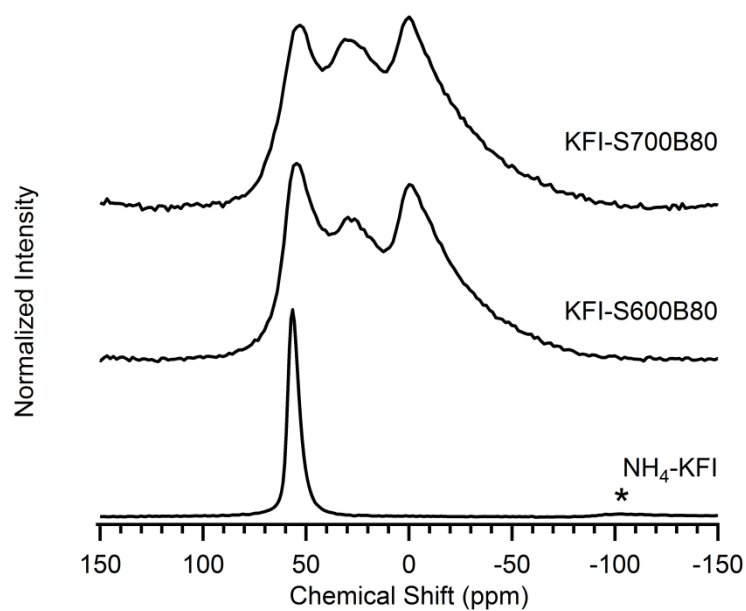


Figure 3-4. ^{27}Al NMR spectra of as-synthesized and 600-700°C steamed KFI (bottom to top) * denotes spinning sideband

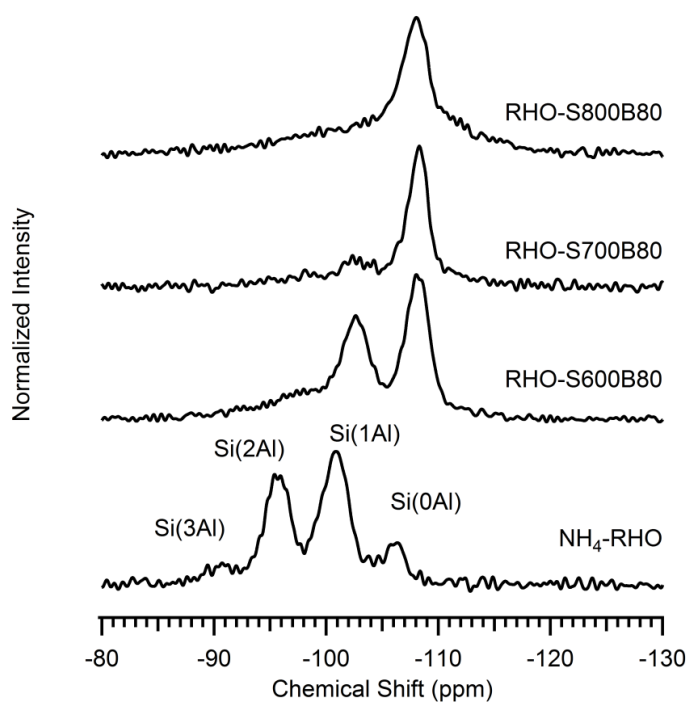


Figure 3-5. ^{29}Si NMR spectra of as-synthesized and 600-800°C steamed RHO (bottom to top)

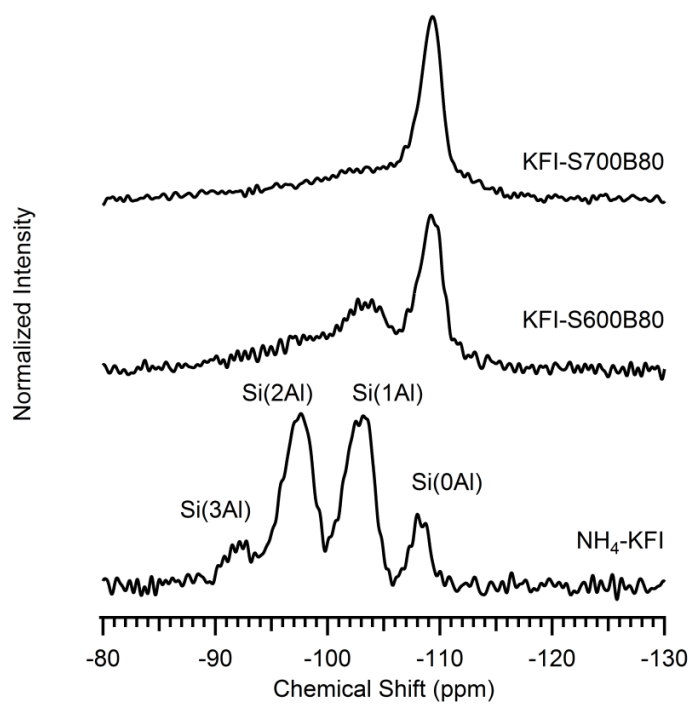


Figure 3-6. ^{29}Si NMR spectra of as-synthesized and 600-800°C steamed KFI (bottom to top)

EDS) were used to estimate the silicon to tetrahedral aluminum ratios ($\text{Si}/\text{Al}_\text{T}$) of the steamed samples (Table 3-1), that ranged from 25-27 for the steamed RHO samples and 17-23 for the steamed KFI samples. The ^{29}Si NMRs (Figures 3-5 and 3-6) show that the signals associated with SiO_4 tetrahedra coordinated to AlO_4 tetrahedra ($\text{Si}(1\text{Al})$, $\text{Si}(2\text{Al})$ and $\text{Si}(3\text{Al})$ located at approximately -107, -98 and -92 ppm, respectively) decrease significantly while the signal associated with $\text{Si}(0\text{Al})$ (approximately -112 ppm) increases in intensity after steaming, suggesting that there is increasingly less aluminum coordinated to the framework silicon.

Changes to the accessible pore volume were characterized by Ar physisorption at 87 K. Figures 3-7 and 3-8 shows the full adsorption and desorption isotherms of the steamed RHO and KFI samples, respectively. In both cases, steaming leads to a reduction in the accessible micropore volume (Figures 3-7A and 3-8A insets) due to partial structural collapse. As with CHA, the micropore volumes decrease with increasing steaming temperature (Table 3-2).

Table 3-2. Micropore volumes of RHO and KFI samples

Sample	Micropore Volume (cc/g)
H-RHO	0.26
RHO-S600B80	0.18
RHO-S700B80	0.096
RHO-S800B80	0.059
RHO-S800B90	0.051
RHO-S800B60	0.033
H-KFI	0.18
KFI-S600B80	0.13
KFI-S700B80	0.062

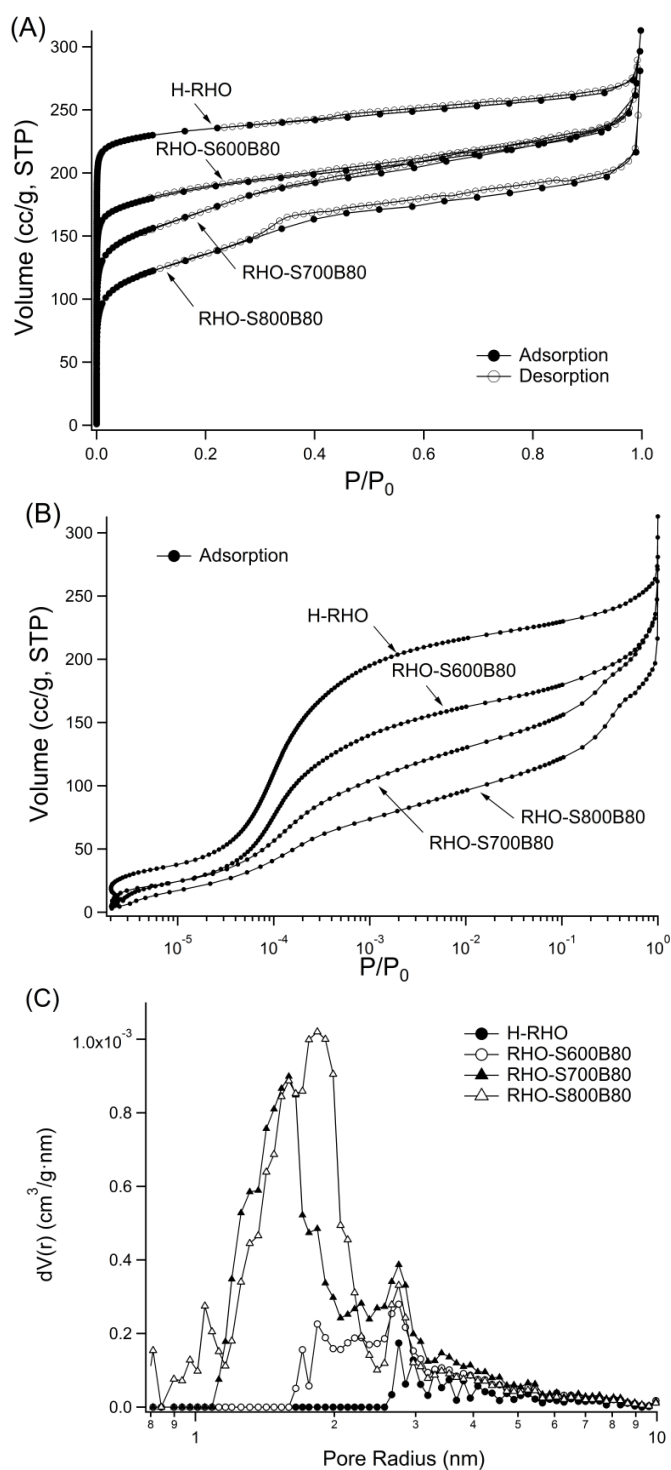


Figure 3-7. (A) Ar physisorption isotherms of the as-synthesized and steamed RHO samples, (B) adsorption isotherms in the micropore filling region and (C) NLDFT pore size distributions plotted on a semi-logarithmic scale

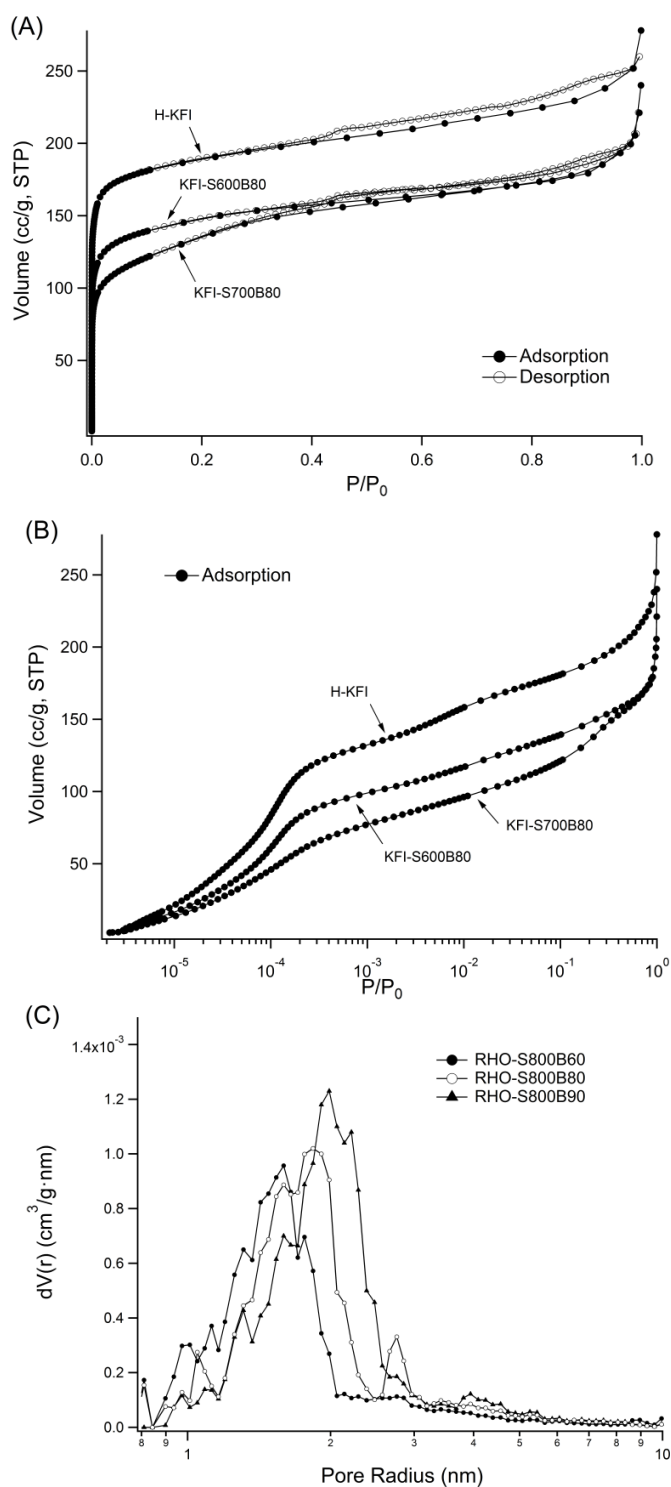


Figure 3-8. (A) Ar physisorption isotherms of the as-synthesized and steamed KFI samples, (B) adsorption isotherms in the micropore filling region and (C) NLDFT pore size distributions plotted on a semi-logarithmic scale

Pore size distribution analyses were performed using the NLDFT method on the adsorption branch of the isotherms, and the mesopore range of the distributions is shown in Figures 3-7C and 3-8C. In contrast to the unsteamed H-RHO, the steamed RHO samples show an increasingly greater contribution from pores of approximately 2-5 nm in diameter with increasing steaming temperature, while contributions in this range are not seen in the unsteamed H-RHO. Similarly for KFI, an increasing contribution from pores with diameter 2-4 nm is observed as the steaming temperature is increased from 600 to 700°C that are greater than what is observed for the H-KFI. These data suggest that mesopores are introduced during the steam treatments and that their contribution increases with the severity of steaming.

As with CHA, we attempted to remove the extra-framework aluminum from the steamed RHO and KFI samples via acid washing treatments. A summary of the treatment conditions and characterizations are provided in the supporting information Table 3-4 and Figures 3-16 through 3-21. ^{27}Al NMR spectra of the acid washed materials showed that while there was a small decrease in the peak corresponding to penta-coordinated aluminum, a significant amount of octahedral aluminum still remained after acid treatment. One possibility for the difference in acid washing results seen for RHO and KFI compared to CHA is that the extra-framework aluminum species in RHO and KFI may be located in regions that do not accommodate diffusion of hydrated alumina. Although Ar physisorption data indicate that mesoporosity is generated in the steamed materials, there may be additional isolated cavities that are inaccessible and thus limits the amount of extra-framework aluminum that can be removed.

3.4.2. Effects of Steam Partial Pressure

Previously, it was observed for CHA that lowering the steam partial pressure during steaming leads to increased degradation (Chapter 2). This trend was attributed to the presence of water during the initial heating period that helped stabilize the framework. To verify whether this behavior is also seen in another 8MR zeolite, a series of experiments was carried out with RHO where samples were steamed for 8 h at 800°C under varying steam partial pressures (water saturator temperatures of 60, 80 and 90°C).

Figure 3-9 shows the powder XRD patterns of the RHO samples steamed under varying steam partial pressures. The samples steamed with the water saturator held at 80°C and 90°C (corresponding to steam partial pressures of 47.3 kPa and 70.1 kPa, respectively) are very similar to each other, as with CHA. However, lowering the bubbler temperature from 80°C to 60°C (17.7 kPa of steam) results in increased structural degradation. Like CHA, dry calcination of NH₄-RHO in air for 8 h at 800°C results in essentially an X-ray amorphous material.

As with the CHA samples, the ²⁷Al NMR spectra of the steamed samples do not show significant differences in the relative intensities of the tetrahedral, pentacoordinated, and hexacoordinated aluminum signals. On the other hand, the ²⁹Si NMR spectra of the samples (Figure 3-11) show a large peak centered at approximately -105 ppm that corresponds to Si(0Al) and overlaps with smaller upfield peaks. With increasing steam partial pressure, an increasing portion of the silicon exists in the Si(0Al) environment.

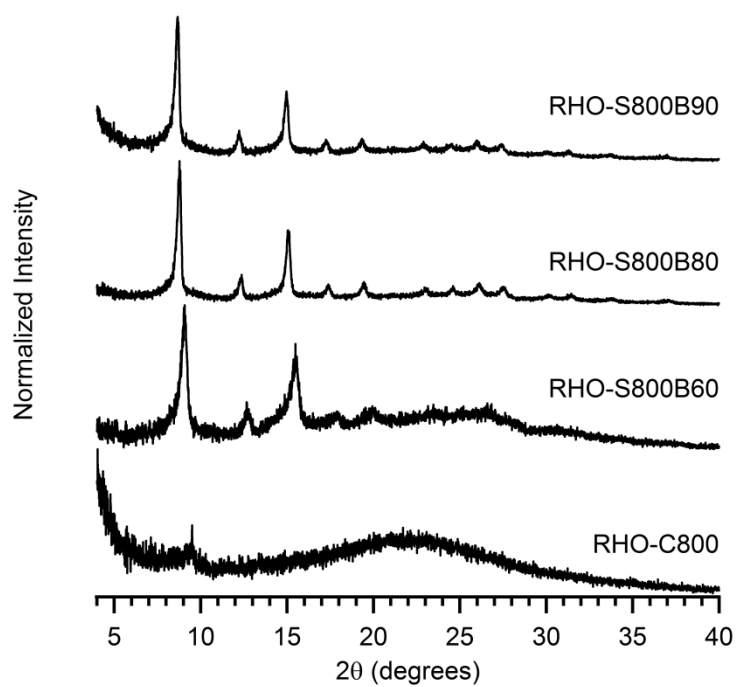


Figure 3-9. Powder XRD patterns of RHO steamed at 800°C under increasing steam partial pressures (bottom to top)

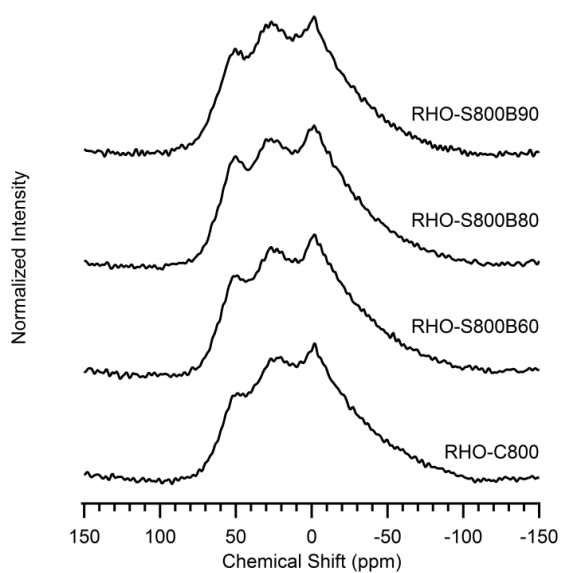


Figure 3-10. ^{27}Al NMR spectra of RHO steamed at 800°C under increasing steam partial pressures (bottom to top)

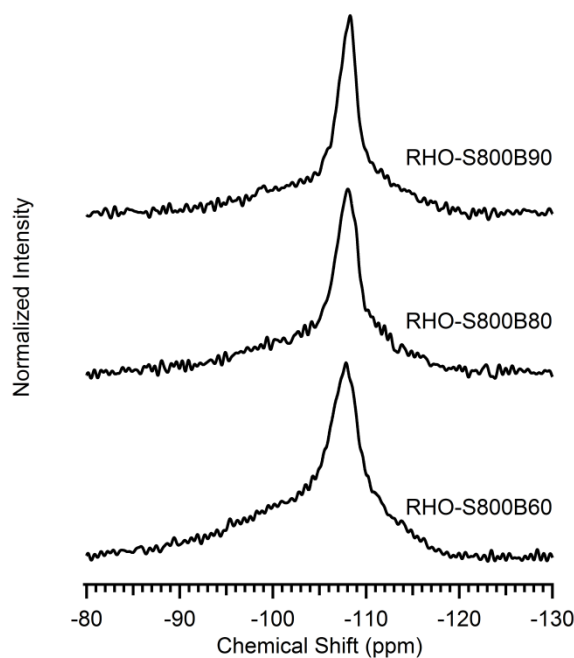


Figure 3-11. ^{31}Si NMR spectra of RHO steamed at 800°C under increasing steam partial pressures (bottom to top)

The Ar physisorption isotherms (Figure 3-12A and 3-12B) indicate that the sample steamed with the water saturator held at 60°C (RHO-S800B60) also has the lowest accessible micropore volume (0.34 cc/g), while the sample steamed with the water saturator at 80°C had the highest accessible micropore volume (0.59 cc/g). Increasing the water saturator temperature to 90°C results in a slightly lower micropore volume of 0.51 cc/g, a trend that was also observed with CHA. The pore size distributions (Figure 3-12C) shows that with increasing steam partial pressure, the range of pore diameters estimated for the mesopores increases slightly. The increased degradation at lower steam partial pressures observed here are consistent with those for CHA and zeolite Y, providing further indication that this is a general trend and not unique to any one 8MR zeolite.

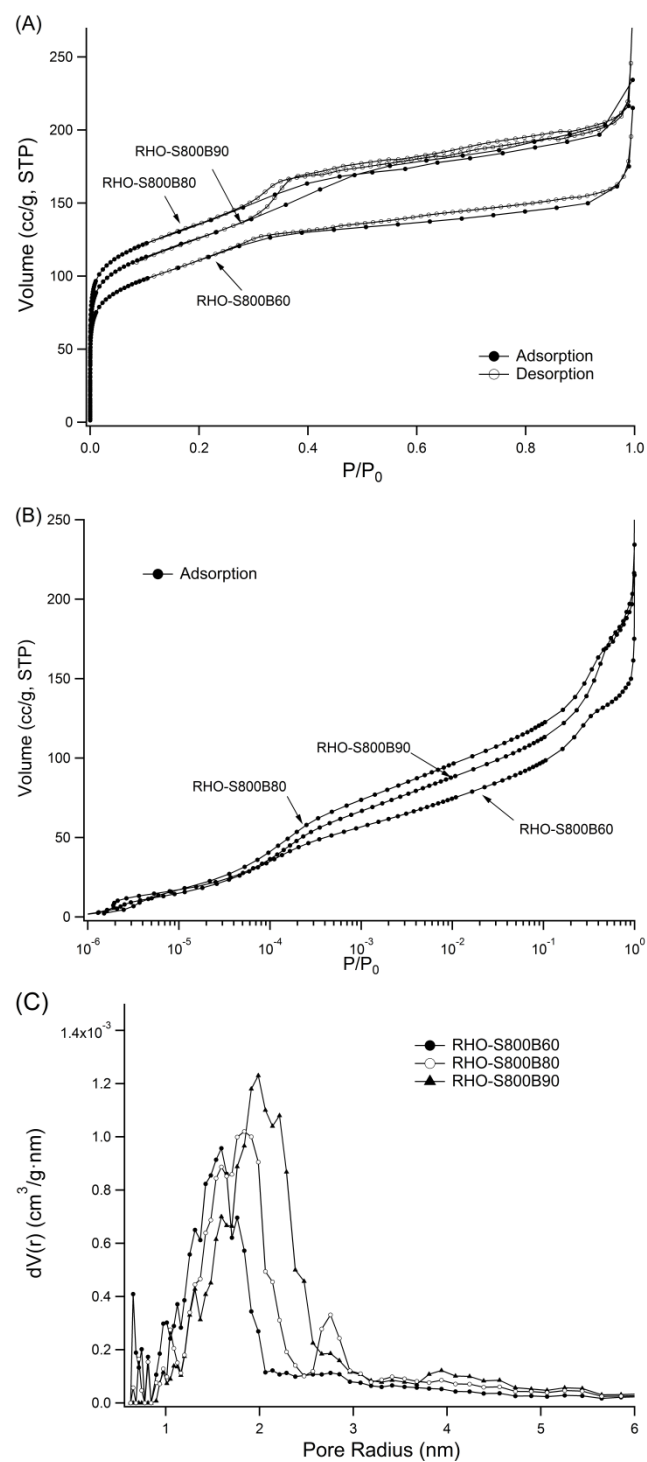


Figure 3-12. Ar physisorption isotherms of the 800°C steamed RHO samples under varying steam partial pressures (A) full isotherms, (B) adsorption isotherms plotted on a log scale and (C) NLDFT pore size distributions

3.4.3. MTO Reaction Testing

3.4.3.1. Effects of steaming temperature

The as-made and steamed zeolites were evaluated as catalysts for the MTO reaction at 400°C and atmospheric pressure, and the time-on-stream reaction profiles are shown in Figures 3-13 and 3-14. The maximum conversions, combined ethylene and propylene selectivities and catalyst lifetimes are summarized in Table 3-3. All of the catalysts tested initially convert methanol at or close to 100%. In addition to C₂-C₄ olefins, C₃-C₅ alkanes (mainly propane), and dimethylether (DME) are also observed in the product

Table 3-3. Maximum combined C₂-C₃ olefin selectivities near complete conversion, and deactivation times of RHO and KFI catalysts tested

Sample	Reaction Temperature	Maximum MeOH Conversion	Combined C ₂ -C ₃ Olefin Selectivity at Max. MeOH Conversion	Time to Deactivation ^a
H-RHO	400°C	100%	43.3%	64 min (1.3 g MeOH/g cat)
RHO-S600B80	400°C	100%	51.6%	125 min (2.6 g MeOH/g cat)
RHO-S700B80	400°C	100%	54.8%	112 min (2.3 g MeOH/g cat)
RHO-S800B80	400°C	96.6%	59.6%	88 min (1.8 g MeOH/g cat)
RHO-S800B80	350°C	91.9%	48.0%	42 min (0.87 g MeOH/g cat)
RHO-S800B80	450°C	100%	66.2%	105 min (2.2 g MeOH/g cat)
H-KFI	400°C	99.7%	44.7%	52 min (1.0 g MeOH/g cat)
KFI-S600B80	400°C	99.6%	51.6%	80 min (1.7 g MeOH/g cat)
KFI-S700B80	400°C	99.3%	52.6%	75 min (1.5 g MeOH/g cat)

^a First time point where conversion drops below 80%

stream. The most prominent changes observed after steaming are an increase in the catalyst lifetime (quantified by comparing the first time point where conversion drops below 80%) and increases in the ethylene and propylene selectivities.

The as-made H-RHO (Figure 3-13A) reaches a maximum combined ethylene and propylene selectivity of 43.3% at 100% conversion but, due to its high aluminum content ($\text{Si/Al} = 2.8$), deactivates rapidly after approximately 64 min (1.3 g MeOH/g cat), after which dimethylether (DME) becomes the main product. Steaming produces catalysts with more stable reaction profiles that depend upon the severity of steaming. RHO steamed at 600°C converts methanol at above 80% for approximately 125 min TOS (2.6 g MeOH/g cat) and reaches a maximum combined ethylene and propylene selectivity of 51.6% at 100% conversion. This sample had the best combination of lifetime and olefin selectivity.

Steaming at higher temperatures (700 and 800°C) produces catalysts with slightly increased ethylene and propylene selectivities, but conversion starts to decrease more quickly (conversion first drops below 80% after approximately 112 and 80 min TOS for RHO-S700B80 and RHO-S800B80, respectively). RHO steamed at 800°C had the highest olefin selectivity (maximum combined $\text{C}_2=$ and $\text{C}_3=$ selectivity of 59.6% at 96.6% conversion) but also deactivated the fastest among the steamed samples.

A similar trend is observed for KFI (Figure 3-14). The unsteamed H-KFI ($\text{Si/Al}=3.1$) deactivates rapidly (after approximately 52 min TOS or 1.0 g MeOH/g cat) and reaches a maximum combined ethylene and propylene selectivity of 44.7% at 99.7% conversion. As with CHA and RHO, higher methanol conversion capacities and olefin

selectivities are observed after steam treatment. KFI steamed at 600°C reaches a maximum combined $C_2=$ and $C_3=$ selectivity of 51.6% at 99.6% conversion, and methanol conversion stays above 80% for 80 min TOS (1.7 g MeOH/g cat). Olefin selectivities are increased slightly for KFI steamed at 700°C (maximum combined $C_2=$ and $C_3=$ selectivity was 52.6% for KFI-S700B80), but as with the other steamed zeolites, deactivation also occurs more quickly.

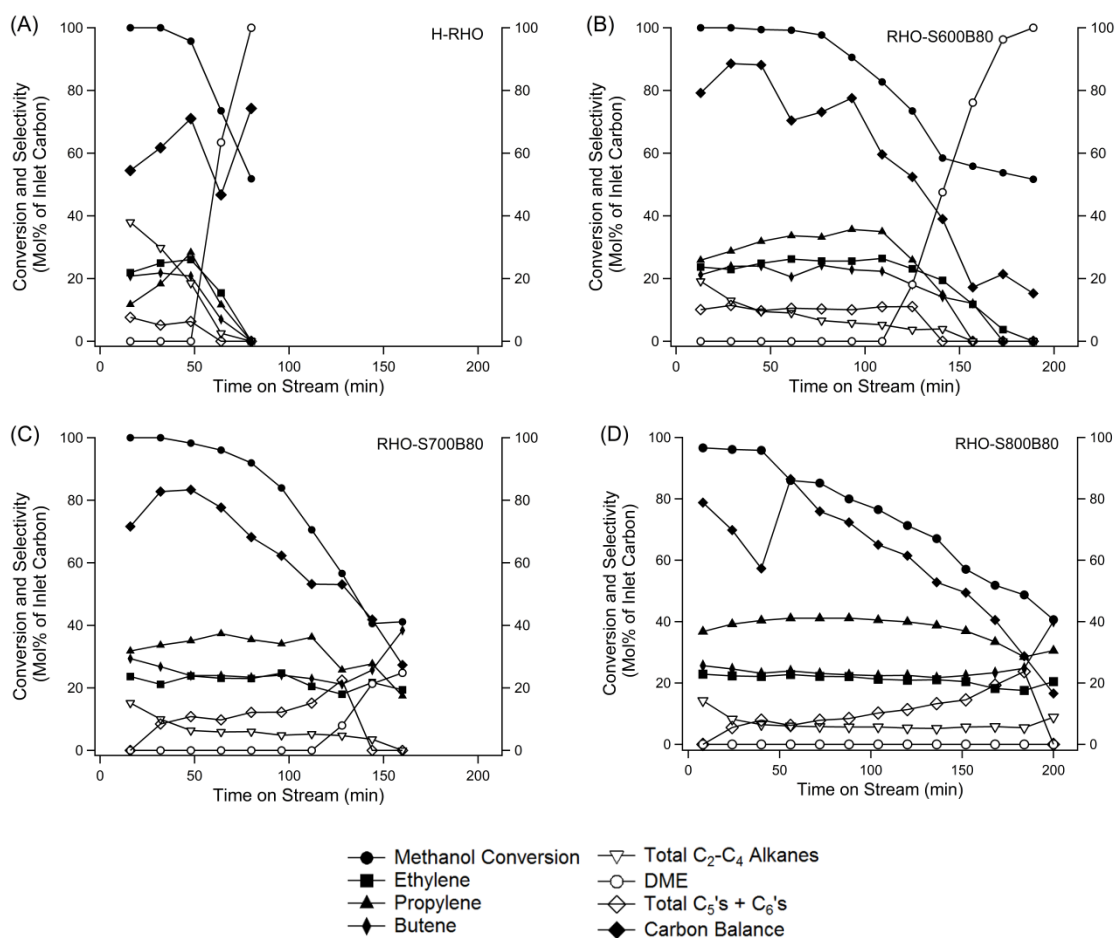


Figure 3-13. MTO reaction data obtained at 400°C for (A) as-synthesized, (B) 600°C steamed, (C) 700°C steamed and (D) 800°C steamed RHO samples.

The fast deactivation of the as-made H-RHO and H-KFI can be attributed to the high framework acid site density of the materials that lead to quick coke deposition. After steaming at 600°C, the framework aluminum content decreases (the estimated Si/AlT ratios are 25 and 17 for the RHO-S600 and KFI-S600, respectively), leading to increased olefin selectivities and lifetimes. The presence of mesopores after steam treatment of these

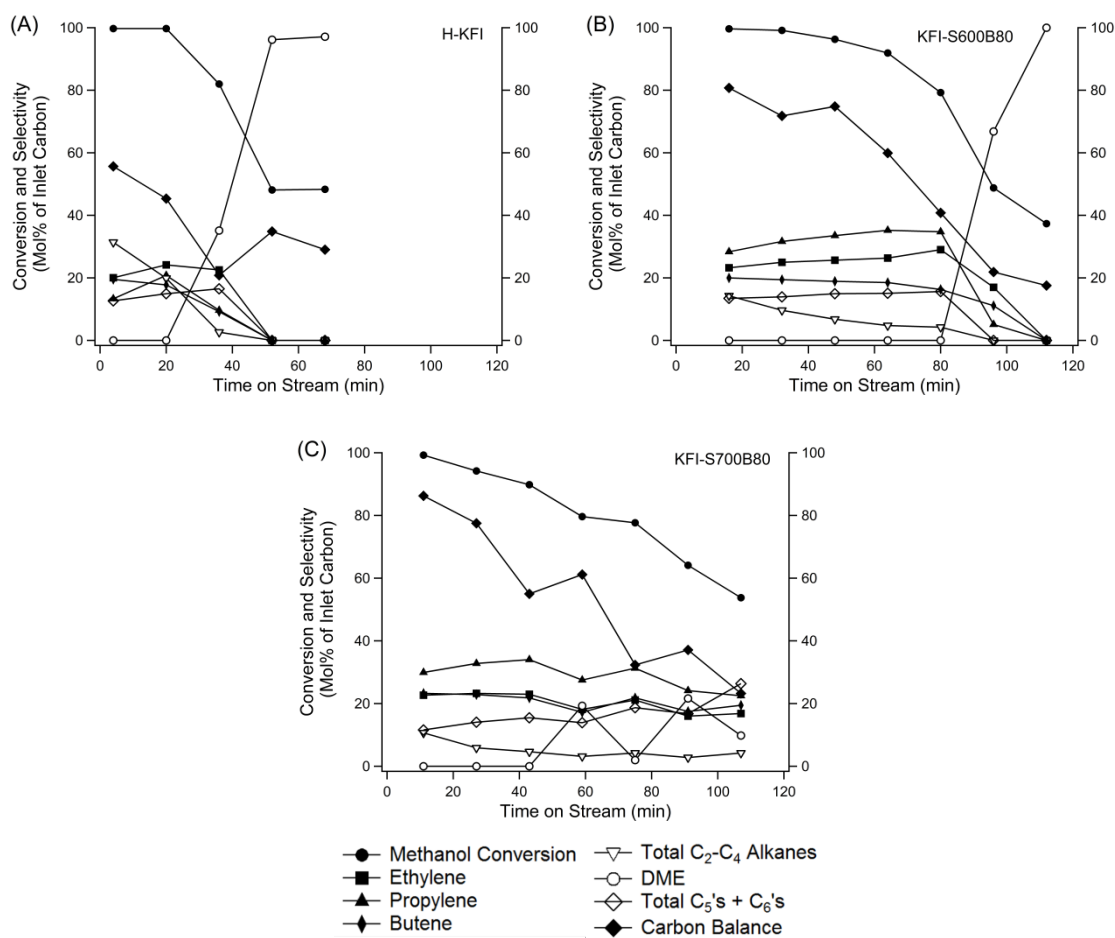


Figure 3-14. MTO reaction data obtained at 400°C for (A) as-synthesized, (B) 600°C steamed and (C) 700°C steamed KFI samples

materials, as indicated by Ar physisorption measurements, likely also contribute to the increased lifetimes of the steamed zeolites by allowing for greater accessibility of reactants to the acid sites in the remaining microporous regions. We have previously observed using NH_3 and *i*-propylamine TPD that steam treatment of high-aluminum CHA-type zeolites lead to decreased total Brønsted acid site densities while simultaneously increasing accessibility of the remaining acid sites via mesopores.¹³ An optimal steaming temperature of 600°C for CHA was found that gave the best balance of intact acid sites and accessibility. The RHO and KFI samples appear to show a similar behavior where steaming at 600°C produces the greatest improvement in catalyst performance. These samples show the best combination of olefin selectivity and catalyst lifetime. Increasing the steaming temperature leads to slight increases in the olefin selectivities but decreased lifetimes, presumably a result of increased degradation and lowered accessibility to the acid sites.

Interestingly, the more severely steamed RHO and KFI (RHO-S700B80, RHO-S800B80 and KFI-S700B80) samples produce little to no DME. This behavior contrasts with the reaction behaviors seen for the steamed CHA samples where deactivation is accompanied by a simultaneous rise in DME production so that DME becomes the main product. Furthermore, higher amounts of butene are produced for the steamed RHO and KFI samples compared to CHA. In particular, the $\text{C}_4=\text{C}_2=$ ratio is nearly 1:1 for the 700 and 800°C steamed RHO samples, while this ratio is typically 1:2 for 600°C steamed CHA. These differences in the product distribution suggest that there may be different reaction mechanisms for RHO and KFI compared to CHA. These differences are investigated further in Chapter 4.

3.4.3.2. Effect of reaction temperature for RHO

The effect of reaction temperature was explored for RHO steamed at 800°C that was tested at temperatures of 350, 400 and 450°C (Figure 3-15). At 350°C, the 800°C steamed RHO deactivates after only 42 min (0.87 g MeOH/g cat) and reaches a maximum combined $C_2=$ and $C_3=$ selectivity of 48% at 91.9% conversion. As with CHA, increasing the reaction temperature leads to an increase in the combined olefin selectivities as well as

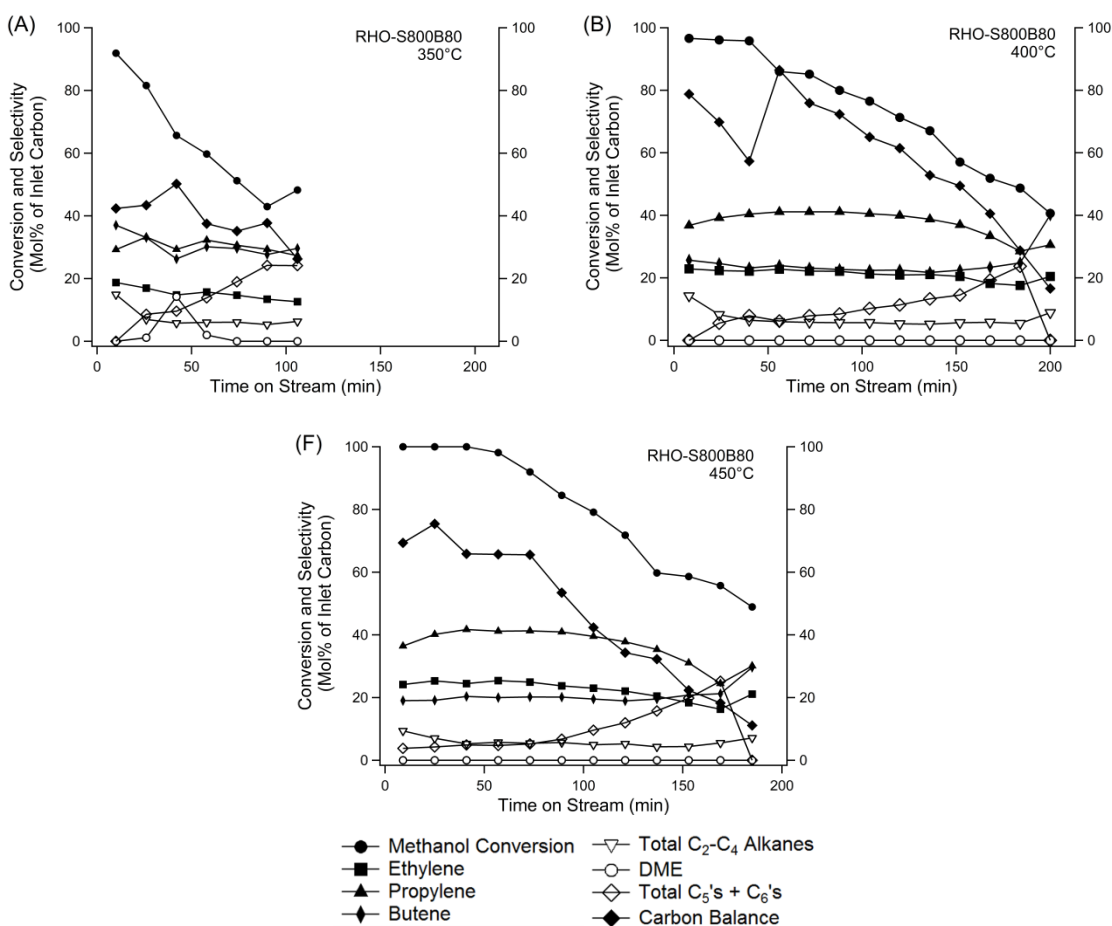


Figure 3-15. MTO reaction data for RHOS800B80 obtained at reaction temperatures of (A) 350°C, (B) 400°C and (C) 450°C

catalyst lifetime. The best activity was obtained at 450°C where the maximum combined C₂₌ and C₃₌ selectivity was 66.2% at 100% conversion, and conversion remained above 80% for 105 min (2.2 g MeOH/g cat).

3.5. Conclusions

High aluminum RHO and KFI-type zeolites were prepared in the absence of OSDAs, dealuminated by steam treatments, and evaluated for MTO. While the proton forms of the as-synthesized RHO and KFI deactivate quickly due to their high aluminum content, the steamed samples show increased lifetimes and olefin selectivities. Characterizations by ²⁷Al and ³¹Si NMR indicate that the steam treatments extract framework aluminum while simultaneously introducing mesoporosity that may facilitate transport of reactants to the micropores. The effects of the steaming temperature and steam partial pressure are investigated and similar trends are observed for all three of the 8MR zeolites studied, indicating that these material and likely other small pore zeolites will behave similarly under steam treatment. The reaction results for RHO and KFI presented here (in addition to CHA shown previously) show that the catalytic behavior of high aluminum 8MR zeolites prepared without OSDAs can be modified by the steam dealumination method to create selective catalysts for MTO. The successful demonstration of this method on three 8MR zeolites suggests that it is likely to be effective on any small-pore zeolite that is prepared without an OSDA to convert them into useful catalysts for reactions like MTO.

3.6. References

- (1) Tian, P.; Wei, Y.; Ye, M.; Liu, Z. Methanol to olefins (MTO): from fundamentals to commercialization. *ACS Catal.* **2015**, *5*, 1922-1938.
- (2) Wilson, S.; Barger, P. The characteristics of SAPO-34 which influence the conversion of methanol to light olefins. *Micropor. Mesopor. Mater.* **1999**, *29*, 117-126.
- (3) Olsbye, U.; Svelle, S.; Bjørgen, M.; Beato, P.; Janssens, T.V.W.; Joensen, F.; Bordiga, S.; Lillerud, K.P. Conversion of methanol to hydrocarbons: how zeolite cavity and pore size controls product selectivity. *Angew. Chem. Int. Ed.* **2012**, *51*, 5810-5831.
- (4) Arstad, B.; Nicholas, J.B.; Haw, J.F. Theoretical study of the methylbenzene side-chain hydrocarbon pool mechanism in methanol to olefin catalysis. *J. Am. Chem. Soc.* **2004**, *126*, 2991-3001.
- (5) Haw, J.F.; Marcus, D.M. Well-defined (supra)molecular structures in zeolite methanol-to-olefin catalysis. *Top. Catal.* **2005**, *34*, 41-48.
- (6) Schmidt, J.E.; Deimund, M.A.; Xie, D.; Davis, M.E. Synthesis of RTH-Type zeolites using a diverse library of imidazolium cations. *Chem. Mater.* **2015**, *27*, 3756-3762.
- (7) Dusselier, M.; Deimund, M.A.; Schmidt, J.E.; Davis, M.E. Methanol-to-olefins catalysis with hydrothermally treated zeolite SSZ-39. *ACS Catal.* **2015**, *5*, 6078-6085.

- (8) Cartlidge, S.; Patel, R. Hydrothermally stable chabazites for the selective preparation of olefins from methanol, in *Zeolites: Facts, Figures, Future*, P.A. Jacobs and R.A. vanSanten, Editors. 1989, Elsevier: Amsterdam. p. 1151-1161.
- (9) Corma, A.; Rey, F.; Rius, J.; Sabater, M.J.; Valencia, S. Supramolecular self-assembled molecules as organic directing agent for synthesis of zeolites. *Nature* **2004**, *431*, 287-290.
- (10) Chatelain, T.; Patarin, J.; Farré, R.; Pétigny, O.; Schulz, P. Synthesis and characterization of 18-crown-6 ether-containing KFI-type zeolite, *Zeolites* 1996, *17*, 328-333.
- (11) Chatelain, T.; Soulard, M.; Guth, J.L.; Schulz, P. Synthesis and characterization of high-silica zeolite-Rho prepared in the presence of 18-crown-6 ether as organic template. *Microporous Mater.* **1995**, *4*, 231-238.
- (12) Zones, S.I. Translating new materials discoveries in zeolite research to commercial manufacture. *Micropor. Mesopor. Mater.* **2011**, *144*, 1-8.
- (13) Ji, Y.; Deimund, M.A.; Bhawe, Y.; Davis, M.E. Organic-free synthesis of CHA-type zeolite catalysts for the methanol-to-olefins reaction. *ACS Catal.* **2015**, *5*, 4456-4465.
- (14) Baerlocher, C.; McCusker, L.B.; Olson, D.H. *Atlas of Zeolite Framework Types*. 6th revised ed. 2007, Amsterdam: Elsevier.
- (15) Corbin, D.R.; Schwarz, S.; Sonnichsen, G.C. Methylamines synthesis: a review. *Catal. Today* **1997**, *37*, 71-102.
- (16) Robson, H.E. Zeolite RHO, U.S. Patent 3,904,738, September 9, 1975.

- (17) Robson, H.E. Method for preparing a small pore synthetic zeolite, U.S. Patent 3,720,753, February 22, 1971.

3.7. Supporting Information for Chapter 3

Table 3-4. Summary of acid washing treatments for steamed RHO and KFI samples and bulk Si/Al Ratios

	Steaming Conditions ^a	Acid Washing Conditions ^b	Si/Al Ratio
RHO	700°C Steamed	-	2.9
	700°C Steamed	0.1 N HCl 2 h 100°C	3.0
	700°C Steamed	1 N HCl 2 h 100°C	4.2
	800°C Steamed	-	2.8
	800°C Steamed	0.1 N HCl 2 h 100°C	3.2
	800°C Steamed	1 N HCl 2 h 100°C	4.2
KFI	700°C Steamed	-	3.2
	700°C Steamed	0.1 N HCl 2 h 100°C	4.3

^a Samples were steamed for 8 h at the steaming temperature with the water saturator at 80°C

^b Acid washing was performed with 100 mL liquid per gram solid. Solids were recovered by filtration, washed with water and dried at 100°C

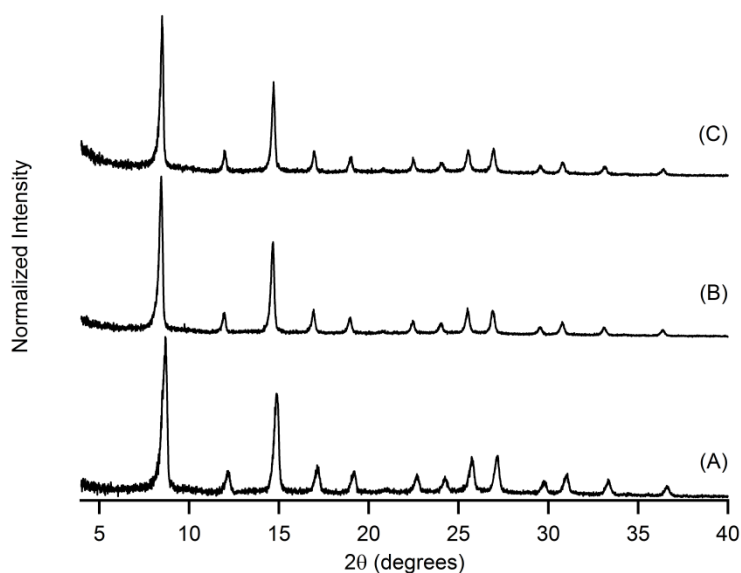


Figure 3-16. Powder XRD patterns for (A) 700°C steamed RHO and 700°C steamed RHO after acid washing with (B) 0.1 N HCl or (C) 1 N HCl for 2 h at 100°C

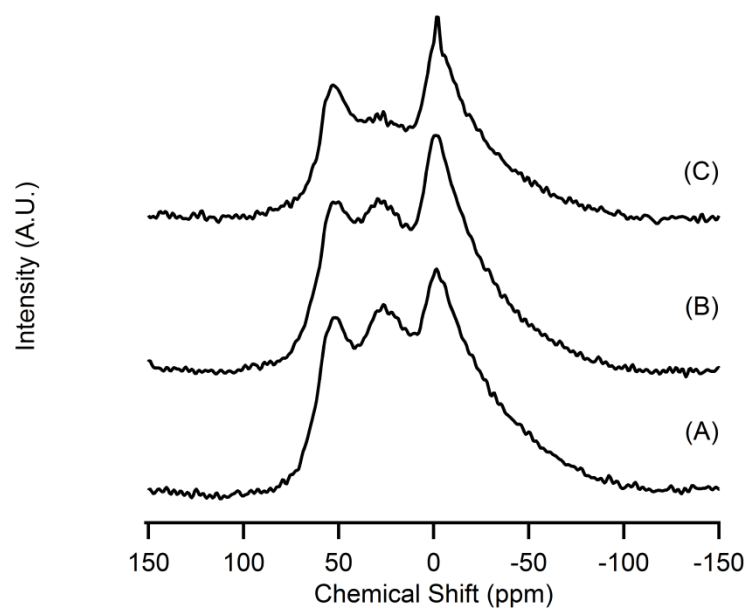


Figure 3-17. ^{27}Al MAS NMR for (A) 700°C steamed RHO and 700°C steamed RHO after acid washing with (B) 0.1 N HCl or (C) 1 N HCl for 2 h at 100°C

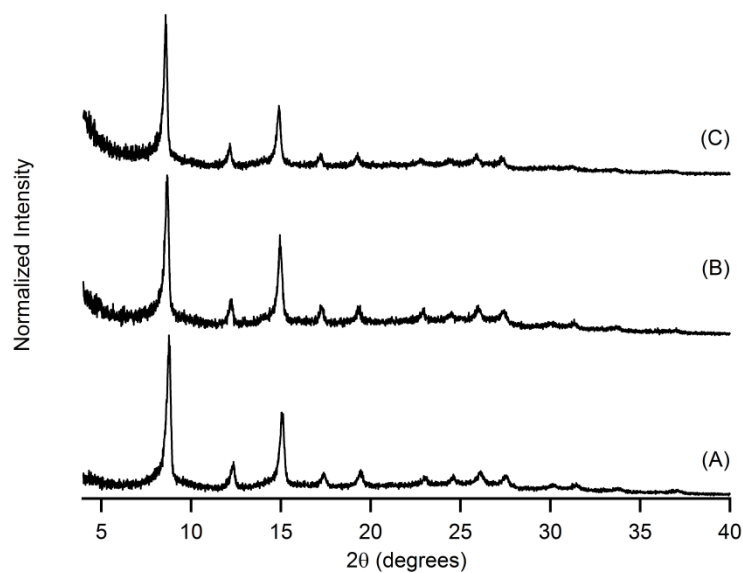


Figure 3-18. Powder XRD patterns for (A) 800°C steamed RHO and 800°C steamed RHO after acid washing with (B) 0.1 N HCl or (C) 1 N HCl for 2 h at 100°C

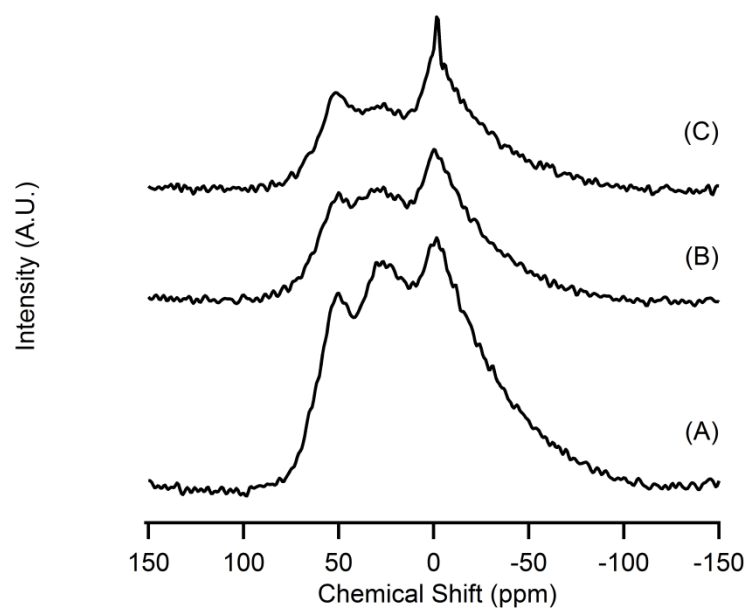


Figure 3-19. ^{27}Al MAS NMR for (A) 800°C steamed RHO and 800°C steamed RHO after acid washing with (B) 0.1 N HCl or (C) 1 N HCl for 2 h at 100°C

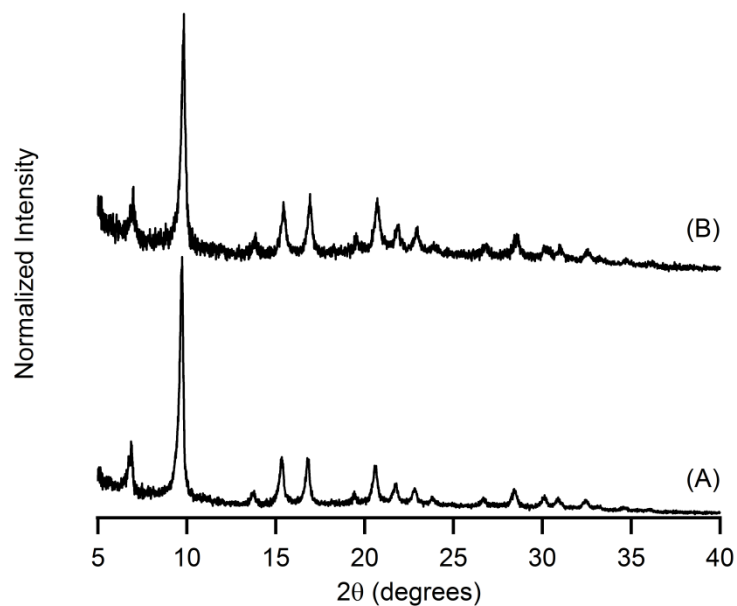


Figure 3-20. Powder XRD patterns for (A) 700°C steamed KFI and (B) 700°C steamed and acid washed KFI.

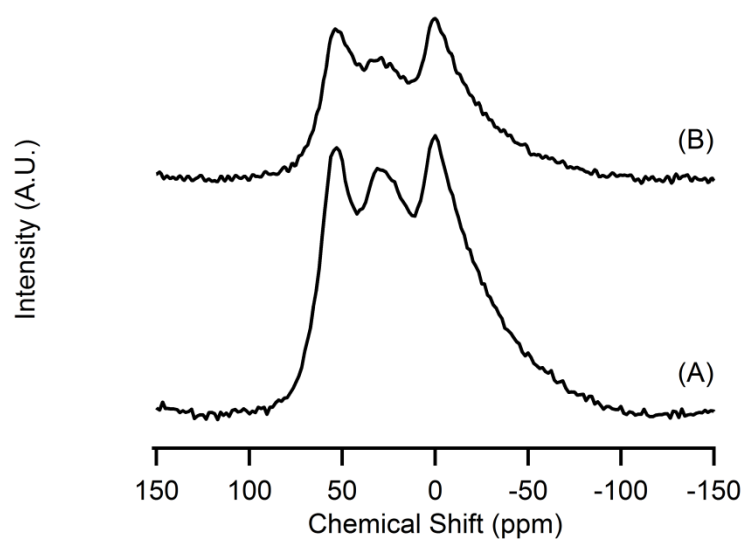


Figure 3-21. ^{27}Al MAS NMR for (A) 700°C steamed KFI and (B) 700°C steamed and acid washed KFI.

4. Role of acid sites internal vs. external to 8MR cages of steamed 8MR zeolites

Information in this chapter has previously appeared in: Y. Ji, J. Birmingham, M.A. Deimund, M.E. Davis, Steam-Dealuminated, OSDA-free RHO and KFI-Type Zeolites as Catalysts for the Methanol-to-Olefins Reaction, *Micropor. Mesopor. Mater.* 232, (2016) 126-137. doi:10.1016/j.micromeso.2016.06.012.

4.1. Abstract

Three 8MR zeolites: CHA, RHO and KFI, are prepared in the absence of OSDAs, dealuminated by steam treatments and poisoned with trimethylphosphite to eliminate acid sites in the mesopores and on the external surface of the crystallites to investigate the role of these sites in the product distributions observed for the steamed materials. Characterizations by EDS, ^{31}P NMR and ^{27}Al NMR provide evidence of attachment of phosphorus to aluminum species after phosphite treatment. Elimination of acid sites external to the 8MR pores is verified by *i*-propylamine TPD. When evaluated for MTO activity, all of the phosphite-treated samples show longer catalyst lifetimes (and less coke content) but no changes in olefin selectivities are observed, suggesting that olefins do not undergo secondary dimerization or methylation reactions that affect the resulting product distributions observed for the steamed zeolites. Differences in the product distributions are instead attributed to differences in the unique pore structures of each of the zeolites.

4.2. Introduction

Previously, we showed that high aluminum 8MR zeolites (CHA, RHO and KFI) prepared without using OSDAs could be dealuminated by steam treatments to convert them into catalysts with improved activity for MTO. A comparison of the reaction profiles for the three 8MR zeolites evaluated (CHA, RHO and KFI) shows differences in their selectivities towards ethylene, propylene, butene and DME. The origins of these differences are investigated here via poisoning experiments.

Evaluation of the steamed materials for MTO showed that the steamed RHO and KFI catalysts have higher selectivities towards butylene (2-butylene and isobutylene) compared to the CHA-type zeolites. All of the steamed RHO samples produce ethylene and butylene at ratios close to 1:1 while this ratio is typically around 2:1 for the steamed CHA-type zeolites that are prepared without OSDAs. For instance, the average $C_2=/C_3=/C_4=$ ratio near complete conversion for the 800°C steamed RHO is 1/1.7/1.1 while for a representative 600°C steamed CHA sample, the ratio is 1/1.2/0.5. Similarly, the steamed KFI samples show higher butylene selectivities compared to CHA. The 600°C steamed KFI sample has a $C_2=/C_3=/C_4=$ ratio of 1/1.3/0.77. Increasing the steaming temperature to 700°C results in increased butylene selectivity (average $C_2=/C_3=/C_4=$ ratio of 1/1.3/0.99), similar to the 800°C steamed RHO.

Further, olefin selectivities remain stable with increasing time on stream even as conversion decreases and little to no DME is observed among the products for both the 800°C steamed RHO and 700°C steamed KFI samples. This behavior contrasts that

observed for the steamed CHA samples as well as the RHO and KFI samples steamed at lower temperatures where, with increasing time on stream, coke formation at strong Brønsted acid sites responsible for converting methanol to olefins leads to decreasing conversion and olefin selectivities (resulting in DME, produced from the dehydration of methanol on weak acid sites, becoming the main product in the effluent).

We have previously shown with NH_3 and *i*-propylamine TPD experiments on steamed CHA samples (Chapter 2) that Brønsted acid sites are located both in the intact 8MR cages as well as in the mesopores and external surface of the steamed samples. To assess whether these external sites are the origin of the differences in DME production or secondary reactions of olefins (such as dimerization of ethylene to butylene) that are responsible for the differences in product selectivities observed for the three zeolite structures, poisoning experiments with trimethylphosphite are performed to eliminate the mesoporous and surface sites and the resulting materials are tested for MTO. Similar trimethylphosphite treatments have been commonly used to modify the acidity and shape selectivity of ZSM-5 for various catalytic processes.¹⁻³ Trimethylphosphite may be exchanged onto zeolites where it binds to aluminum sites. Calcination to remove the organic ligands then leaves phosphate groups permanently attached onto the acid sites in the zeolites. In the steamed 8MR zeolites, trimethylphosphite is able to access acid sites in the mesopores and external surface but is too large to diffuse into 8MR cages and thus can be used to selectively poison acid sites external to the 8MR pore system.

In this study, batches of the three zeolites (CHA, RHO and KFI) were synthesized, steamed, treated with trimethylphosphite and evaluated for MTO reactivity. CHA steamed

at 600°C (CHA-S600) was prepared following the OSDA-free method that we previously reported (Chapters 2 and 3) and compared to 800°C steamed RHO (RHO-S800) and 700°C steamed KFI (KFI-S700). These samples were chosen because they showed the most stable $C_{4=}/C_{2=}$ ratio and lowest DME production. Elimination of mesoporous and external surface sites after trimethylphosphite treatment is verified by *i*-propylamine TPD.

4.3. Experimental Section

4.3.1. Synthesis and treatment of 8MR zeolites

CHA, RHO and KFI-type zeolites were synthesized without using OSDAs following the procedures previously described in Chapters 2 and 3. CHA was synthesized via the interzeolite transformation from FAU, following the method of Bourgonne et al.⁴ RHO⁵ was prepared from a synthesis gel with molar composition $0.3 \text{ Na}_2\text{O} / 0.1 \text{ Al}_2\text{O}_3 / 1 \text{ SiO}_2 / 0.04 \text{ Cs}_2\text{O} / 8\text{H}_2\text{O}$ that was aged for 3 days at room temperature and then heated for 1 day at 100°C. KFI⁶ was prepared from a synthesis gel with molar composition $0.24 \text{ K}_2\text{O} / 0.167 \text{ Al}_2\text{O}_3 / 1 \text{ SiO}_2 / 0.030 \text{ Cs}_2\text{O} / 7.5 \text{ H}_2\text{O}$. The gel was heated for 4.5 days at 100°C. The solids were recovered by centrifugation, washed with water and acetone and dried overnight at 100°C. Prior to reaction testing and steam treatment, the as-synthesized samples were exchanged three times with aqueous 1 M NH_4NO_3 solution (100 mL liquid per gram solid) for 2 h at 90°C. After the final exchange, the solids were centrifuged, washed with water and acetone and dried overnight at 100°C.

Steaming was conducted in a horizontal tube furnace (MTI OTF-1200X) under a flowing mixture of steam and air that was generated by bubbling zero-grade air (50 cc/min)

through a water saturator held at 80°C upstream of the sample. Samples were loaded in ceramic boats, exposed to flowing steam and heated at 1°C/min to the desired steaming temperature (600, 700 or 800°C) and held there for 8 h.

4.3.2. Trimethylphosphite Treatment

Trimethylphosphite was exchanged onto the zeolites via a liquid phase exchange, similar to those that have been carried out for ZSM-5.⁷ Prior to exchanging with trimethylphosphite, steamed samples were dried under vacuum at 300°C to remove adsorbed water. The steamed CHA was dried for 2 h at 300°C while the steamed RHO and KFI samples were dried for 16 h as it was determined a longer drying time was necessary to remove adsorbed water from the samples. Exchanges were carried out by refluxing 1 g of dried solids in 1.6 mL trimethylphosphite (Aldrich, 99.99%) and 5 mL octane (Aldrich, anhydrous) for 20 h at 125°C under flowing argon. The amount of trimethylphosphite added was approximately a three-fold excess of the total aluminum present in the zeolite sample. The solids were then filtered, washed with dichloromethane followed by pentane, and dried at 100°C. A final calcination was performed to remove the organic components by heating the samples for 2 h at 150°C and 5 h at 500°C (1°C/min) in a flow of breathing-grade air. The phosphite-treated samples are designated CHA-S600-P, RHO-S800-P and KFI-S700-P. This procedure was also performed on H-ZSM-5 (Zeolyst CBV3024E, Si/Al = 15) where each framework aluminum is accessible to trimethylphosphite to verify that the method is effective in poisoning all Brønsted acid sites. Characterizations for the H-ZSM-5 sample are provided in the supporting information (Figures 4-5 through 4-7).

4.3.3. Characterizations

Powder X-ray diffraction (XRD) patterns were obtained on a Rigaku MiniFlex II instrument with Cu K α radiation ($\lambda = 1.54184$ Å) at a sampling window of 0.01° and scan speed of $0.3^\circ/\text{min}$. Powder patterns were normalized to the highest intensity peak. Bulk elemental analysis was conducted by energy dispersive spectroscopy (EDS) on a ZEISS 1550VP instrument equipped with an Oxford X-Max SDD.

Solid-state ^{27}Al and ^{31}P MAS NMR spectra were acquired on a Bruker DSX 500 MHz spectrometer. ^{27}Al NMR spectra were recorded with the spectrometer operating at 130.3 MHz using a 90° pulse length of $6\ \mu\text{s}$, a recycle time of 2 s, and a spinning rate of 12 kHz. Samples were hydrated overnight over a saturated KCl solution and loaded in a 4 mm ZrO_2 rotor. Chemical shifts were referenced to 1 M aqueous aluminum nitrate solution.

^{31}P NMR spectra were recorded with the spectrometer operating at 202.4 MHz with ^1H decoupling using a 90° pulse length of $8.5\ \mu\text{s}$, a recycle time of 40 s, and spinning rate of 12 kHz. Chemical shifts were referenced to aqueous phosphoric acid. ^{31}P NMR spectra were obtained for trimethylphosphite-treated samples in both hydrated and dehydrated states. To prepare dehydrated samples, the sample was packed in the rotor and then heated for 1 h at 150°C followed by 1 h at 500°C (at a $5^\circ\text{C}/\text{min}$ ramp rate) under vacuum.

i-Propylamine TPD was performed on samples to assess whether acid sites external to the 8MR pores of the steamed zeolites (on the surface and within the mesopores) were eliminated by the trimethylphosphite treatments. As described in Chapter 2, *i*-Propylamine is too large to diffuse through 8MR pores and thus can only access acid sites located on the

surface and in mesoporous regions of the steamed zeolites. Reaction of the probe molecule at acid sites produces NH_3 and propylene that can be monitored and quantified. Samples were pelletized, crushed, and sieved to obtain particle sizes between 0.18 and 0.6 mm. In a typical measurement, approximately 200 mg of the sample was loaded between supporting quartz wool beds in a continuous flow quartz tube reactor (Altamira AMI-200). Any initially adsorbed species were removed by heating the samples at $10^\circ\text{C}/\text{min}$ to 150°C for 1 h, followed by heating at $10^\circ\text{C}/\text{min}$ to 600°C for 1 h, in 30 sccm flowing helium. Samples were then cooled to 50°C and dosed with *i*-propylamine by means of a vapor saturator, purged for 2 h at the dosing temperature under 30 sccm flowing helium to remove weakly physisorbed species and then heated to 600°C at $10^\circ\text{C}/\text{min}$ and held there for 2 h. Desorbing products, NH_3 ($m/z = 17$) and propylene ($m/z = 41$), were monitored by an online mass spectrometer.

4.3.4. MTO Reaction Testing

Catalysts for reaction testing were pelletized, crushed and sieved to obtain particles between 0.15 mm and 0.6 mm. Approximately 200 mg of the sieved catalyst was supported between quartz wool beds in a tubular, continuous flow reactor (Autoclave Engineers BTRS, Jr. SS-316). Samples were calcined in-situ by heating (at a rate of $1^\circ\text{C}/\text{min}$) for 3 h at 150°C and then 12 h at 580°C under a flow of breathing-grade air. Reactions were conducted at 400°C and atmospheric pressure with a feed of 10% methanol in inert (5% Ar, bal. He) pumped at a WHSV of 1.3 h^{-1} . Effluent gases were monitored by an on-stream GC/MS (Agilent 6890/MSD5793N). Conversions, selectivities and carbon balances are reported on a carbon mole basis as previously described (Equations 2-1 through 2-3).

Coke contents of the spent catalysts were determined from the organic mass losses measured by thermogravimetric analysis (TGA). TGAs were performed in a PerkinElmer STA 6000 instrument by heating the solids to 900°C at a rate of 10°C/min under a flow of zero-grade air (20 sccm).

4.4. Results and Discussion

4.4.1. Characterizations

Elemental analysis by EDS showed that the steamed and phosphite-treated CHA, RHO and KFI samples have P/Al ratios of 0.046, 0.023 and 0.026, respectively, after the phosphite exchange and calcination (Table 4-1). From fraction of tetrahedral Al (Al_T/Al_{Total}) estimated from the ^{27}Al NMR and the bulk P/Al ratio, the ratio of phosphorus to tetrahedral Al (P/Al_T) is estimated to be 0.38 for CHA-S600-P. From our previous work⁸, the ratio of acid sites measured by *i*-propylamine TPD to that measured by NH_3 TPD for CHA steamed at 600°C was 0.32. This ratio is equivalent to the ratio of accessible

Table 4-1 Si/Al and P/Al ratios of phosphite-treated samples and their estimated tetrahedral / penta-coordinated / octahedral Al ($Al_T/Al_P/Al_O$) ratios from ^{27}Al NMR

Sample	Si/Al	P/Al	$Al_T/Al_P/Al_O$
CHA-S600	2.5	-	1/1.86/5.49
CHA-S600-P	2.5	0.046	1/2.35/6.65
RHO-S800	2.7	-	1/2.41/1.43
RHO-S800-P	2.6	0.023	1/2.95/1.94
KFI-S700	2.8	-	1/0.82/1.32
KFI-S700-P	2.8	0.026	1/1.09/1.53

mesoporous and external surface acid sites to the total number of accessible acid sites (observed to correspond one-to-one with the number of tetrahedral aluminum). The P/Al ratio measured for CHA-S600-P is thus consistent with the ratio that would be expected if each phosphorus is attached to an accessible acid site external to the 8MR cages. The P/Al_T ratios are estimated to be 0.11 and 0.08 for RHO-S800-P and KFI-S700-P, respectively. While these ratios are lower than that of the CHA sample, the *i*-propylamine TPD results (Figure 4-3) indicate that a significant portion of the accessible mesoporous and external surface sites are poisoned by the treatments. The PXRD patterns (Supporting Information Figures 4-8 through 4-10) of the samples after treatment are essentially unchanged from the starting steamed materials, suggesting that the treatments do not cause significant degradation of the framework.

Incorporation of phosphorus into the steamed zeolites was further confirmed by ³¹P MAS NMR (Figure 4-1). In the hydrated samples, the ³¹P NMRs show a broad peak that spans from approximately 0 to -40 ppm, and can be assigned to overlapping signals from phosphate groups that may be either free or coordinated to aluminum. For example, the ³¹P signals occurring at -6 and -12 ppm are typically assigned to terminal and middle phosphate groups in short chain polyphosphates.^{9,10} ³¹P signals occurring at lower frequencies of approximately -15 to -40 ppm have been attributed to highly condensed polyphosphate species, aluminum-bound polyphosphates in phosphorus-modified ZSM-5, as well as amorphous aluminum phosphate.⁹⁻¹³ For instance, ³¹P signals at approximately -17 ppm and -20 to -30 ppm have been assigned to phosphate groups located at terminal and middle positions, respectively, of polyphosphates coordinated to

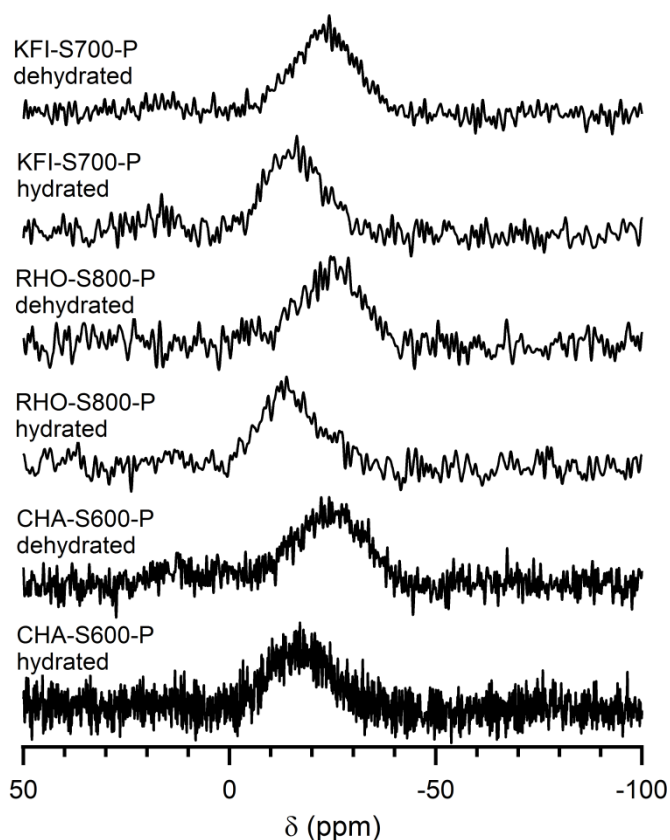


Figure 4-1. ^{31}P MAS NMR of steamed and phosphite-treated zeolites

aluminum.⁹ The ^{31}P signal of branching groups in P_4O_{10} occurs at -46 ppm,¹² while signals occurring at approximately -40 ppm have been assigned to branched groups in highly condensed polyphosphates bound to aluminum.¹⁰

Since the TPD and MTO reactivity data were obtained for samples that had been dehydrated, ^{31}P NMR spectra were also obtained on dehydrated samples in order to observe the coordination environment of the phosphorus under similar conditions. After dehydration at 500°C, the lower frequency ^{31}P signals increase in intensity relative to the higher frequency signals, resulting in a single broad peak centered at approximately -25 ppm that is observed for all of the samples. The shift towards lower frequencies suggests

that the shorter chain polyphosphates condense to form longer chain polyphosphates during the dehydration procedure. We note that the chemical shifts observed in these samples are also consistent with those reported for microporous aluminophosphates (AlPO_4 's) and SAPO's (typically -20 to -35 ppm).¹⁴

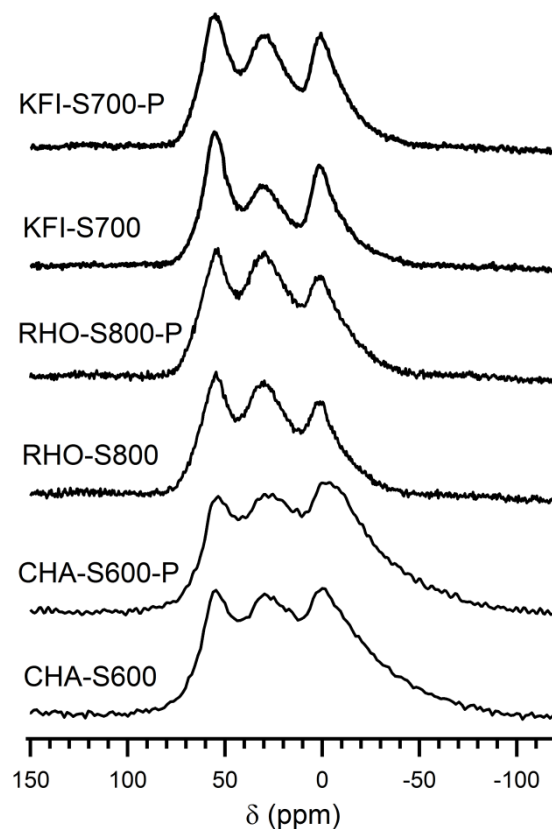


Figure 4-2. ^{27}Al MAS NMR spectra of the steamed zeolites before and after phosphite treatment

The ^{27}Al NMRs of the phosphite-treated samples show that the peak corresponding to octahedral aluminum increases in intensity relative to the downfield peaks (Figure 4-2). This peak is further shifted to a slightly lower frequency and may be assigned to

tetrahedral, framework aluminum that is converted to octahedrally-coordinated aluminum by the presence of phosphate groups.¹⁵ The increase in intensity of the octahedral aluminum species is most prominent for the CHA sample, which has the highest phosphorus content. The bulk Si/Al ratios of the phosphite-treated samples (Table 4-1) were the same as that of the parent zeolites, indicating that no aluminum was further extracted from the zeolites during the treatments.

TPD with *i*-propylamine was performed on the steamed zeolites before and after phosphite treatment in order to verify that the acid sites external to the 8MR cages have been poisoned. *i*-Propylamine TPD of trimethylphosphite-treated H-MFI (Si/Al ratio of 15), where each framework aluminum corresponds to a Brønsted acid site that is accessible to *i*-propylamine, shows that the treatment results in nearly complete elimination of the accessible acid sites (Figure 4-7). Figure 4-3 shows the *i*-propylamine TPDs of the steamed 8MR zeolites before and after phosphite treatment. Unreacted *i*-propylamine as well as molecules associated with Lewis acid sites, hydroxyl defects and molecules that are hydrogen bonded to protonated amines at Brønsted acid sites desorb below approximately 500 K.¹⁶ Above 500 K, propene and ammonia desorption peaks are observed that are the result of the decomposition of *i*-propylamine at Brønsted acid sites. Since *i*-propylamine is too large to diffuse through 8MR pores, these higher temperature propene peaks represent decomposition reactions that occur at acid sites located either in the mesopores or on the external surface. These peaks are significantly reduced to near-baseline levels after phosphite treatment for all three of the steamed samples, suggesting that a significant portion of the sites external to the 8MR pore system have been poisoned.

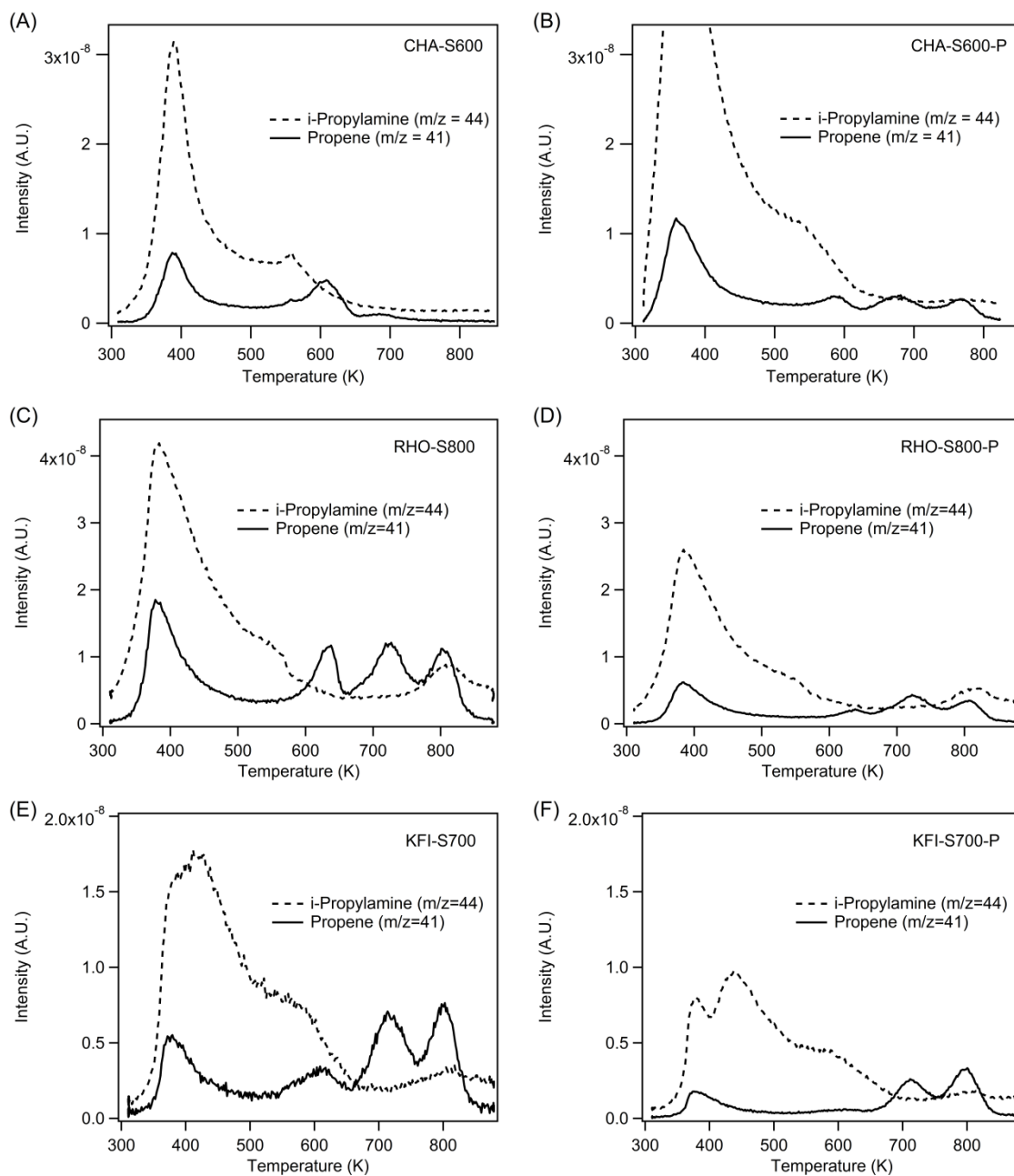


Figure 4-3. *i*-Propylamine TPD for steamed and phosphite-treated zeolite samples

4.4.2. MTO Reaction Testing

The steamed samples were tested for MTO reactivity, and they did not show significant differences in their $C_2=/C_3=/C_4=$ selectivities after phosphite treatment (Figure

4-4 and Table 4-2). The main difference after treatment is an increase in lifetime that is observed for all three of the zeolites studied. Whereas the steamed samples show a deactivation that is marked by a sudden decrease in conversion and olefin selectivities, conversion decreases more gradually for the phosphite-treated samples. This behavior was most apparent for KFI, that showed the greatest relative increase in lifetime after phosphite treatment (conversion remained above 80% for 102 min for KFI-S700-P compared to 72 min for the KFI-S700). The coke content of the phosphite-treated KFI after reaction was also significantly lower than that of the untreated KFI-S700 (9.8% vs. 18.7%). The phosphite-treated CHA and RHO samples similarly had lower coke content after reaction compared to the untreated samples (Table 4-2), though the change was not as significant compared to that of the KFI samples. We note that while the selectivities for C₅ and C₆ hydrocarbons appear higher in the RHO and KFI samples before phosphite treatment (Figure 4-4C through F), the total products that can be accounted for is lower for the untreated samples and thus causes the C₅ and C₆ selectivities to appear higher for those samples. ³¹P NMR spectra of the spent catalysts were obtained (Figure 4-11), and they show a broad signal spanning from approximately 0 to -50 ppm (as with the fresh catalysts), suggesting that phosphorus remains in the catalysts during the reactions.

The increased lifetime and lower coke content of the phosphite-treated samples suggest that acid sites in the mesopores may serve as sites for coke deposition. For small-pore zeolites such as CHA, it has been established that deactivation occurs via the formation of polycyclic aromatic compounds inside the cavities that hinders diffusion

Table 4-2. Summary of MTO reaction data for steamed zeolites before and after trimethylphosphite treatment

Sample	Maximum MeOH Conversion	Maximum C ₂ +C ₃ = Selectivity at Maximum Conversion	Average C ₂ =/C ₃ =/C ₄ = Ratio Near Complete Conversion	Catalyst Lifetime ^a	Coke Content ^b
CHA-S600	100%	71.5%	1.0/1.2/0.49	119 min	16.9%
CHA-S600-P	100%	69.1%	1.0/1.1/0.46	160 min	16.7%
RHO-S800	99.5%	60.6%	1.0/1.8/1.0	101 min	16.9%
RHO-S800-P	99.6%	61.6%	1.0/1.8/0.99	134 min	16.8%
KFI-S700	99.4%	55.3%	1.0/1.6/1.0	72 min	18.7%
KFI-S700-P	98.5%	54.6%	1.0/1.5/1.0	102 min	9.8%

^a First time point where conversion drops below 80%

^b Estimated from TGA of spent catalyst

through the crystal and leads to blockage of the pore structure.¹⁷⁻¹⁹ In the steamed zeolites studied here, coke may also adsorb onto the acid sites located in the mesopores and contribute to pore blockage. It has been reported that while introduction of mesopores in SSZ-13 results in increased catalyst lifetimes for MTO by facilitating greater utilization of the micropores, the coke content of the spent catalysts increased with increasing mesopore volume.²⁰ For the 8MR zeolites studied here, poisoning of the mesoporous sites with trimethylphosphite likely limits coking reactions that occur at acid sites external to the 8MR pores and thus maintains the accessibility of the pore structure for a longer period of time on stream (consistent with the lower coke content observed in the spent phosphite treated samples). As conversion decreases for the phosphite-treated samples, the fraction of

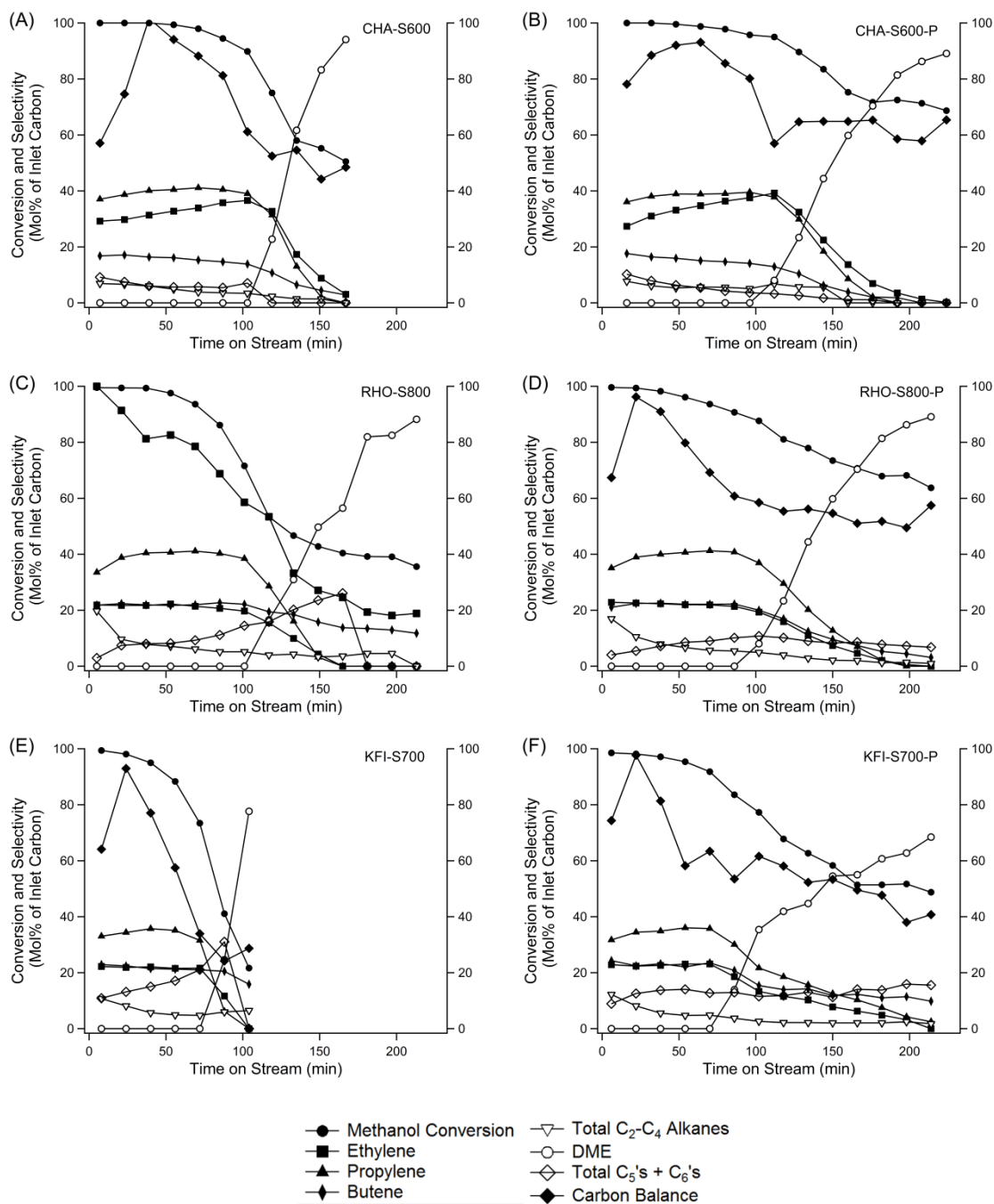


Figure 4-4. MTO reaction data for steamed zeolites before and after phosphite treatment

methanol converted to products that can be accounted for remains higher than that of the corresponding untreated samples.-

The lack of changes in the observed olefin selectivities after poisoning the mesoporous and surface acid sites suggest that the olefins produced inside the 8MR cages do not undergo further dimerization or methylation and that the increased $C_4=/C_{2=}$ ratios observed for RHO and KFI compared to CHA likely do not result from dimerization of ethylene to butylene at the mesoporous and external surface sites. Differences in olefin selectivities among the three zeolites may instead result from differences in their pore structures (has been reported previously to play a significant role in differing olefin selectivities.²¹⁻²³ It has been observed, for example, that the maximum ethylene selectivity decreases as the cage size is increased in a comparison of LEV, CHA and AFX zeolites.²¹ On the other hand, increased propylene and butylene formation (compared to that of CHA) have been observed for AEI-type materials (SSZ-39²⁴ and SAPO-18²²), whose cages are pear-shaped and wider at the bottom compared to the CHA cage. Li et al²³ have studied the effects of cavity size on the product distribution of SAPO-type catalysts, SAPO-35 (LEV), SAPO-34 (CHA) and DNL-6 (RHO), and also observed increasing butylene production with increasing cage size. Quenching and isotopic tracing experiments indicated that smaller cavities limit the size of polymethylbenzene intermediates and result in higher ethylene selectivities. The finding was supported by DFT calculations suggesting that the larger cavity size of the RHO structure could stabilize polymethylbenzenium cations with butyl side chains while the CHA cavity better stabilizes polymethylbenzeium cations with shorter alkyl chains (ethyl and propyl).

In this work, RHO and KFI contain cubic *lta* cages that can accommodate larger species compared to the elongated cages found in CHA (the maximum diameter of a sphere

that can be accommodated in the cages are 7.37 Å, 10.43 Å and 10.67 Å for CHA, RHO and KFI, respectively²⁵) and likely also contributes to the higher propylene and butylene selectivities observed for RHO and KFI. Further, RHO and KFI have larger channel dimensions (the maximum free sphere diameter that can diffuse through the channels along the a-, b-, or c-axis is approximately 3.72 Å for CHA, 4.04 Å for KFI and 4.06 Å for RHO²⁴) that may accommodate better diffusion of higher-chain molecules like butylene.

4.5. Conclusions

The origins of the differences in the product distributions observed for steamed CHA, RHO and KFI are investigated by trimethylphosphite treatments that selectively poison acid sites external to the 8MR pore structures of the materials. When evaluated for MTO activity, the poisoned samples show longer catalyst lifetimes and lower coke contents but maintain the same olefin selectivities. This finding suggests olefins do not undergo secondary reactions at mesoporous and external surface acid sites, such as dimerization of ethylene to butylene, that are responsible for the increased $C_4=/C_2=$ ratios observed for steamed RHO and KFI compared to CHA. Instead, differences in the $C_2=/C_3=/C_4=$ ratios likely result from the unique pore structure of each zeolite. The increased lifetimes and lower coke contents of the trimethylphosphite-treated samples compared to the untreated steamed samples suggest that the mesoporous and surface sites serve as sites for coke deposition.

4.6. References

- (1) Tynjälä, P.; Pakkanen, T.T. Modification of ZSM-5 zeolite with trimethyl phosphite part 1. structure and acidity. *Micropor. Mesopor. Mater.* **1998**, *20*, 363-369.
- (2) Védrine, J.C.; Auroux, A.; Djaifve, P.; Ducarme, V.; Hoser, H.; Zhou, S. Catalytic and physical properties of phosphorus-modified ZSM-5 zeolite. *J. Catal.* **1982**, *73*, 147-160.
- (3) van der Bij, H.E.; Weckhuysen, B.M. Phosphorus promotion and poisoning in zeolite-based materials: synthesis, characterisation and catalysis. *Chem. Soc. Rev.* **2015**, *44*, 7406-7428.
- (4) Bourgogne, M.; Guth, J. L.; Wey, R. Process for the preparation of synthetic zeolites, and zeolites obtained by said process. U.S. Patent 4,503,024, March 5, 1985.
- (5) Robson, H.E. Zeolite RHO, U.S. Patent 3,904,738, September 9, 1975.
- (6) Robson, H.E. Method for preparing a small pore synthetic zeolite, U.S. Patent 3,720,753, February 22, 1971.
- (7) Kaeding, W.W.; Butter, S.A. Conversion of methanol and dimethylether, U.S. Patent 3,911,041, September 23, 1974.
- (8) Ji, Y.; Deimund, M.A.; Bhawe, Y.; Davis, M.E. Organic-free synthesis of CHA-type zeolite catalysts for the methanol-to-olefins reaction. *ACS Catal.* **2015**, *5*, 4456-4465.

- (9) Damodaran, K.; Wiench, J.W.; Cabral de Menezes, S.M.; Lam, Y.L.; Trebosc, J.; Amoureux, J.P.; Pruski, M. Modification of H-ZSM-5 zeolites with phosphorus. 2. Interaction between phosphorus and aluminum studied by solid-state NMR spectroscopy. *Micropor. Mesopor. Mater.* **2006**, *95*, 296-305.
- (10) Blasco, T.A.; Corma, A.; Martínez-Triguero, J. Hydrothermal stabilization of ZSM-5 catalytic-cracking additives by phosphorus addition. *J. Catal.* **2006**, *237*, 267-277.
- (11) Caro, J.; Bülow, M.; Derewinski, M.; Haber, J.; Hunger, M.; Kärger, J.; Pfeifer, H.; Storek, W.; Zibrowius, B. NMR and IR studies of zeolite H-ZSM-5 modified with orthophosphoric acid. *J. Catal.* **1990**, *124*, 367-375.
- (12) Grimmer, A.R.; Haubenreisser, U. High-field static and MAS ^{31}P NMR: Chemical shift tensors of polycrystalline potassium phosphates $\text{P}_2\text{O}_5 \cdot x\text{K}_2\text{O}$ ($0 \leq x \leq 3$). *Chem. Phys. Lett.* **1983**, *99*, 487-490.
- (13) Bautista, P.M.; Campelo, J.M.; Garcia, A.; Luna, D.; Marinas, J.M.; Romero, A.A. $\text{AlPO}_4\text{-Al}_2\text{O}_3$ catalysts with low alumina content: I. Structural and textural characterization of catalysts obtained with aqueous ammonia. *Appl. Catal. A-Gen.* **1993**, *96*, 175-199.
- (14) Blackwell, C.S.; Patton, R.L. Solid-state NMR of silicoaluminophosphate molecular sieves and aluminophosphate materials. *J. Phys. Chem.* **1988**, *92*, 3965-3970.
- (15) van der Bij, H.E.; Weckhuysen, B.M. Local silico-aluminophosphate interfaces within phosphated H-ZSM-5 zeolites. *Phys. Chem. Chem. Phys.* **2014**, *16*, 9892-9903.

- (16) Gorte, R.J. What do we know about the acidity of solid acids? *Catal. Lett.* **1999**, *62*, 1-13.
- (17) Haw, J.F.; Marcus, D.M. Well-defined (supra)molecular structures in zeolite methanol-to-olefin catalysis. *Top. Catal.* **2005**, *34*, 41-48.
- (18) Mores, D.; Stavitski, E.; Kox, M.H.F.; Kornatowski, J.; Olsbye, U.; Weckhuysen, B.M. Space- and time-resolved in-situ spectroscopy on the coke formation in molecular sieves: methanol-to-olefin conversion over H-ZSM-5 and H-SAPO-34. *Chem.-Eur. J.* **2008**, *14*, 11320-11327.
- (19) Aguayo, A.T.; Campo, A.E.S.d.; Gayubo, A.G.; Tarrío, A.; Bilbao, J. Deactivation by coke of a catalyst based on a SAPO-34 in the transformation of methanol into olefins. *J. Chem. Technol. Biot.* **1999**, *74*, 315-321.
- (20) Wu, L.; Degirmenci, V.; Magusin, P.C.M.M.; Lousberg, N.J.H.G.M.; Hensen, E.J.M. Mesoporous SSZ-13 zeolite prepared by a dual-template method with improved performance in the methanol-to-olefins reaction. *J. Catal.* **2013**, *298*, 27-40.
- (21) Bhawe, Y.; Moliner-Marín, M.; Lunn, J.D.; Liu, Y.; Malek, A.; Davis, M.E. Effect of cage size on the selective conversion of methanol to light olefins. *ACS Catal.* **2012**, *2*, 2490-2495.
- (22) Chen, J.; Li, J.; Wei, Y.; Yuan, C.; Li, B.; Xu, S.; Zhou, Y.; Wang, J.; Zhang, M.; Liu, Z. Spatial confinement effects of cage-type SAPO molecular sieves on product distribution and coke formation in methanol-to-olefin reaction. *Catal. Commun.* **2014**, *46*, 36-40.

- (23) Li, J.; Wei, Y.; Chen, J.; Xu, S.; Tian, P.; Yang, X.; Li, B.; Wang, J.; Liu Z. Cavity controls the selectivity: insights of confinement effects on MTO reaction. *ACS Catal.* **2015**, 5, 661-665.
- (24) Dusselier, M.; Deimund, M. A.; Schmidt, J. E.; Davis, M. E. Methanol-to-olefins catalysis with hydrothermally treated zeolite SSZ-39, *ACS Catal.* **2015**, 5, 6078-6085.
- (25) Baerlocher, C.; McCusker, L.B.; Olson, D.H. Atlas of Zeolite Framework Types. 6th revised ed. 2007, Amsterdam: Elsevier.

4.7. Supporting Information for Chapter 4

4.7.1. Trimethylphosphite Treatment of H-ZSM-5

The trimethylphosphite treatment method was applied to a commercial ZSM-5 (MFI) sample (Zeolyst CBV3024E, Si/Al=15) to verify that the method effectively poisons all accessible Brønsted acid sites. 1.5 g of the calcined (H-form) zeolite was dried for 2 h at 300°C under vacuum and then refluxed for 20 h at 125°C in 7.5 mL octane and 1.6 mL trimethylphosphite. The solids were filtered, washed with dichloromethane and pentane, and dried at 100°C. The dried solids were then calcined in breathing-grade air by heating at 1°C/min to 150°C, holding for 2 h, and then 5 h at 500°C.

Elemental analysis by EDS of the phosphite-exchanged and calcined H-ZSM-5 samples shows that the sample has a P/Al ratio of 1.14, suggesting that all of the aluminum sites were exchanged. The ^{31}P NMR spectra of the hydrated trimethylphosphite-treated H-ZSM-5 (Figure 4-5) shows overlapping peaks that can be assigned to free and coordinated phosphorus species. The peak at approximately 0 ppm is likely free phosphate species, while signals at -6 and -12 ppm are typically assigned to terminal and middle phosphate groups in short chain polyphosphates.^{9,10} On the other hand, signals at lower frequencies (approximately -15 to -40 ppm) have been typically assigned to highly condensed polyphosphate species and polyphosphates coordinated to aluminum.⁹⁻¹³ Dehydration of the trimethylphosphite-treated H-MFI shifts the peaks to lower frequencies, consistent with condensation of the shorter chain phosphates to longer chain polyphosphates. The ^{27}Al NMR of the trimethylphosphite-treated sample (Figure 4-6) shows that after phosphite exchange and calcination, a peak occurs at approximately -8 ppm that can be assigned to

tetrahedral framework aluminum that is converted to octahedral coordination by the coordination of phosphate groups.¹⁵ These characterization data are consistent with coordination of phosphate to aluminum in the zeolite sample.

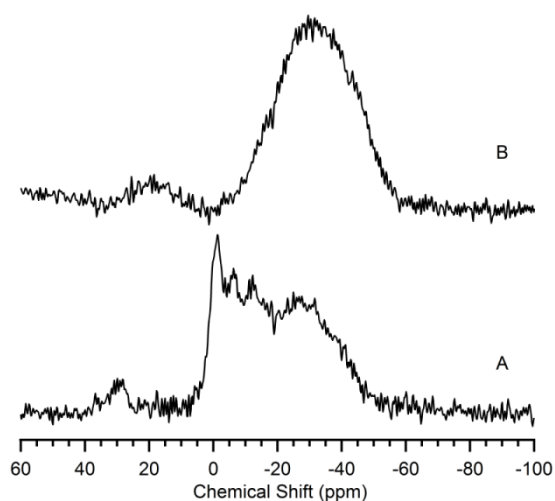


Figure 4-5. ^{31}P NMR spectra of trimethylphosphite-exchanged and calcined H-ZSM-5 (A) hydrated and (B) dehydrated

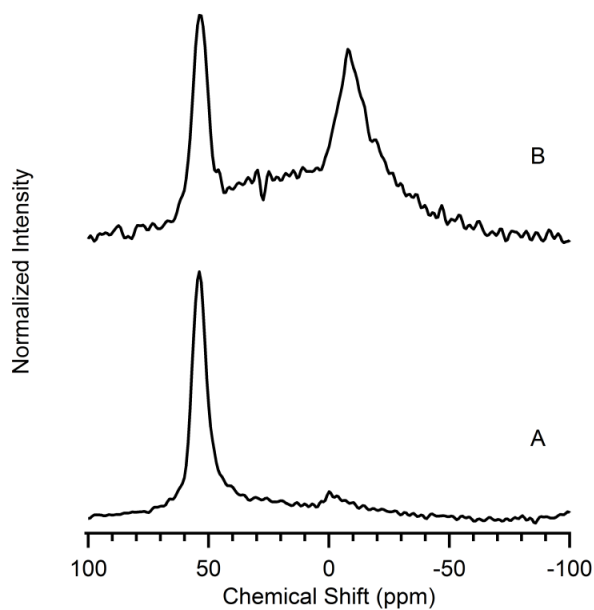


Figure 4-6. ^{27}Al NMR spectra of (A) H-ZSM-5 and (B) trimethylphosphite-exchanged and calcined H-ZSM-5

i-Propylamine TPD was performed on the samples to verify that Brønsted acid sites are poisoned by the treatment (Figure 4-7). The TPD results show that the higher temperature propene peak above 550 K (associated with the reaction of *i*-propylamine at Brønsted acid sites to form propene and ammonia) is significantly reduced to near-baseline levels after treatment.

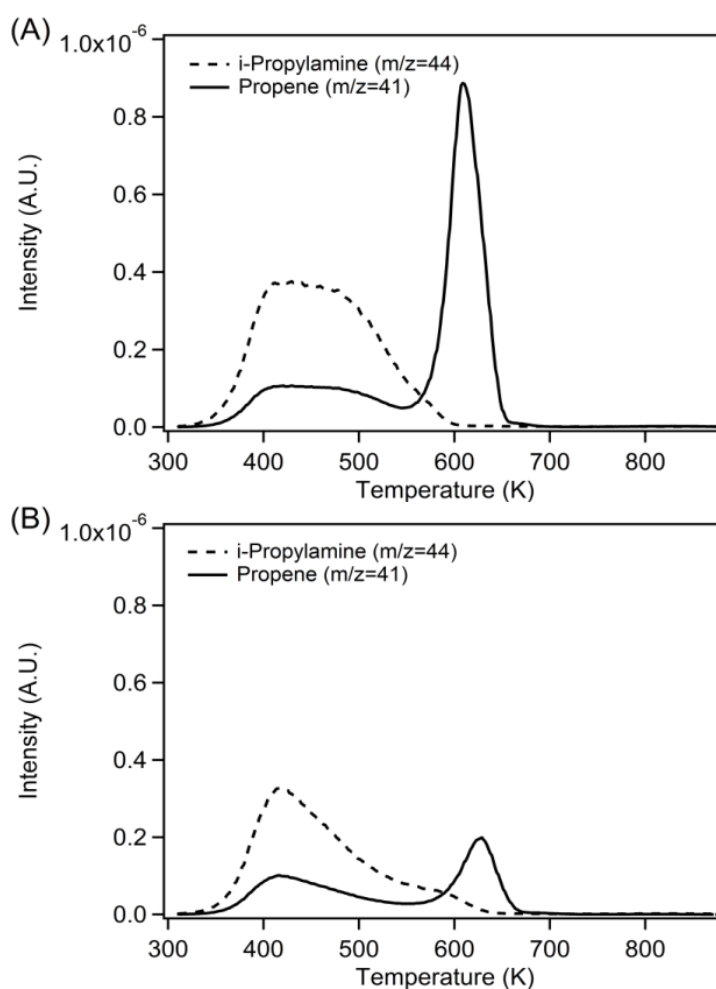
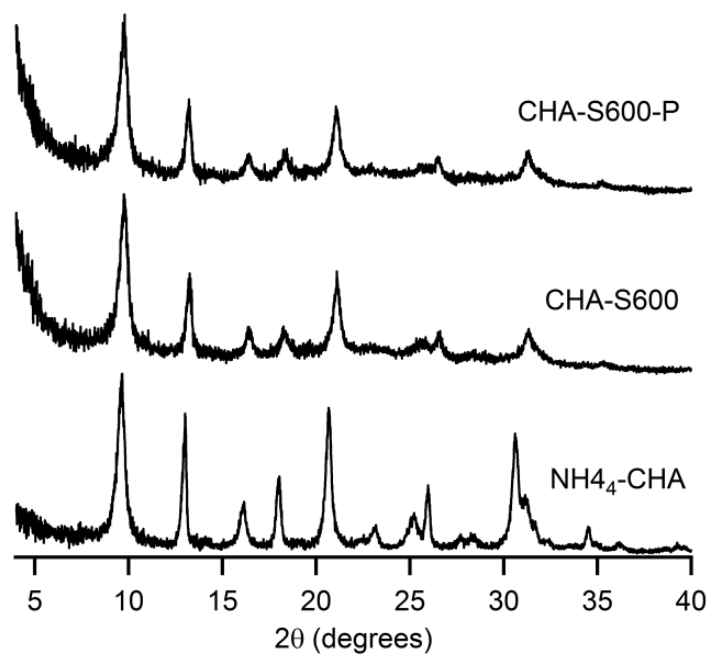
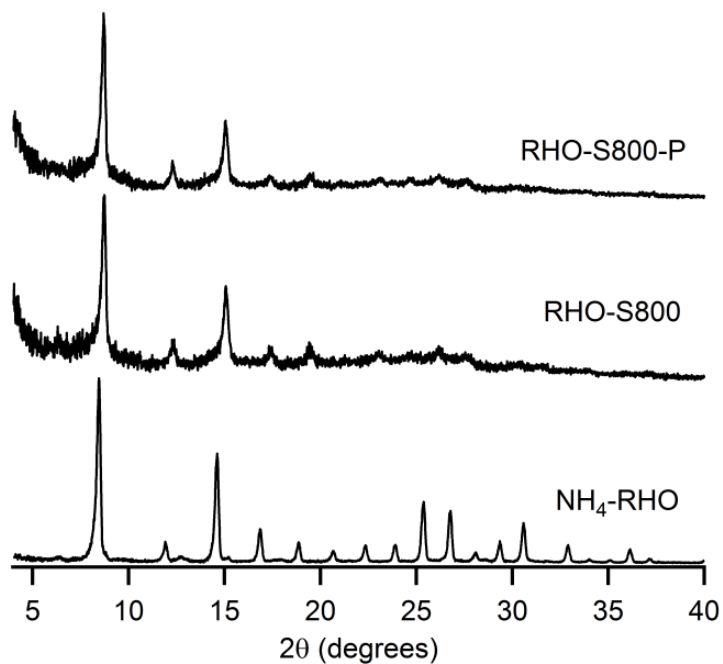


Figure 4-7. *i*-Propylamine TPDs of (A) H-MFI and (B) H-MFI after trimethylphosphite treatment

4.7.2. Additional Characterizations of Trimethylphosphite-Treated 8MR zeolites

Figure 4-8. Powder XRD patterns of NH_4 -exchanged, steamed and phosphite-treated CHAFigure 4-9. Powder XRD patterns of NH_4 -exchanged, steamed and phosphite-treated RHO

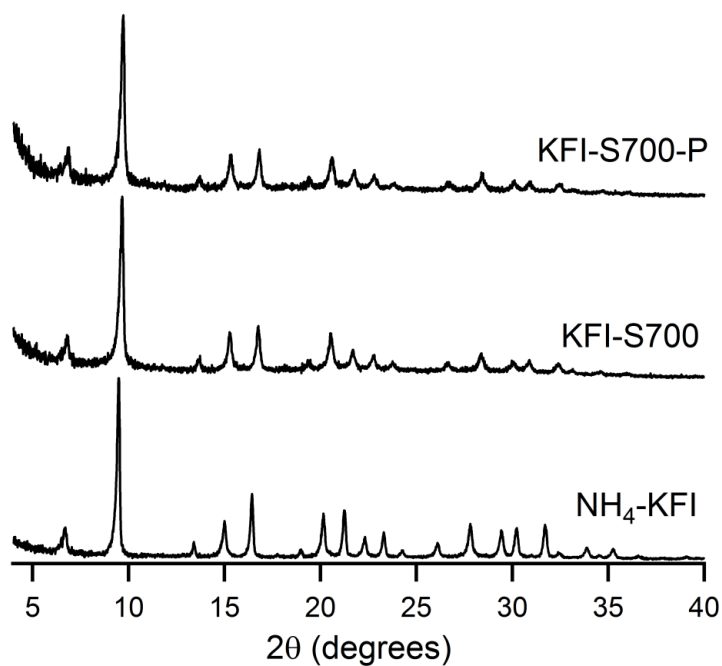


Figure 4-10. Powder XRD patterns of NH_4 -exchanged, steamed and phosphite-treated KFI

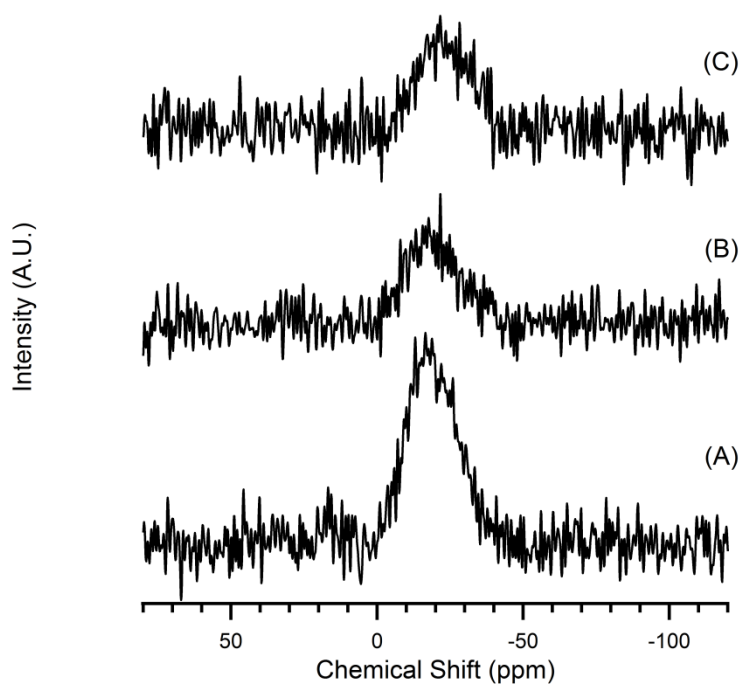


Figure 4-11. ^{31}P NMR spectra of trimethylphosphite-treated samples post MTO reaction: (A) CHA-S600-P, (B) RHO-S800-P and (C) KFI-S700-P

5. Conclusion and Future Directions for OSDA-free synthesis of 8MR zeolite catalysts for MTO

5.1. Conclusions

This part of the thesis explored a low-cost synthesis method for preparing small pore zeolite catalysts for the MTO reaction without using OSDAs. The preparation method entails synthesizing high aluminum 8MR zeolites (Si/Al typically less than 5) in the absence of OSDAs and extracting a portion of the framework aluminum via high temperature steam treatments to convert the materials into catalysts that may be useful for MTO. This dealumination method was first demonstrated successfully on CHA and then extended to two other 8MR zeolites, RHO and KFI. These materials can be synthesized reliably and on a large scale in the absence of OSDAs by using alkali cations, but they have not yet been explored for MTO in the as-synthesized form because of their high aluminum contents.

The effects of steaming temperature and steam partial pressure on the structures were investigated. Characterizations by XRD and argon physisorption indicate that steaming causes partial structural collapse of the frameworks (including loss of micropore volume), with the extent of degradation increasing with increasing steaming temperature, while simultaneously introducing mesopores. Extraction of framework aluminum is supported by ^{27}Al NMR that shows the conversion of tetrahedral (framework) aluminum to

penta-coordinated and octahedral aluminum. These data were consistent with ^{29}Si NMR spectra of the steamed samples that showed decreasing aluminum in the second coordination spheres of the framework silicon. Extraction of framework aluminum leads to decreased Brønsted acid site concentrations in the steamed samples, as titrated by TPD using ammonia on steamed CHA samples. The accessibility of these remaining acid sites is increased via the introduced mesopores, as titrated by reactive TPD with *i*-propylamine.

The effects of steam partial pressure were investigated for CHA and RHO by changing the water saturator temperature (60°C, 80°C or 90°C, corresponding to 19.9, 47.3 and 70.1 kPa, respectively). Interestingly, increased degradation is observed when the zeolites are steamed under lower steam partial pressures (19.9 kPa) for both materials. It is believed that the presence of steam is necessary during the initial heating period to stabilize the zeolite framework particularly at temperatures where the framework would normally collapse under dry calcination conditions. Steaming of zeolite Y under these same steaming conditions exhibits the same trend of increased degradation at lower steam partial pressures, suggesting that this trend is not unique to 8MR zeolites.

Evaluation of the materials for MTO showed that the steam treatments lead to improved olefin selectivities as well as lifetimes. The improved MTO activity is attributed to the extraction of framework aluminum that reduces the concentration of Brønsted acid sites as well as the introduction of mesopores that facilitate transport of reactants into the crystallites. For CHA, an optimal steaming temperature of 600°C (at a water saturator temperature of 80°C) was identified that gave the best lifetime and olefin selectivities

comparable to SAPO-34. The MTO activity of this sample was retained upon regeneration of the spent catalyst. Extra-framework aluminum could be removed from this sample by acid washing, leading to a further enhancement in the lifetime. 600°C was also the optimal steaming temperature for RHO and KFI. Samples steamed at this temperature had the best combination of catalyst lifetime and olefin selectivity, while samples steamed at higher temperatures had lower lifetimes with only minimal improvements in olefin selectivities.

Overall, CHA performed the best out of the three 8MR zeolites studied in terms of combined olefin selectivities and lifetimes. At a reaction temperature of 450°C, CHA steamed at 600°C (and water saturator temperature of 80°C) reached a combined ethylene and propylene selectivity of 74.2% at 100% conversion, approaching that of the commercial catalyst. On the other hand, the highest selectivity towards propylene was achieved with 800°C steamed RHO that had an average $C_3=/C_2=$ ratio of 1.8/1 compared to 1.2/1 for 600°C steamed CHA. The higher propylene selectivity for RHO makes it an interesting material given that propylene demand is growing and has a higher value than ethylene.

Comparison of the reaction profiles of the three zeolites studied here showed differences in their product distributions. In particular, the RHO and KFI samples showed higher butylene and lower ethylene selectivities ($C_4=/C_2=$ ratios of approximately 1:1) compared to CHA ($C_4=/C_2=$ ratios of approximately 1:2) as well as lower DME production. To assess whether these differences arise from secondary reactions at the mesoporous and

external surface acid sites of the steamed zeolites, trimethylphosphite treatments are carried out to selectively poison these sites. The attachment of phosphorus onto the steamed zeolites is verified by ^{31}P NMR and ^{27}Al NMR, and elimination of acid sites external to the 8MR pores is verified by *i*-propylamine TPD. When evaluated for MTO activity, all of the phosphite-treated samples show longer catalyst lifetimes and less coke content but no changes in olefin selectivities are observed. These results suggest that olefins do not undergo secondary dimerization or methylation reactions that affect the resulting product distributions observed for the steamed zeolites, and instead, the mesoporous and surface acid sites serve as sites for coke deposition. Differences in the product distributions are instead attributed to differences in the unique pore structures of each of the zeolites.

5.2. Recommended Future Work

The results presented here show that high aluminum 8MR zeolites that are synthesized without OSDAs can be dealuminated by steam treatments to convert them into useful catalysts for MTO. The successful demonstration of this low-cost method on three 8MR zeolite structures suggests that it may be effective on many other small pore zeolites that are synthesized without using OSDAs. Other structures with 8MR pores that may be interesting to explore are LEV and RTH. These materials can be synthesized via OSDA-free, seeded synthesis methods and show interesting MTO behavior in the as-synthesized forms.^{1,2} If new OSDA-free synthesis methods are discovered for additional 8MR zeolites, those materials may also be of interest to investigate.

The MTO reaction data for CHA, RHO and KFI suggest that the cage size plays a role in controlling the selectivities towards different olefins. This effect may be better understood by investigating the types of aromatic intermediates in each of the structures. Occluded carbon analyses and mechanistic studies would provide greater insight into the underlying mechanisms that give rise to the differing olefin selectivities observed. The study with trimethylphosphite treatment suggests that olefins do not undergo secondary methylation and cracking reactions at acid sites located external to the 8MR pore system. The absence of secondary reactions may be further confirmed by cofeeding of ethylene and ^{13}C -labeled methanol. The production of propylene with one ^{13}C atom incorporated would indicate occurrence of secondary methylation. Comparison of the reaction results on the steamed samples with and without phosphite treatment would thus provide further confirmation of whether secondary reactions occur at the mesoporous and external surface sites.

Finally, in addition to MTO, 8MR zeolites are also currently of interest as deNO_x catalysts (via ammonia selective catalytic reduction of NO_x species) for diesel engines. Small-pore zeolites with high Si/Al ratios are also desirable as deNO_x catalysts due to their robust hydrothermal stability. Thus, the dealumination method presented here may also be of interest to investigate as catalysts for deNO_x.

5.3. References

- (1) Zhang, H.; Yang, C.; Zhu, L.; Meng, X.; Yilmaz, B.; Müller, U.; Feyen, M.; Xiao, F. Organotemplate-free and seed-directed synthesis of levyne zeolite. *Micropor. Mesopor. Mater.*, **2012**, *155*, 1-7.
- (2) Yokoi, T.; Yoshioka, M.; Imai, H.; Tatsumi, T. Diversification of RTH-Type zeolite and its catalytic application. *Angew. Chem. Int. Ed.*, **2009**, *48*, 9884–9887.

A. Microporous zincosilicate molecular sieves as catalysts for propane dehydrogenation

A.1 Abstract

Three microporous zincosilicate molecular sieves are explored as catalysts for propane dehydrogenation: Zn-MFI (zincosilicate of the MFI framework), CIT-6 (BEA) and VPI-8 (VET). Both Zn-MFI and CIT-6 are active for dehydrogenation, but their activity depend upon the treatment conditions. In CIT-6, framework zinc sites without associated alkali, *e.g.*, lithium, (resembling Zn^{2+} sites on amorphous silica) are identified as catalytically active for propane dehydrogenation while alkali-bearing zinc sites are inactive. CIT-6 that has been ammonium exchanged to remove lithium shows high initial activity for dehydrogenation, reaching maximum propylene selectivities above 90% but deactivates faster than supported platinum catalysts. The stability of the catalyst could be improved by a reduction treatment prior to reaction or by the addition of nickel as a promoter. However, the addition of platinum to CIT-6 provided the most stable catalyst.

A.2 Introduction

Propylene is currently predominantly obtained via steam cracking or catalytic cracking of crude oil where it is viewed mainly as a byproduct. However, the recent abundance of shale gas has both lowered propane prices and caused a shift in feedstocks for cracking operations from heavier (naphtha) to lighter fractions (mainly ethane) that produce

relatively low yields of propylene compared to cracking of heavier fractions. At the same time, propylene demand is expected to rise faster than production, creating opportunities for on-purpose propylene production technologies, particularly via propane dehydrogenation.

Nonoxidative alkane dehydrogenation is highly endothermic ($\Delta H_{298}^0 = 124.3$ kJ/mol for the dehydrogenation of propane: $\text{C}_3\text{H}_8 \leftrightarrow \text{C}_3\text{H}_6 + \text{H}_2$) and thus equilibrium limited. At the high temperatures required to obtain significant olefin yields, undesired side reactions such as cracking and coking (generally regarded as the major cause of catalyst deactivation)¹ are also favorable. A suitable dehydrogenation catalyst must therefore possess good activity and be selective for activation of C-H bonds over C-C bonds.

Two types of catalysts have typically been used in commercial dehydrogenation processes: chromium oxide-based catalysts and supported platinum catalysts with various promoters. Chromia supported on alumina has been studied extensively for dehydrogenation of alkanes² and is the basis of the Catofin process (CB&I Lummus). Platinum is also active for dehydrogenation in the metallic state and identified to be superior for activation of C-H bonds compared to other noble metals. Both the Pacol and the Oleflex processes developed by UOP are based on a platinum supported on alumina catalyst. While dehydrogenation of alkanes is structure insensitive (the reaction rate is independent of the size of the platinum particles), the rates of undesired side reactions such as hydrogenolysis, isomerization and coking increase with increasing particle size. The addition of promoters modifies the catalytic properties of the platinum and improves its

activity.³ Tin is the most studied promoter, and it is generally accepted that the addition of tin (forming a Pt-Sn alloy) increases the platinum dispersion, thus suppressing the rate of the undesired structure-sensitive reactions.¹ It has also been proposed that Sn modifies the electronic properties of platinum and decreases the energy barrier for desorption of propylene.⁴ Another common promoter is zinc that improves the performance of supported platinum catalysts for similar reasons.^{5,6} The nature of the support plays a role in the reactivity. Desirable supports must be thermally stable, allow for high dispersion of metal particles (high surface area and porosity), and have limited Brønsted acidity to avoid side reactions.⁷ Two common supports are alumina as well as zeolites with added alkali metals that neutralize the acidity of the support.

Recently, it was reported that single site Zn^{2+} supported on amorphous silica are active and highly selective (greater than 95%) catalysts for propane dehydrogenation, albeit with low reaction rates.⁸ The active site was identified to be isolated, 3-coordinate Lewis acidic Zn^{2+} sites. The proposed mechanism involves cleavage of a terminal C-H bond on propane to form a zinc alkyl (with a proton transferred to a bridging oxygen) followed by beta hydride elimination to form propylene and zinc hydride. In addition to zinc, several other single-site Lewis acid catalysts have also been identified to be active for dehydrogenation including Fe^{2+} and Co^{3+} .^{9,10}

The results reported for these single site Lewis acid catalysts suggested to us that Lewis acid molecular sieves (pure silica based microporous molecular sieves with isolated metal (IV) centers) may also be active for dehydrogenation without the use of platinum.

The objective of this project was to screen a variety of Lewis acid molecular sieves for dehydrogenation activity focusing on microporous zincosilicates. While Lewis acidic zeotypes have been investigated for a wide range of reactions (*e.g.*, Baeyer-Villiger oxidation, Meerwein-Ponndorf-Verley-Oppenauer reduction, and isomerization of sugars),^{11,12} they have not yet been explored for alkane dehydrogenation. Moreover, in zinc-containing catalysts that have been studied for dehydrogenation, zinc is either added as a promoter for a second metal, *e.g.*, platinum, in a bimetallic system or exchanged onto aluminosilicate supports. For instance, zinc- and gallium-exchanged ZSM-5 (aluminosilicate of the MFI type) have been studied extensively for alkane dehydrogenation and aromatization.^{13,14} Zhang et al. investigated platinum supported on H-ZSM-5 and found improved activity and stability when Sn or Zn was incorporated in the zeolite framework.^{15,16} Similarly, workers at BP reported high activity and selectivity for platinum-impregnated Zn-MFI (zincosilicate of the MFI type).¹⁷

CIT-6 is a zincosilicate molecular sieve with the beta (BEA) framework that was first synthesized in the M.E. Davis group.^{18,19} Framework zinc sites in CIT-6 are accessible to guest molecules and behave as Lewis acid centers in probe molecule IR spectroscopy.²⁰ Previously, CIT-6 has mainly been studied as a support for other metals and not yet explored as a direct catalyst for dehydrogenation (though it is reported to be a selective catalyst for the Diels-Alder cycloaddition-dehydration reactions of ethylene and substituted furans). Previous work in our lab showed that platinum supported on CIT-6 is an active and selective catalyst for propane dehydrogenation with performance comparable to the platinum supported on Zn-MFI catalyst developed by BP (CIT-6 was never tested by itself

in this study),²¹ while Ni^{2+} exchanged on CIT-6 has been investigated as a catalyst for propylene oligomerization.²² The propane dehydrogenation results with zinc supported on amorphous silica suggested to us to explore zincosilicates as direct catalysts for the reaction. In addition to CIT-6, two other microporous zincosilicates, Zn-MFI and VPI-8 (VET), were explored.

A.3 Experimental Section

A.3.1 Synthesis of Materials

A.3.1.1 *Zn-MFI*

Zincosilicate MFI (Zn-MFI) was synthesized following the BP patent method.¹⁷ In a typical synthesis, 0.9 g of $\text{ZnSO}_4 \cdot 7\text{H}_2\text{O}$ (Aldrich 99.7%) was dissolved in 3 g distilled water. NH_4OH solution (JT Baker 25-30% in water) was added dropwise until the pH was 6. The precipitated solids were filtered, washed with water, dried at room temperature, and then dissolved in a solution of 0.404 g NaOH (Mallinckrodt pellets) in 4.626 g distilled water. 3.985 g of tetrapropylammonium hydroxide (TPAOH) (Acros Organics 25 wt% aqueous solution) was then added to the solution followed by 6.984 g colloidal silica (Ludox AS-40). The final gel had molar composition: 1.6 Na_2O /1.57 TPAOH/14.9 SiO_2 /1 ZnO/217 H_2O . The gel was loaded in Teflon-lined autoclaves and heated for 4 days at 175°C with tumbling. The solids were then centrifuged, washed with water and acetone and dried overnight at 100°C.

A.3.1.2 CIT-6 and VPI-8

CIT-6 was synthesized following the method reported by Takewaki et al.¹⁸ In a typical synthesis, 40.055 g tetraethylammonium hydroxide (TEAOH) (Aldrich, 35 wt% aqueous solution) was diluted with 39.651 g distilled water. 0.307 g LiOH·H₂O (Aldrich, 98+%) was added to the solution followed by 0.964 g Zn(OAc)₂·2H₂O (Aldrich, 99.999%). Once dissolved, 22 g of colloidal silica (Ludox AS-40) was added, and the solution was stirred for 2 h at room temperature. The final gel molar composition was 1 SiO₂/0.03 Zn(OAc)₂/0.65 TEAOH/0.05 LiOH/30 H₂O. This gel was loaded into three Teflon liners and then heated for 12 days at 140°C. The solids were recovered by centrifugation as described previously. Three batches of CIT-6 were used in this study and are designated CIT-6A, CIT-6B and CIT-6C. VPI-8 was prepared from a synthesis gel that was prepared in the same manner as CIT-6, but the gel was heated at 150°C for 15 days. The as-synthesized product was calcined for 6 h at 580°C in breathing air, exchanged with 1 M NH₄NO₃ for 24 h at 80°C, and calcined again for 6 h at 580°C.

A.3.1.3 Si-BEA

Pure silica BEA (Si-BEA) was prepared following previously reported procedures.²³ 3.862 g tetraethylammonium fluoride dihydrate (TEAF·2H₂O) (Aldrich, 98.5%) was dissolved in 10 g of distilled water, and then 10.204 g tetraethylorthosilicate (TEOS) (Aldrich, 98%) was added. The solution was covered and stirred overnight to hydrolyze. The solution was then allowed to evaporate until the desired composition was reached. The final composition was 1 SiO₂/0.55 TEAF/7.25 H₂O. The gel was transferred to a Teflon-line autoclave and heated for 7 days at 140°C with tumbling.

A.3.1.4 Zn/SiO₂

Zn supported on amorphous silica (Zn/SiO₂) was prepared following the method reported by Schweitzer et al.⁸ 10 g of silica (Davisil 646, 35-60 mesh, 300 m²/g) was stirred in 80 g distilled water, and the pH was adjusted to 11 using NH₄OH (JT Baker 25-30 wt% in water). A separate solution was prepared by dissolving 2 g Zn(NO₃)₂·6H₂O (Aldrich, 98%) in 20 g distilled water that was pH adjusted to 11 using NH₄OH. The zinc solution was rapidly added to the silica, and the resulting mixture was stirred for approximately 10 min before the liquid was decanted. The solids were filtered, washed with water, dried overnight at 100°C and finally calcined for 3 h at 300°C in breathing air.

A.3.2 CIT-6 Exchange Treatments

To investigate the catalytically active zinc sites in CIT-6 for dehydrogenation, Li and N(CH₃)₄ exchanges were performed following the method reported by Orazov et al.²⁰ that shift the distribution of sites. Exchanges were performed with CIT-6 that had been calcined for 2 h at 150°C and then 10 h at 550°C (1°C/min) in breathing air. Li exchange was performed using 1 M LiNO₃ (with pH adjusted to 10 using 5 wt% LiOH solution) for 12 h at room temperature (100 mL liquid/g solid). N(CH₃)₄ exchange was performed using 1 M N(CH₃)₄Cl (pH adjusted to 10 using NH₄OH) for 12 h at room temperature (100 mL liquid/g solid). The solids were recovered by centrifugation, washed with water and acetone, and dried overnight at 100°C. The resulting products were calcined again for 10 h at 550°C in breathing air. A portion of the N(CH₃)₄ exchanged sample was back exchanged with Li to determine the effect on reactivity. This sample was exchanged with LiNO₃, calcined in the same manner as previously described and designated (CIT-6B-N(CH₃)₄-Li).

Zinc-exchanged CIT-6 was prepared by stirring as-synthesized CIT-6 in 0.01 M $\text{Zn}(\text{OAc})_2 \cdot 2\text{H}_2\text{O}$ (Aldrich, 99.999%) solution (100 mL liquid/g solid) for 5 h at 75°C. The pH of the zinc solution was adjusted to 7 using NH_4OH solution to avoid excessive extraction of framework zinc during the exchange. The solids were recovered by centrifugation, washed with water and acetone and dried at 100°C. The dried solids were then calcined for 2 h at 150°C and then 10 h at 550°C (1°C/min) in breathing air.

A.3.3 Platinum and Nickel Impregnation

Platinum-impregnated Zn-MFI (Pt/Zn-MFI) was prepared following the BP patent method.¹⁷ As-made Zn-MFI was calcined for 6 h at 550°C, exchanged twice with 1 M NH_4NO_3 for 1 h at room temperature, and calcined again for 6 h at 550°C. 1 g of the dried solids was stirred in a solution of 0.0091 g $\text{Pt}(\text{NH}_4)_4\text{Cl}_2$ hydrate (Aldrich, 98%) and 3.9 g distilled water and dried in a rotary evaporator under vacuum. The resulting solids were dried overnight at 70°C. The amount of platinum added was calculated to be 0.5 wt% of the solids.

Platinum-impregnated CIT-6 (Pt/CIT-6) was prepared according to the method reported by Andy et al.²¹ As-made CIT-6 was contacted four times with 1 M NH_4NO_3 solution for 10 h at 80°C to extract a portion of the OSDA. The resulting solids were calcined for 10 h at 550°C in breathing air, and then exchanged with 1 M NH_4NO_3 for 10 h at 80°C. The solids were recovered by centrifugation, washed with water and acetone and dried at 100°C. Platinum impregnation of the NH_4 -exchanged CIT-6 was performed in the same manner as described above.

Nickel-impregnated CIT-6 was carried out by stirring 0.7 g of solids (CIT-6 that had been contacted with NH_4NO_3 , calcined and NH_4 exchanged) in a solution of 1.4 g distilled water and 0.0173 g $\text{Ni}(\text{NO}_3)_2 \cdot 6\text{H}_2\text{O}$ (Aldrich) (the amount of nickel added was 0.5 wt% of the solids). The liquid was removed in a rotary evaporator under vacuum, and the remaining solids were dried overnight at 70°C. A 2.5 wt% nickel-loaded CIT-6 sample was prepared in the same manner but with five-fold the nickel loading.

A.3.4 Reaction Testing

Reaction testing was conducted in a Parker Autoclave Engineers BTRS-JR reactor system fitted with a stainless steel reactor tube that had been passivated with a silicon coating (SilcoNert 1000). Catalysts were pelletized, crushed and sieved to obtain particles between 0.15 and 0.6 mm in diameter. Approximately 400 mg of the sieved material was suspended between quartz wool beds in the reactor tube. Reactions were conducted at atmospheric pressure and 540°C with a propane WHSV of 2.2 h^{-1} and propane to inert molar ratio of 4:1. 5% argon bal. helium was used as the inert gas with argon serving as the internal standard. Effluent gases were monitored by an online GC (Agilent 7890A) with FID and TCD detectors.

Once loaded in the reactor, samples were heated in helium (approximately 50 cc/min) at 1°C/min to 150°C, held there for 2 h, and then heated at 1°C/min to the reaction temperature. Once the temperature stabilized, the reactant streams were switched to flow over the sample. For NH_4 exchanged CIT-6 samples, the materials were calcined in-situ in breathing air prior to reaction by heating at 1°C/min to 550°C and held for 10 h. Afterward,

the reactor was cooled to 540°C, and flushed with helium (approximately 50 cc/min) for at least 1 h before starting the reaction. For platinum and nickel impregnated samples, the catalysts were first calcined in-situ in breathing air (approximately 50 cc/min) for 2 h at 150°C and then 8 h at 400°C (1°C/min ramp rate). After cooling, the sample was flushed with helium for at least 1 h and then reduced in hydrogen (20 cc/min) by heating at 1°C/min to 540°C and held there for 6 h. At the end of the reduction period, the sample was flushed with helium before starting the reaction.

Propane conversions ($X_{C_3H_8}$) and selectivities (S_i) are computed on a carbon mole basis according to Equations A-1 and A-2, respectively. Carbon balances are calculated based on the moles of carbon converted (Equation A-3), where n_i and $n_{c,i}$ represent the molar flow rate and carbon number for species i , respectively

$$X_{C_3H_8} = \frac{n_{C_3H_8,in} - n_{C_3H_8,out}}{n_{C_3H_8,in}} \cdot 100\% \quad (A-1)$$

$$S_i = \frac{n_{i,out} \cdot n_{c,i}}{3(n_{C_3H_8,in} - n_{C_3H_8,out})} \cdot 100\% \quad (A-2)$$

$$Carbon\ balance = \frac{\sum_{i=All\ Products} n_{i,out} \cdot n_{c,i}}{3(n_{C_3H_8,in} - n_{C_3H_8,out})} \cdot 100\% \quad (A-3)$$

Coke contents of the spent catalysts were measured by thermogravimetric analysis (TGA) that were performed in a PerkinElmer STA 6000 instrument by heating the solids to 900°C at a rate of 10°C/min under a flow of zero-grade air (20 sccm).

Table A-1. Summary of catalyst treatments and Si/Zn ratios

Sample	Treatment					Si/Zn
	Step 1	Step 2	Step 3	Step 4	Step 5	
Zn-MFI-NH₄	Calcination	NH ₄ exchange	Calcination	-	-	32.3 ± 1.9
Pt/Zn-MFI	Calcination	NH ₄ exchange	Calcination	0.5 wt% Pt impregnation	-	25.5 ± 1.9
CIT-6A-C	Calcination	-	-	-	-	14.2 ± 1.4
CIT-6A-Li	Calcination	Li exchange	Calcination	-	-	13.3 ± 1.1
CIT-6B-Li						13.2 ± 1.1
CIT-6A-N(CH₃)₄	Calcination	N(CH ₃) ₄ exchange	Calcination	-	-	14.7 ± 1.8
CIT-6B-N(CH₃)₄						13.3 ± 1.9
CIT-6B-N(CH₃)₄-Li	Calcination	N(CH ₃) ₄ exchange	Calcination	Li exchange	Calcination	15.0 ± 1.6
CIT-6A-Zn	Zn exchange	Calcination	-	-	-	8.2 ± 0.4
CIT-6A-NH₄	SDA extraction with NH ₄ NO ₃	Calcination	NH ₄ exchange	-	-	20.1 ± 2.4
CIT-6B-NH₄						18.7 ± 1.6
CIT-6C-NH₄						22.3 ± 1.3
CIT-6A-Pt	SDA extraction with NH ₄ NO ₃	Calcination	NH ₄ exchange	0.5 wt% Pt impregnation	-	18.5 ± 1.0
Ni/CIT-6B-0.5	SDA extraction with NH ₄ NO ₃	Calcination	NH ₄ exchange	0.5 wt% Ni impregnation	-	21.2 ± 3.0
Ni/CIT-6C-2.5	SDA extraction with NH ₄ NO ₃	Calcination	NH ₄ exchange	2 wt% Ni impregnation	-	23.6 ± 2.5
VPI-8-C	Calcination	-	-	-	-	27.9 ± 4.9
VPI-8-NH₄	Calcination	NH ₄ exchange	Calcination	-	-	29.7 ± 4.6

A.4 Results and Discussion

Table A-1 provides a summary of the catalysts tested, the post-synthetic treatments that were performed and the Si/Zn ratios as measured by EDS. Three separate batches of CIT-6 were used for reaction testing, and samples from different batches that underwent the same treatments are grouped together in Table A-1 where applicable. A summary of the reaction testing results is provided in Table A-2, which shows conversions and propylene

selectivities at two time points: approximately 1 h and 10 h time on stream (or the final time point if the reaction was stopped before 10 h).

Table A-2. Reaction data at specific time points for Zn-MFI and CIT-6 samples. Reaction conditions: 540°C, 4:1 (mol/mol) propane:inert, 2.2 h⁻¹ WHSV and 0.4 gcat. unless otherwise specified

Entry	Sample	Time (min)	Conversion (%)	Propylene Selectivity (%)
1	Pt/Zn-MFI	63	30.2	99.5
		434	28.5	100
2	Zn-MFI-NH ₄	54	15.2	100
		592	8.9	95.9
3	CIT-6A-Pt	55.2	29.5	92.5
		445	29.6	98.8
4	CIT-6A-NH ₄	66	27.3	75.6
		529	15.3	97.0
5	CIT-6B-NH ₄	55	27.1	66.0
		595	15.2	89.5
6	CIT-6C-NH ₄	62	26.1	64.4
		600	15.8	92.2
7	CIT-6C-NH ₄ ^a	68	21.7	91.5
		608	14.0	95.8
8	CIT-6C-NH ₄ ^b	69	8.4	79.9
		609	4.3	91.4
9	CIT-6A-C	67	11.6	86.9
		605	8.7	66.1
10	CIT-6A-Zn	68	23.9	84.9
		605	11.9	86.4
11	CIT-6A-Li	53	2.6	68.2
		591	1.7	74.3
12	CIT-6A-N(CH ₃) ₄	53	28.7	77.9
		608	15.8	86.2
13	CIT-6B-N(CH ₃) ₄ -Li	54	3.5	95.0
		594	2.7	80.8
14	Ni/CIT-6B-0.5	62	22.8	85.8
		602	15.0	88.1
15	Ni/CIT-6C-2.5	53	19.6	73.5
		612	12.1	79.8

^a In-situ pre-treatment used Pt/CIT-6 conditions

^b Reaction was carried out using 0.05 gcat for a propane WHSV of 17.6 h⁻¹

A.4.1 Zn-MFI Reaction Testing Results

Figure A-1 shows the reaction data for Zn-MFI with and without platinum. The Pt/Zn-MFI (Figure A-1A) sample achieves nearly 100% propylene selectivity, maintains a stable propane conversion averaging 29% and is resistant to coke (the catalyst had approximately 0.6 wt% coke post-reaction). While the equilibrium conversion of 28.3% for 540°C and a propane:inert ratio of 4:1 is slightly below this value, it is within error. This result is consistent with previously reported results for Pt/Zn-MFI by Andy et al.²¹ and verifies that the reactor system is working correctly. On the other hand, the Zn-MFI-NH₄ sample (Figure A-1B and Table A-2 entry 2) shows a similarly high propylene selectivity but deactivates gradually with time on stream. Minor amounts of lower hydrocarbons including methane, ethylene and ethane (less than 1% selectivity), as well as small amounts of (unidentified) higher molecular weight species (C₆ and higher), were also observed in the reactor effluent.

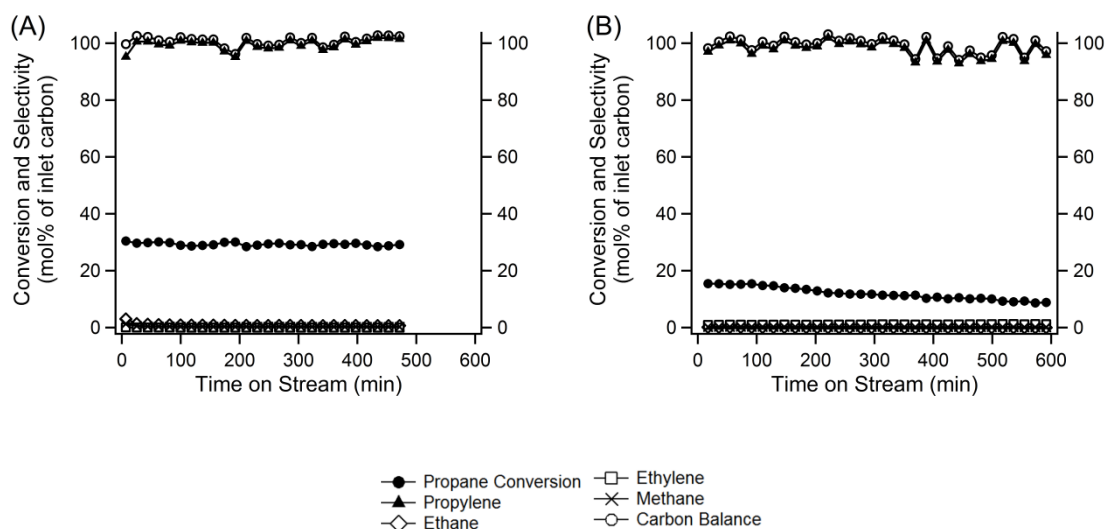


Figure A-1. Reaction data for (A) Pt/Zn-MFI and (B) Zn-MFI-NH₄

A.4.2 Zn/SiO₂ Reaction Testing Results

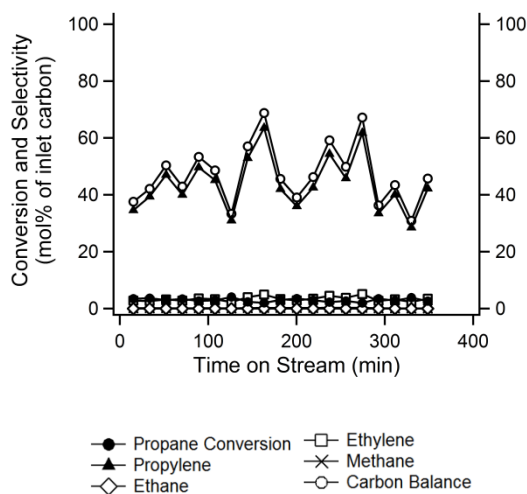


Figure A-2. Reaction data for Zn/SiO₂

EDS measurement of the Zn/SiO₂ catalyst indicates that this material has approximately 5.2 wt% zinc, consistent with results reported by Schweitzer et al.⁸ Figure A-2 shows the reaction profile for zinc on amorphous silica (Zn/SiO₂). Under the reaction conditions here, the material shows very low activity and is not selective for dehydrogenation. Conversion was between 2 and 4% for this material.

A.4.3 CIT-6 Reaction Testing Results

A.4.3.1 *Effect of Exchange Treatments*

Figure A-3 shows representative reaction profiles for platinum-impregnated CIT-6 (Pt/CIT-6A), NH₄-exchanged CIT-6 (CIT-6A-NH₄), zinc-exchanged CIT-6 (CIT-6A-Zn), and a pure-silica beta control. Similar to Pt/Zn-MFI, the platinum-impregnated CIT-6 (Figure A-3A) maintains a stable, near-equilibrium conversion of 29% and high C₃=

selectivity of near 100% for over 7 h time on stream, in agreement with previously reported results.²¹

The reaction profile for NH_4 -exchanged CIT-6 without platinum (CIT-6A- NH_4) is shown in Figure A-3B that indicates the material is also active for dehydrogenation but deactivates faster than Pt/CIT-6. Conversion initially starts at 31% and gradually decreases with time on stream, reaching 50% of its initial value after approximately 8.5 h while

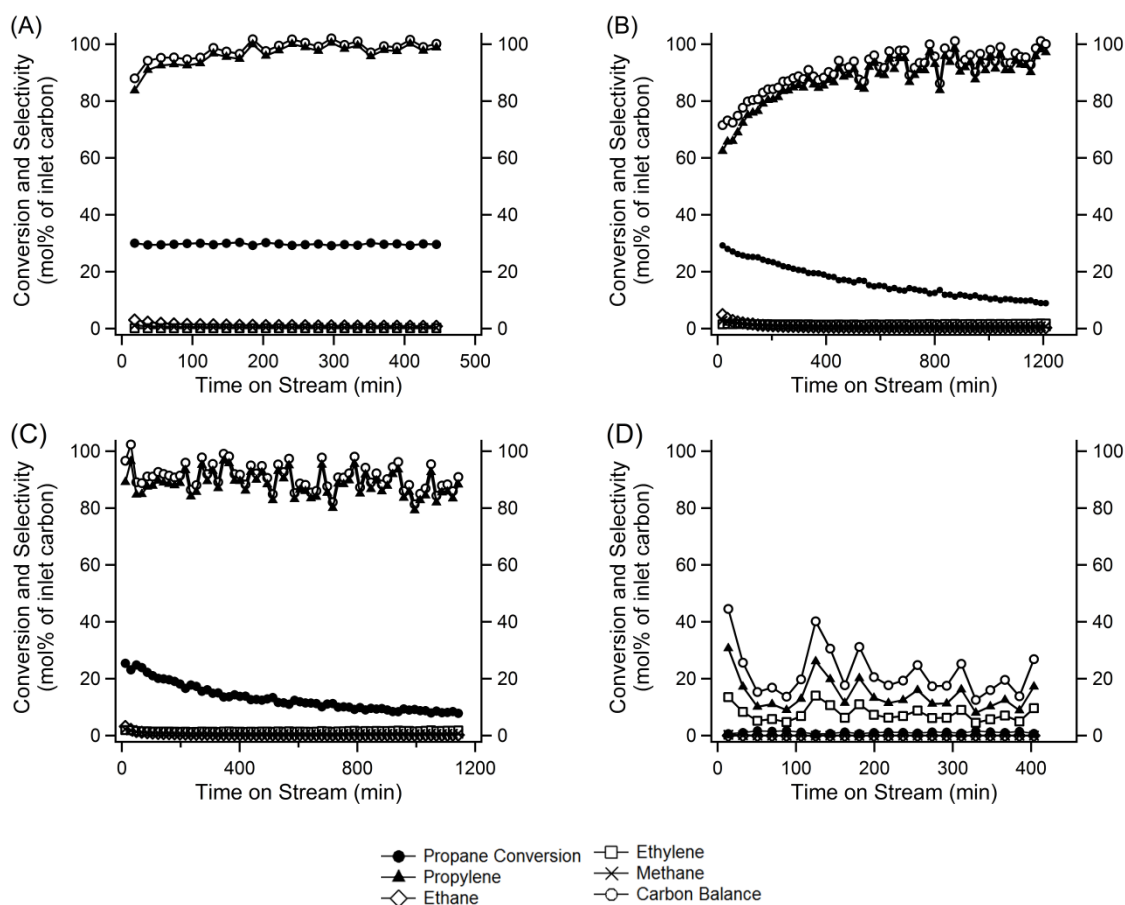


Figure A-3. Reaction data for (A) Pt/CIT-6A, (B) CIT-6A- NH_4 , (C) CIT-6A-Zn and (D) pure silica BEA.

propylene selectivity starts at 64% and increases to between 95-98% gradually. This material had approximately 21.3 wt% coke compared to approximately 5.2 wt% for Pt/CIT-6A. The zinc-exchanged CIT-6 (Figure A-3C) shows a similar deactivation profile. Initial conversion is at 25% and drops to 50% of the initial value after approximately 8 h, but propylene selectivity remains stable near an average of 88%. A pure-silica beta sample was prepared and reaction tested as a control (Figure A-3D). Conversion remained below 2% during the entire reaction period for this sample.

Reaction testing of NH_4 exchanged CIT-6 samples (Figures A-3B and A-4A) consistently show that when the conversion is near equilibrium at the start of the reaction, propylene selectivity is initially low and then increases with time on stream as conversion decreases below the equilibrium value. The initial conversion that is above equilibrium suggests that side reactions such as cracking or polymerization of olefins may be occurring that lead to coke deposition responsible for the low carbon balance initially observed. As the deactivation zone moves down the catalyst bed, the conversion capacity decreases while selectivity increases. To observe the true reactivity below equilibrium conversion, an NH_4 -exchanged CIT-6 sample was reaction tested where the propane WHSV was increased 8 fold (17.6 h^{-1}) by lowering the catalyst mass from 400 mg to 50 mg. Figure A-4 shows a comparison of reaction data for CIT-6C- NH_4 obtained at space velocities of 2.2 and 17.6 h^{-1} . At the higher space velocity, conversion starts near 11% and decreases to 50% of the initial conversion after approximately 5.5 h. The initial transient period where propylene selectivity rises is shorter (selectivity reaches 90% after approximately 3 h at a WHSV of 17.6 h^{-1} vs. 7.5 h at a WHSV of 2.2 h^{-1}).

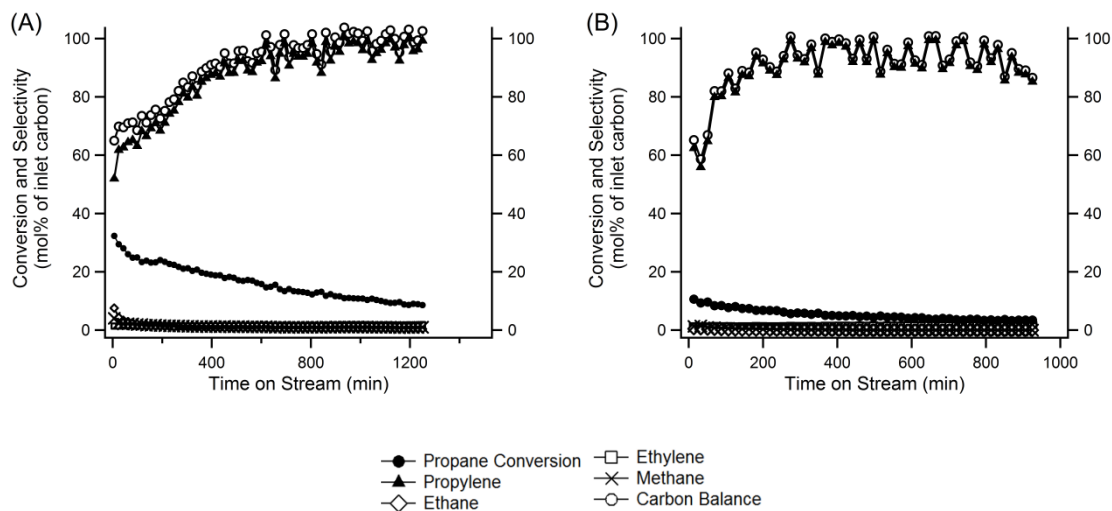


Figure A-4. Reaction data for CIT-6C-NH₄ tested at a propane WHSV of (A) 2.2 h⁻¹ and (B) 17.6 h⁻¹

We also note that the CIT-6 used in this study was synthesized using Ludox colloidal silica that may contain trace aluminum and iron impurities. The presence of these impurities can give rise to Brønsted acid sites that can lead to cracking reactions and coke deposition and may also contribute to the initially lower selectivity observed in these samples. Deactivation via coke formation at these Brønsted acid sites would then lead to the observed rise in propylene selectivity as well as decrease in conversion. While it has been reported that CIT-6 can be synthesized using fumed silica that is higher purity,¹⁹ we were not successful in synthesizing a phase-pure sample. Reaction testing of a CIT-6 sample prepared using fumed silica would allow one to determine whether Brønsted acid sites play a significant role in the reactivity observed for the CIT-6 samples studied here.

A.4.3.2 Catalytically Active Zinc Sites in CIT-6

Previous investigation of CIT-6 with probe molecule spectroscopy showed that there are two types of framework zinc sites in the as-synthesized material: lithium-bearing, ion-exchangeable zinc sites that are analogous to framework aluminum sites in zeolites (Z_1 and Z_2 sites in Figure A-5) and sites that resemble zinc supported on amorphous silica (Z_0 in Figure A-5).²⁰ The distribution of sites can be shifted to obtain CIT-6 with predominantly Z_1 and Z_2 or Z_0 sites via lithium and $N(CH_3)_4$ exchanges, respectively, in near-neutral pH. While both types of sites behave as Lewis acid centers, it was found via these exchange treatments that Z_0 sites are the catalytically active sites for Diels Alder cycloaddition-dehydration reaction of methyl 5-(methoxymethyl)furan-2-carboxylate (MMFC) with ethylene. To determine the catalytically active zinc sites in CIT-6 for dehydrogenation, similar exchange treatments were performed.



Figure A-5. Proposed framework zinc sites in microporous zincosilicates, from ref. 20

Figure A-6A shows the reaction data for as-made (calcined) CIT-6 that contains both types of zinc sites. Conversion starts at 14% and gradually decreases to 8% after approximately 10 h while selectivity reaches a maximum of approximately 95% and decreases with time on stream. Lithium exchange of the calcined CIT-6 generates a material with predominantly Z_1 and Z_2 sites. This material (Figure A-6B) shows very low

activity when tested for dehydrogenation. Conversion remained between 1 and 3% during the entire reaction period while the average propylene selectivity was 68%. Exchange with $\text{N}(\text{CH}_3)_4$, on the other hand, generates a material with predominantly sites that resemble zinc on amorphous silica (Z_0 sites), and this material shows the highest activity out of the exchanged samples. Conversion initially starts at 31% and decreases to approximately 50% of the initial value after 10 h while propylene selectivity approaches 90%.

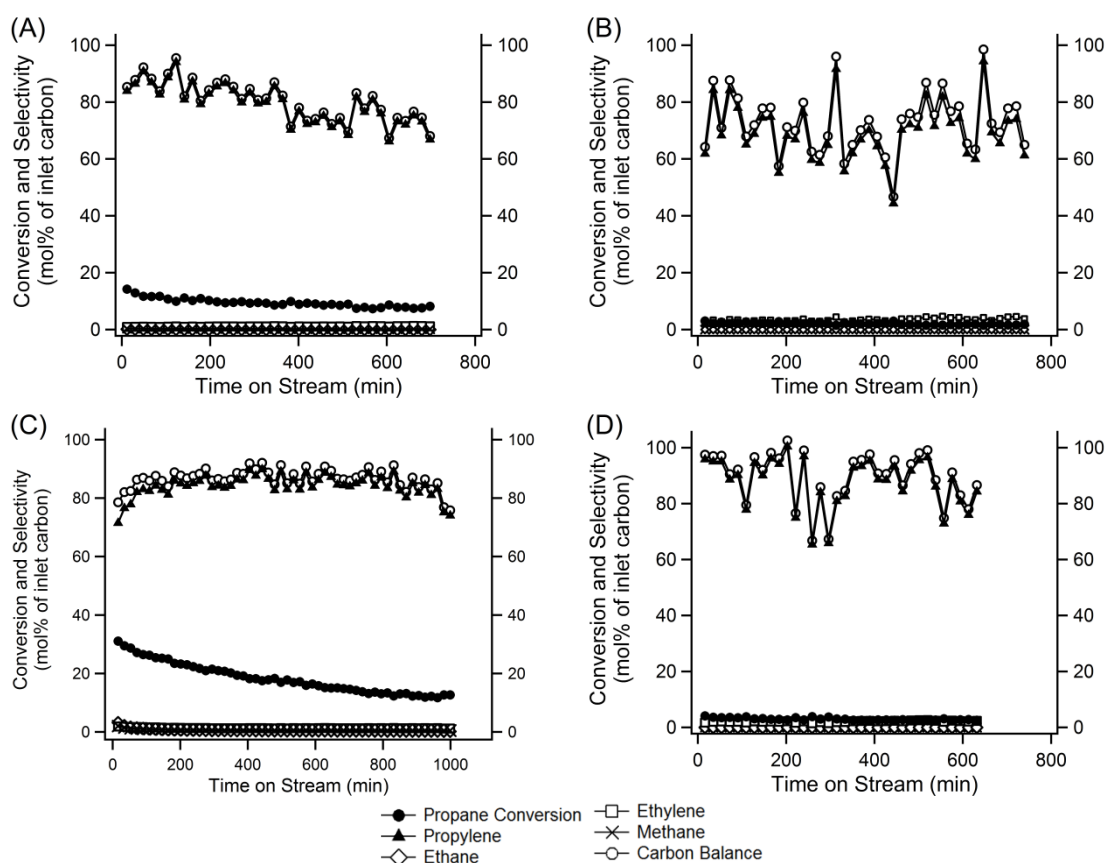


Figure A-6. Reaction data for (A) CIT-6A-C, (B) CIT-6A-Li, (C) CIT-6A-N(CH₃)₄, (D) CIT-6B-N(CH₃)₄-Li,

Comparison of these reaction data suggests that the Z_0 sites are the catalytically active sites for dehydrogenation while the lithium-bearing zinc sites appear to be inactive. To further confirm that lithium-bearing sites are not active for dehydrogenation, a $N(CH_3)_4$ exchanged CIT-6 sample (CIT-6B- $N(CH_3)_4$) was prepared that was then back-exchanged with lithium (CIT-6B- $N(CH_3)_4$ -Li). After back exchange of lithium, the material loses activity and resembles the lithium-exchanged CIT-6 (Figure A-6D and Table A-2 entry 13), providing further indication that the lithium-bearing zinc sites are not catalytically active for dehydrogenation. While this sample was prepared from a different batch of CIT-6 (CIT-6B), the lithium and $N(CH_3)_4$ exchanged samples for this batch (CIT-6B-Li and CIT-6B- $N(CH_3)_4$, respectively) were reaction tested (Figure A-10 and A-11, respectively) and show the same trend as that shown in Figure A-6. These data are consistent with the reaction data for NH_4 -exchanged CIT-6 (Figure A-3B), where the exchange treatment most likely converts lithium-bearing zinc sites into the more catalytically active Z_0 sites.

We also note that the bulk Si/Zn ratios for CIT-6A-Li and CIT-6A- $N(CH_3)_4$ (Si/Zn=13.3 and 14.7, respectively) do not deviate significantly from the parent CIT-6A-C (Si/Zn = 14.2). Back-exchange of lithium onto $N(CH_3)_4$ exchanged CIT-6 does not produce a significant change in the bulk zinc content (Table A-1) either. These data would suggest that the changes in reactivity observed cannot be wholly attributed to the loss of zinc from the materials.

A.4.3.3 Nickel Impregnation

The reaction results with Zn-MFI and CIT-6 suggest that certain zirconosilicate molecular sieves may directly catalyze the dehydrogenation reaction. While they are active and can reach propylene selectivities above 95% depending upon the treatment conditions, the materials deactivate faster compared to their platinum-impregnated counterparts. In supported platinum catalysts, it is generally believed that the addition of promoters such as zinc and tin reduce the size of platinum particles, thereby lowering the rate of undesired side reactions, and modify the electronic properties of platinum that lower the energy barrier for desorption of propylene, leading to improved selectivity and stability. However, in the zirconosilicate samples studied here, platinum appears to act as a promoter that improves the stability of the catalyst though the exact mechanism is unclear at present. These results prompted us to try using nickel as a replacement for platinum on CIT-6. Nickel supported on alumina catalysts have been explored previously for dehydrogenation of cyclohexane and were shown to have comparable activity to platinum catalysts.²⁴

NH₄-exchanged CIT-6 samples were impregnated with either 0.5 or 2.5 wt% nickel (Ni/CIT-6B-0.5 and Ni/CIT-6C-2.5, respectively) in the same manner as the platinum-impregnated samples. Figure A-7 shows the reaction data for the CIT-6 samples before and after nickel loading. Loading with 0.5 wt% nickel (Figure A-7B and Table A-2 entry 14) results in more stable propylene production (selectivities remained between 85-90%) as well as a minor improvement in the deactivation profile (time for conversion to reach 50% of its initial value was approximately 12.8 h for Ni/CIT-6B-0.5 vs. approximately 10.3 h for CIT-6B-NH₄).

Increasing the nickel loading to 2.5 wt% (Figure A-7D and Table A-2 entry 15)

does not significantly change the deactivation profile (the time for conversion to reach 50% of the initial value was approximately 12.2 h) but results in lower propane selectivities compared to Ni/CIT-6B-0.5. Furthermore, both nickel-impregnated samples produced greater methane compared to Pt/CIT-6A with Ni/CIT-6B-2.5 producing greater methane compared to Ni/CIT-6B-0.5. In addition to dehydrogenation, nickel is also known to catalyze hydrogenolysis of alkanes²⁵ with methane being one of the main products. The

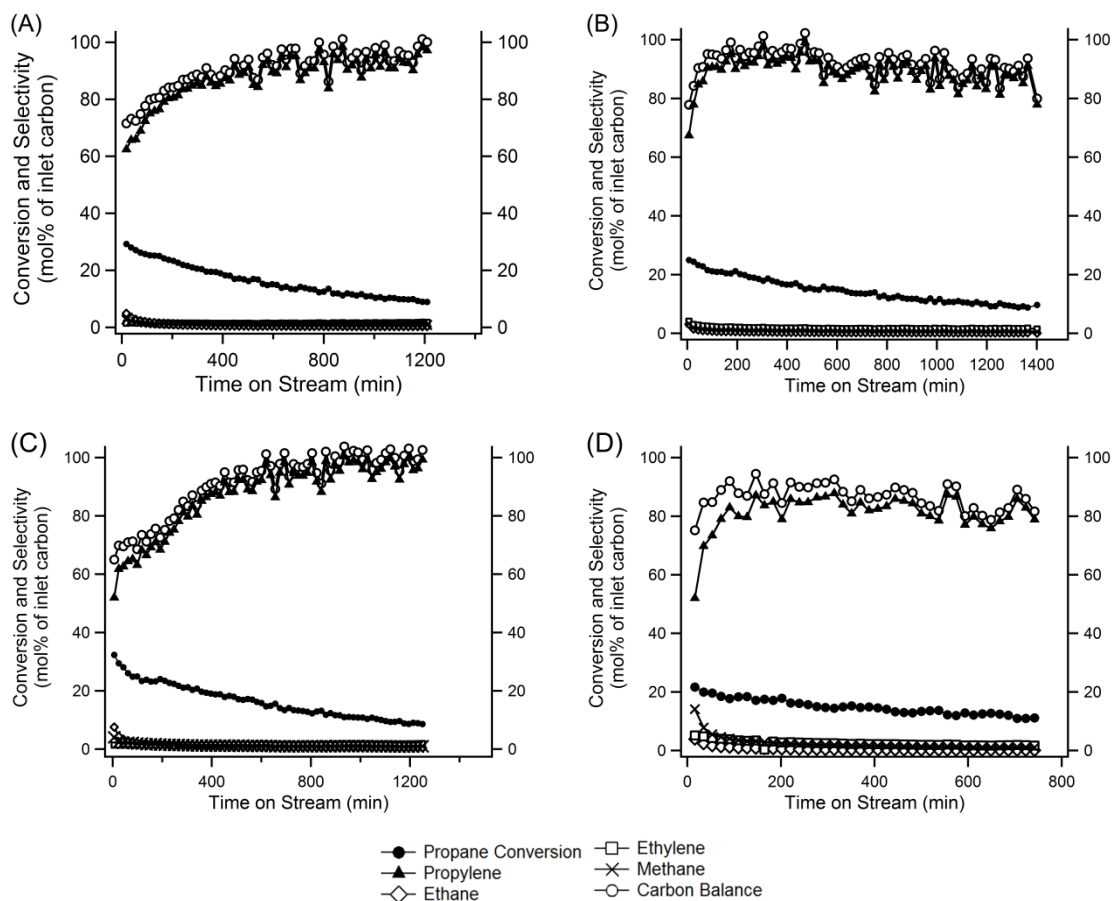


Figure A-7. Reaction data for (A) CIT-6B-NH₄, (B) Ni/CIT-6B-0.5, (C) CIT-6C-NH₄ and (D) Ni/CIT-6C-2.5

lower propylene selectivity and higher methane production would suggest that hydrogenolysis rates (a structure-sensitive reaction) increase at the higher nickel loading.

A.4.3.4 Effect of In-Situ Pretreatment

In-situ pretreatment of CIT-6 samples differ for those containing platinum or nickel compared to samples without a second metal where Pt/CIT and Ni/CIT-6 samples are calcined and reduced successively while NH_4 exchanged CIT-6 is only calcined prior to reaction. To assess whether the reduction pretreatment causes a difference in the reactivity of CIT-6 itself, two samples of NH_4 -exchanged CIT-6 (CIT-6C- NH_4) were each subjected to either the standard in-situ pretreatment (calcine 10 h at 550°C in air) for CIT-6 or the pretreatment for platinum-impregnated samples (calcine 8 h at 400°C in air and then reduce 6 h at 540°C in H_2) and then reaction tested.

Figure A-8 shows the reaction data for these two samples. The most apparent

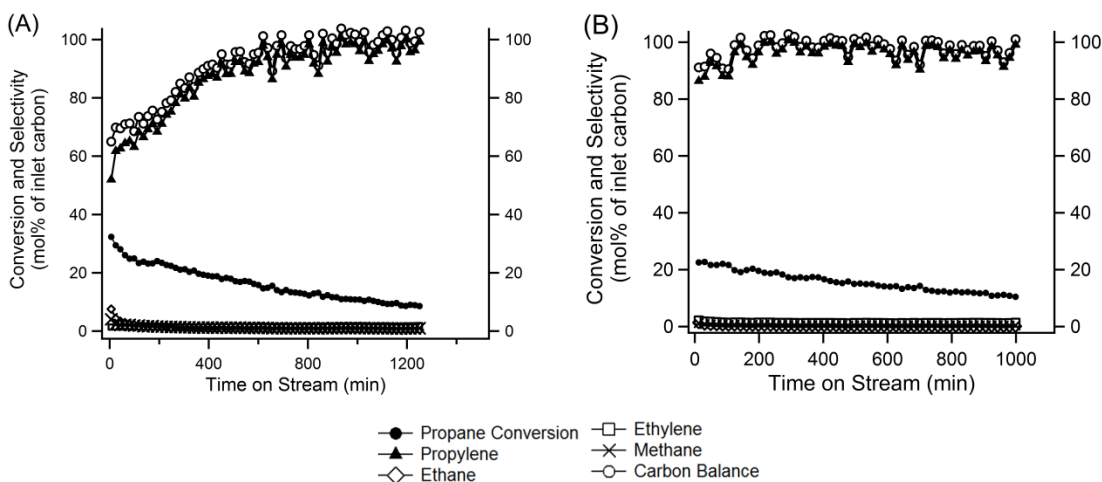


Figure A-8. Reaction data for CIT-6C- NH_4 samples (A) after the standard in-situ pre-treatment and (B) after in-situ pre-treatment for platinum-impregnated samples

differences when the NH_4 -exchanged CIT-6 receives pretreatment for platinum-impregnated samples are a lower initial conversion (initial conversion was 22.6% vs. 32.3% for CIT-6C- NH_4 receiving pretreatment for platinum-containing samples vs. pretreatment under standard conditions) and the disappearance of the initial transient rise in propylene production so that propylene selectivities are stable, averaging 95%, for the entire reaction period.

The change in reactivity may be attributed to a change in the state of zinc as a result of reduction treatment. It is well-known that framework zinc in CIT-6 may be removed during high temperature calcination and presumably exists as ZnO in the pore space. In the NH_4 exchanged CIT-6 samples, there is likely extra-framework ZnO that is generated during the two calcination treatments prior to reaction that may be contributing to the initial dehydrogenation activity observed for samples that undergo the standard pre-treatment.

Liu et al.²⁶ have recently investigated ZnO supported on alumina ($\text{ZnO}/\text{Al}_2\text{O}_3$) for propane dehydrogenation and found that the addition of trace amounts (0.1%) of platinum lead to improved stability (rate of deactivation was significantly slower). Via XPS characterization of the fresh and spent catalysts, it was found that the addition of platinum inhibits the reduction of Zn^{2+} to Zn^0 during the course of the reaction, leading to greater stability of the catalyst (Zn^{2+} is generally believed to be active for dehydrogenation while Zn^0 is inactive¹⁴). It is thus likely that extra-framework ZnO in CIT-6C- NH_4 that underwent standard pretreatment contributes to an initially high propane conversion. The rising selectivity may be attributed to the reduction of ZnO during the course of the

reaction as well as possibly the deactivation via coking of Brønsted acid sites that may be present due to impurities in the catalyst. On the other hand, ZnO in CIT-6C-NH₄ sample that underwent the reduction pretreatment should be completely reduced to Zn⁰ prior to reaction and thus a more stable reaction profile is observed. These data would also suggest that the stabilization observed for the nickel and platinum-impregnated CIT-6 samples may be due in part to the reduction of ZnO species.

A.4.4 VPI-8 Reaction Testing

Figure A-9 shows the reaction data for VPI-8. Neither the calcined (lithium-bearing) nor the NH₄-exchanged material is active for dehydrogenation with observed conversions of less than 2% for both samples. It may also be the case that framework zinc sites in VPI-8 possess weaker Lewis acidity compared to those found in CIT-6 and Zn-MFI that is insufficient for activating C-H bonds. IR spectroscopy of deuterated acetonitrile (CD₃CN) adsorption and desorption on these samples would allow for a comparison of the

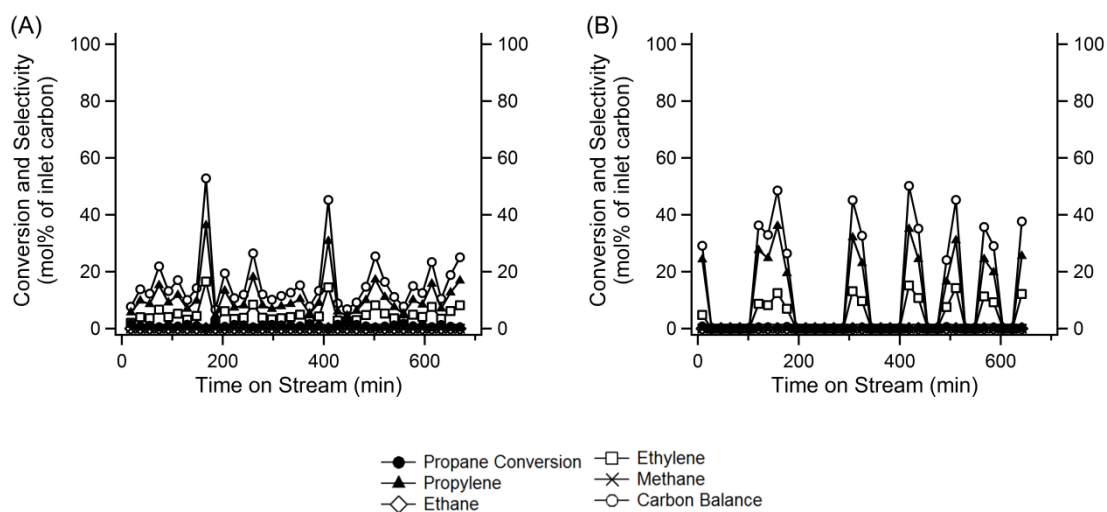


Figure A-9. Reaction data for (A) VPI-8-C and (B) VPI-8-NH₄

relative strengths of the Lewis acid centers in the materials studied here. Further, VPI-8 possesses a 1-dimensional channel system that may hinder diffusion of reactants and therefore limit its activity.

A.5 Conclusions and Recommended Future Work

This work investigated microporous zincosilicate molecular sieves as direct catalysts for propane dehydrogenation. Zn-MFI and CIT-6 were both found to be active for dehydrogenation with the activity depending upon their post-synthetic treatments while VPI-8 was inactive. In CIT-6, framework zinc sites resembling isolated zinc centers on amorphous silica were identified as the catalytically active sites for dehydrogenation while zinc sites bearing lithium are inactive. Thus, CIT-6 that was treated to remove the lithium via exchange with NH_4 or $\text{N}(\text{CH}_3)_4$ was found to be active for dehydrogenation and reached maximum propylene selectivities of 90% or higher. These samples had initial conversions near equilibrium but deactivated faster compared to platinum-impregnated samples. In-situ reduction of NH_4 -exchanged CIT-6 prior to reaction improved the stability of the catalyst likely by reducing Zn^{2+} to Zn^0 species. The stability could also be improved by the addition of nickel.

Overall, this work shows that zincosilicate molecular sieves, particularly CIT-6, may be active and selective for propane dehydrogenation but lack the stability of supported platinum catalysts. The nickel impregnation results with CIT-6 hint that the stability of catalyst may be further improved to be comparable to platinum-based catalysts. Further work may be performed to investigate the mechanistic role of platinum (and nickel) in the

Pt/CIT-6 and Pt/Zn-MFI catalyst system that might provide greater insight into improving the stability of CIT-6. In addition to zincosilicates, other Lewis acid molecular sieves may also be of interest to explore as direct catalysts for dehydrogenation. These materials include Sn-BEA, Sn-MFI and Zr-BEA where their interaction strengths with CD₃CN observed via IR are comparable to those seen for CIT-6 and thus may show interesting activity.

A.6 References

- (1) Sattler, J.J.H.B.; Ruiz-Martinez, J.; Santillan-Jimenez, E.; Weckhuysen, B.M. Catalytic dehydrogenation of light alkanes on metals and metal oxides. *Chem. Rev.*, **2014**, *114*, 10613-10653.
- (2) Weckhuysen, B.M.; Schoonheydt, R.A. Alkane dehydrogenation over supported chromium oxide catalysts. *Catal. Today*, **1999**, *51*, 223-232.
- (3) Hill, J.M.; Cortright, R.D.; Dumesic, J.A. Silica- and L-zeolite-supported Pt, Pt/Sn and Pt/Sn/K catalysts for isobutane dehydrogenation. *Appl. Catal. A: Gen.*, **1998**, *168*, 9-21.
- (4) Yang, M.-L.; Zhu, Y.-A.; Zhou, X.-G.; Sui, Z.-J.; Chen D. First-principles calculations of propane dehydrogenation over PtSn catalysts. *ACS Catal.*, **2012**, *2*, 1247-1258.
- (5) Yu, C.; Xu, H.; Ge, Q.; Li, W. Properties of the metallic phase of zinc-doped platinum catalysts for propane dehydrogenation. *J. Mol. Catal. A: Chem.*, **2007**, *266*, 80-87.

- (6) Silvestre-Albero, J.; Sanchez-Castillo, M.A.; He, R.; Sepúlveda-Escribano, A.; Rodríguez-Reinoso, F.; Dumesic, J.A. Microcalorimetric, reaction kinetics and DFT studies of Pt-Zn/X-zeolite for isobutane dehydrogenation. *Catal. Lett.*, **2001**, *74*, 17-25.
- (7) Zhang, Y.; Zhou, Y.; Shi, J.; Zhou, S.; Sheng, X.; Zhang, Z.; Xiang S. Comparative study of bimetallic Pt-Sn catalysts supported on different supports for propane dehydrogenation. *J. Mol. Catal. A: Chem.*, **2014**, *381*, 138-147.
- (8) Schweitzer, N.M.; Hu, B.; Das, U.; Kim, H.; Greeley, J.; Curtiss, L.A.; Stair, P.C.; Miller, J.T.; Hock, A.S. Propylene hydrogenation and propane dehydrogenation by a single-site Zn²⁺ on silica catalyst. *ACS Catal.*, **2014**, *4*, 1091-1098.
- (9) Hu, B.; Schweitzer, N.M.; Zhang, G.; Kraft, S.K.; Childers, D.J.; Lanci, M.P.; Miller, J.T.; Hock A.S. Isolated FeII on silica as a selective propane dehydrogenation catalyst. *ACS Catal.*, **2015**, *5*, 3494-3503.
- (10) Hu, B.; Getsoian, A.; Schweitzer, N.M.; Das, U.; Kim, H.; Niklas, J.; Poluektov, O.; Curtiss, L.A.; Stair, P.C.; Miller, J.T.; Hock A.S. Selective propane dehydrogenation with single-site CoII on SiO₂ by a non-redox mechanism. *J. Catal.*, **2015**, *322*, 24-37.
- (11) Van de Vyver, S; Román-Leshkov, Y. Metalloenzyme-like zeolites as Lewis acid catalysts for C-C bond formation. *Angew. Chem. Int. Ed.*, **2015**, *54*, 12554-12561.
- (12) Moliner, M., State of the art of Lewis acid-containing zeolites: lessons from fine chemistry to new biomass transformation processes. *J. Chem. Soc., Dalton Trans.*, **2014**, *43*, 4197-4208.

- (13) Ono, Y., Transformation of lower alkanes into aromatic hydrocarbons over ZSM-5 zeolites. *Catal. Rev.*, **1992**, *34*, 179-226.
- (14) Almutairi, S.M.T ; Mezari, B.; Magusin, P. C. M. M.; Pidko, E.A.; Hensen, E.J.M. Structure and reactivity of Zn-modified ZSM-5 zeolites: the importance of clustered cationic Zn complexes. *ACS Catal.*, **2012**, *2*, 71-83.
- (15) Zhang, Y.; Zhou, Y.; Huang, L.; Xue, M. Zhang, S. Sn-Modified ZSM-5 as support for platinum catalyst in propane dehydrogenation. *Ind. Eng. Chem. Res.*, **2011**, *50*, 7896-7902.
- (16) Zhang, Y.; Zhou, Y.; Huang, L.; Zhou, S.; Sheng, X.; Wang, Q.; Zhang C. Structure and catalytic properties of the Zn-modified ZSM-5 supported platinum catalyst for propane dehydrogenation. *Chem. Eng. J.*, **2015**, *270*, 352-361.
- (17) Barri, S.A.; Tahir, R. Chemical process and catalyst, U.S. Patent 5,208,201, May 4, 1993.
- (18) Takewaki, T.; Beck, L.W.; Davis, M.E. Zincosilicate CIT-6: a precursor to a family of *BEA-type molecular sieves. *J. Phys. Chem. B*, **1999**, *103*, 2674-2679.
- (19) Takewaki, T.; Beck, L.W.; Davis, M.E. Synthesis of CIT-6, a zincosilicate with the *BEA topology. *Top. Catal.*, **1999**, *9*, 35-42.
- (20) Orazov, M.; Davis, M.E. Catalysis by framework zinc in silica-based molecular sieves. *Chem. Sci.*, **2016**, *7*, 2264-2274.
- (21) Andy, P.; Davis, M.E. Dehydrogenation of propane over platinum containing CIT-6. *Ind. Eng. Chem. Res.*, **2004**, *43*, 2922-2928.
- (22) Deimund, M.A.; Labinger, J.A.; Davis, M.E. Nickel-exchanged zincosilicate catalysts for the oligomerization of propylene. *ACS Catal.*, **2014**, *4*, 4189-4195.

- (23) Orazov, M.; Davis, M.E. Tandem catalysis for the production of alkyl lactates from ketohexoses at moderate temperatures. *Proc. Natl. Acad. Sci. U.S.A.*, **2015**, *112*, 11777-11782.
- (24) Ahmed, K.; Chowdhury, H.M. Dehydrogenation of cyclohexane and cyclohexene over supported nickel and platinum catalysts. *Chem. Eng. J.*, **1992**, *50*, 165-168.
- (25) David Jackson, S.; Kelly, G. J.; Webb, G. Supported nickel catalysts: Hydrogenolysis of ethane, propane, n-butane and iso-butane over alumina-, molybdena-, and silica-supported nickel catalysts. *Phys. Chem. Chem. Phys.*, **1999**, *1*, 2581-2587.
- (26) Liu, G. Zeng, L.; Zhao, Z.-J.; Tian, H.; Wu, T.; Gong, J. Platinum-modified ZnO/Al₂O₃ for propane dehydrogenation: minimized platinum usage and improved catalytic stability. *ACS Catal*, **2016**, *6*, 2158-2162.

A.7 Supporting Information for Appendix

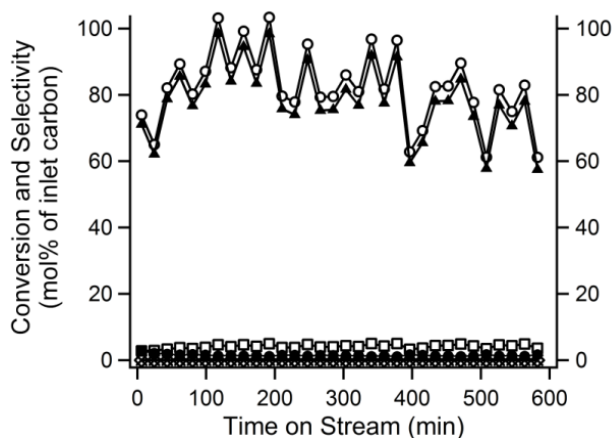


Figure A-10. Reaction data for CIT-6B-Li

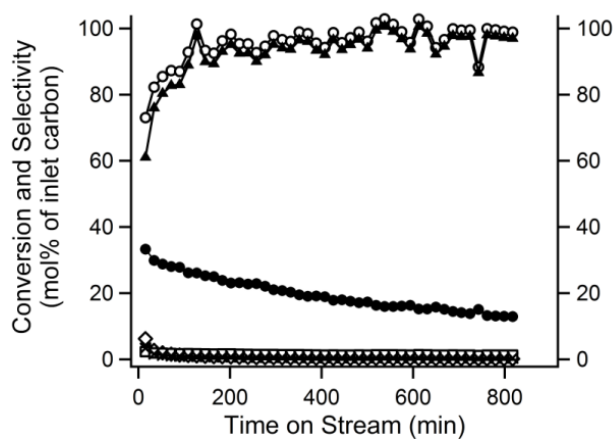


Figure A-11. Reaction data for CIT-6B-N(CH₃)₄